Sarbjyot Nijjer

Deposition and Reduction of Manganese Dioxide on Alternative Anode Materials in Zinc Electrowinning

NTNU Trondheim
Norges teknisk-naturvitenskapelige universitet

Doktor ingeniøravhandling 2000:19
Institutt for materialteknologi og elektrokjemi

IME-rapport 2000:11

Deposition and Reduction of Manganese Dioxide on Alternative Anode Materials in Zinc Electrowinning

by

Sarbjyot Nijjer

Thesis submitted in partial fulfilment of the
requirements for the degree
Doktor Ingeniør

Norwegian University of Science and Technology
Department of Materials Technology and Electrochemistry

January 2000

List of symbols

Symbol	Unit	Explanation
a	Å	lattice axis
a_R		activity of species R
a_O		activity of species O
b	Å	lattice axis
b	V/current decade	Tafel slope
c	Å	lattice axis
c	mol/dm^3, g/l	concentration
$c_R{}^\infty$	mol/dm^3	bulk concentration of species R
c_R	mol/dm^3	concentration of species R
d_o	cm	outer diameter of a cylinder electrode
D	cm^2/s	diffusion coefficient
D_R	cm^2/s	diffusion coefficient of species R
E	V	potential
E°	V	standard potential
E^{rev}	V	reversible potential
E_a	V	anodic potential
E_c	V	cathodic potential
E_p	V	peak potential
$E_p{}^a$	V	anodic peak potential
$E_p{}^c$	V	cathodic peak potential
$E_{1/2}$	V	half peak potential
ΔE_p	V	split in peak potentials
f	Hz	frequency
F	C/mol	Faraday constant
h	cm	high of cylinder a electrode
i	A/cm^2, mA/cm^2	current density
i_o	A/cm^2	exchange current density
$\vec{i}$	A/cm^2	partial cathodic current density
$\overleftarrow{i}$	A/cm^2	partial anodic current density
i_p	mA/cm^2	peak current density

Symbol	Unit	Explanation
$i_{Mn^{2+}}$	mA/cm^2	current density in electrolyte containing Mn^{2+} ions
$i_p{}^a$	mA/cm^2	anodic peak current density
$i_p{}^c$	mA/cm^2	cathodic peak current density
I	A	current
J	mol/cm^2	flux of species
k	s^{-1}	rate constant
$m_{H_2O_2}$	g/h	weight of hydrogen peroxide per hour
m_{MnO_2}	mg/cm^2	weight of manganese dioxide per square cm
Δm	mg/cm^2	change in weight per square cm
n		number of electrons
Q_a	mC	anodic charge
Q_c	mC	cathodic charge
R	J/K·mol	gas constant
S_{MnO_2}	%	current efficiency for MnO_2
t	s	time
t_a	s	time interval for anodic pulse
t_c	s	time interval for cathodic pulse
T	°C, K	temperature
U_a	V	anode potential
v	mV/s	scan rate (SR)
x	cm	distance
Z_{re}	Ω	real component of impedance
Z_{im}	Ω	imaginary component of impedance
α_a		anodic transfer coefficient
α_c		cathodic transfer coefficient
η	V	overpotential
η_a	V	anodic overpotential
η_c	V	cathodic overpotential
λ	s	time interval
Θ_B		fraction of catalyst surface

Acknowledgements

The present work was carried out at Department of Electrochemistry/Department of Materials Science and Electrochemistry at NTNU, in the period from May 1996 to January 2000. The Research Council of Norway (NFR), Norzink A/S in Odda and Permascand AB in Ljungaverk (Sweden), are acknowledged for financial support of this project.

Professor Jomar Thonstad[1] has been my supervisor during these years, and I am grateful for his support, advice and great interest in my work. I also want to thank Geir Martin Haarberg[2], who has been my co-supervisor during the last one and half year, for interesting discussions and advices. Anders Eklund[3], who initiated this project and served as co-supervisor in the initial phase, is acknowledged for his go-ahead spirit.

I want to thank the staff at Norzink A/S, Permascand AB and Eka Chemicals AB for good cooperation during these years. Thanks go to; Agnar Målsnes[4], Anders Eklund, Harald Haarstad[4], Ingemar Johansson[5], Helena Mäkinen[6], Hanna Carlsson[6], Bo Håkansson[7] and Fredrik Herlitz[7] for their support and interest for this project.

I want to thank Kjell Røkke[1] for making equipment for my experimental work. Martha Bjerknes[1] deserves a special thank for encouraging me during these years. Many thanks go to my friends and colleagues at IME/SINTEF, those who are still working here and those who have left the Department, for memorable years.

Finally I want to thank Torstein for supporting me during these years. I am very grateful for his patience and encouragement when I had my tough days. I also thank Øyvind and Ingrid, who made me relax and think about anything else than my thesis.

Sarbjyot Nijjer

---

[1]Department of Materials Science and Electrochemistry
[2]SINTEF, Materials Technology
[3]Avesta Sheffield AB, prior employed at Norzink A/S
[4]Norzink A/S
[5]Permascand AB
[6]Prior employed at Permascand AB
[7]Eka Chemicals AB

Summary

In the present work, deposition of manganese dioxide (MnO_2) from sulphuric acid (H_2SO_4) containing Mn^{2+} ions, was studied on various electrode materials of DSA® type, i.e. an active coating on a titanium substrate, and lead electrodes. The experimental techniques used were; cyclic voltammetry (CV), linear voltammetry (LSV), galvanostatic electrolysis (GE) and Scanning Electron Microscopy (SEM).

The mass transfer of Mn^{2+} ions to the electrode surface was found to be the rate determining step in the oxidation of Mn^{2+} to MnO_2, which was found to follow an ECE-mechanism (electrochemical-chemical-electrochemical). The deposited MnO_2 was found to be completely reduced in the cathodic scan. The reduction process was found to be a combination of electrochemical and chemical dissolution steps. Low acid concentrations, high stirring rate and high temperature raised the oxidation rate of Mn^{2+} to MnO_2, while high acid concentration and low temperature suppressed the deposition of MnO_2. High stirring rates reduced the quantity of deposited MnO_2 on the electrode surface during cyclic voltammetry.

The deposition of MnO_2 was found to block the catalytic sites on the Ti/IrO_2 - Ta_2O_5 anode, and the anode potential was observed to increase during galvanostatic electrolysis. The oxidation of Mn^{2+} is suggested to occur at the interface MnO_2 deposit/electrolyte. When lead anodes (Pb/Ag) and inert anodes (Ti/IrO_2 - Ta_2O_5) were used in electrolysis, the electrolyte was red coloured due to Mn^{3+} ions. The MnO_2 deposit adhered firmly to the anode surface during electrolysis, and no MnO_2 particles were observed suspended in the bulk electrolyte. When platinum was used as anode, huge quantities of MnO_2 particles were suspended in the electrolyte, while only small amounts of MnO_2 were deposited on the electrode surface.

Experiments using rotating cylinder anodes with IrO_2 - Ta_2O_5 coating, showed that the thickness of the deposited MnO_2 (10-20 μm) was nearly independent of the rotation speed (0-3.1 m/s).

New coatings for oxygen evolution were prepared by replacing parts of the Ta_2O_5 in the IrO_2 - Ta_2O_5 coating, with MnO_x ($x \leq 2$). The coating with 5 mol% MnO_x was found to be the most electrocatalytic during electrolysis in 2M H_2SO_4.

When hydrogen peroxide (H_2O_2) was added to the electrolyte during electrolysis, no MnO_2 deposit was observed on the electrode surface. The red colour of the

electrolyte was absent because the Mn^{3+} was reduced to Mn^{2+} by the H_2O_2. Continuous addition of 0.9-1.79 g/h H_2O_2 to the electrolyte during the electrolysis, was found to reduce the deposited MnO_2 without causing any damage to the catalytic coating (IrO_2 - Ta_2O_5) or the Ti substrate. In addition, the anode potential was reduced by 500-700 mV because of the depolarizing effect of the H_2O_2.

Contents

Chapter 1

Introduction

Zinc metal has a wide application today and it is the fourth most produced metal behind iron and steel, aluminium and copper. Some examples of applications are: galvanizing industry (car body, pipe, metal wire), casting alloys, alloying element in brass and other alloys, sacrificial anodes in the offshore industry, chemicals and medical industry. Because of formation of a zinc hydroxide layer on the surface in atmospheric and other environments, zinc coatings are often used to protect steel constructions in corroding environments. Nearly half of the zinc produced is used to protect steel [1].

Since early in this century, zinc has been produced by pyrometallurgical and electrochemical methods (1916). In the pyrometallurgical method, zinc oxide is reduced by CO to form gaseous zinc which is condensed in a reducing atmosphere [2]. Electrochemical production of zinc gives very pure metal, up to about 99.999 % . Because of the high consumption of electrical energy in the electrowinning process, electrode materials with low anodic overpotential are preferred. Lead anodes, which have high overpotential for oxygen evolution, are used in the zinc electrowinning today.

1.1 Zinc electrowinning

A simple outline of the zinc electrowinning process is shown in figure 1.1. Zinc is usually present as zinc sulphide (ZnS) in the zinc ore. In addition, zinc ore contains several other elements (Mn, Mg, Ca, Cd, Cu, Fe, Co, Ni, Al, As, Sb,

Si, Sn, Ge, Hg) [2, 3]. Zinc sulphide is not readily attacked by acid and alkaline solutions [3], so it is converted into zinc oxide (ZnO) by fluidized bed roasting at high temperature (920-950°C) [4, 5]. The roasting reaction is given by equation 1.1 [2, 3].

$$2ZnS + 3O_2 \rightarrow 2ZnO + 2SO_2 \tag{1.1}$$

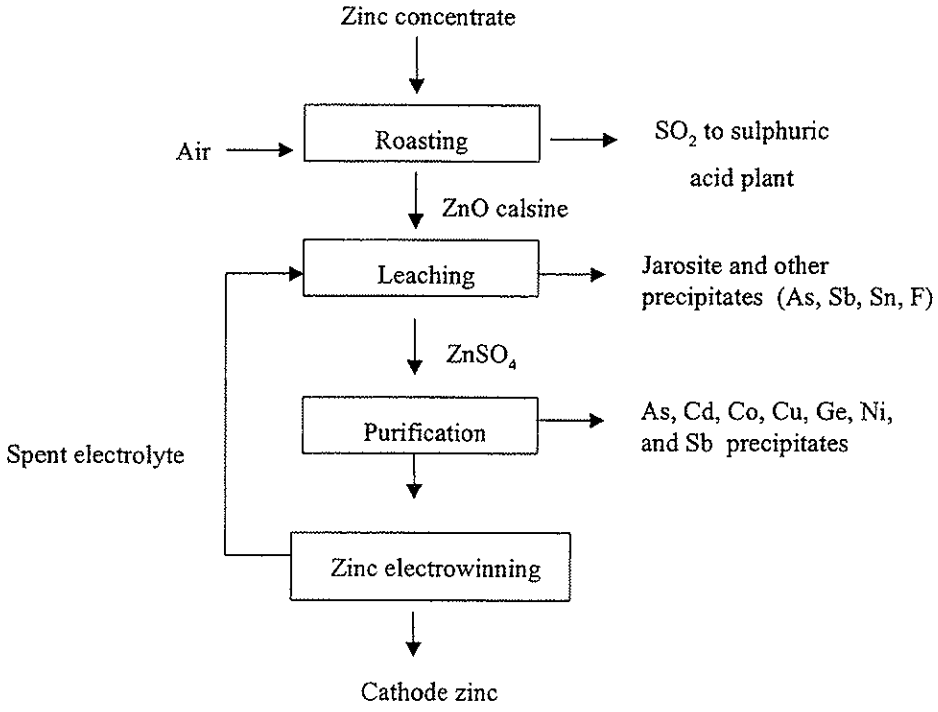

Figure 1.1: *Outline of the zinc electrowinning process.*

The roasting reaction is exothermic and the equilibrium is shifted far to the right. The zinc oxide produced in the roasting process, is easily dissolved in sulphuric acid during the leaching process, to produce zinc sulphate as described by equation 1.2:

$$ZnO + H_2SO_4 \rightleftharpoons ZnSO_4 + H_2O \tag{1.2}$$

The impurities must be removed from the electrolyte before it enters the electrolysis cell. The iron ions in the electrolyte cause reduction in the cathodic current efficiency, because they undergo oxidation from Fe^{2+} to Fe^{3+} on the anode, and are reduced on the cathode from Fe^{3+} to Fe^{2+}. Most of the iron in the zinc concentrate is Fe^{2+}. Some zinc producers use manganese dioxide or/and permanganate as oxidizing agents to oxidize Fe^{2+} to Fe^{3+}. The iron is precipitated as jarosite[1] in a separate process in the leaching step. Small quantities of other elements are removed with the jarosite such as Sb, As, Sn and F etc. [2].

The manganese concentration in the zinc ore corresponds to about 2-5 g/l in the electrolyte, depending on the ore. If chemicals containing manganese are added as oxidizing agents, the concentration of Mn^{2+} ions in the electrolyte can be increased to 10-15 g/l (sometimes more) when it enters the electrolysis cell.

The other elements (Cd, Co, Cu, Ni, As, Sb and Ge) are removed from the electrolyte in the purification steps where zinc dust is used as reducing agent to form precipitates. When the electrolyte enters the electrolysis cell, it mainly contains $ZnSO_4$ (50-55 g/l), $MnSO_4$ (10-15 g/l) and H_2SO_4 (170 g/l) [2]. The temperature of the electrolyte is generally maintained in the range 30-40°C [3]. Small amounts of alkali metal ions are present in the electrolyte, but they have no effect on the electrode reactions.

The electrodes are placed vertically and the distance between the anode and cathode is ~3.5 cm (figure 1.2). The anodes are made of lead, alloyed with small amounts of silver (0.3-0.7 wt%), and the cathodes are aluminium sheets. The main electrode reactions in the zinc electrowinning are reduction of Zn^{2+} on the cathode, and oxygen evolution on the anode as given by equations 1.3 and 1.4 respectively.

$$Zn^{2+} + SO_4^{2-} + 2e^- \rightarrow Zn + SO_4^{2-} \ , \ E^\circ = -0.76V_{NHE} \tag{1.3}$$

$$H_2O \rightarrow \frac{1}{2}O_2 + 2H^+ + 2e^- \ , \ E^\circ = 1.23V_{NHE} \tag{1.4}$$

[1] Jarosite is a complex iron compound ($Na_2Fe_6(SO_4)_4(OH)_{12}$) [2] which is precipitated in acid environment pH = 2 [3].

The overall reaction is given by equation 1.5:

$$ZnSO_4 + H_2O \rightarrow Zn + \frac{1}{2}O_2 + H_2SO_4 \qquad (1.5)$$

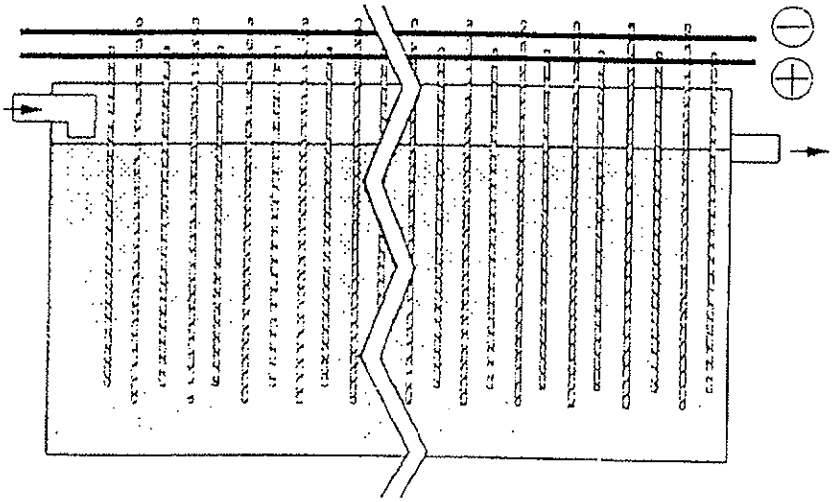

Figure 1.2: *Schematic view of a zinc electrowinning cell [6].*

Mn^{2+} ions in the electrolyte, are being oxidized on the anode to form manganese dioxide (MnO_2) deposit as a parasitic reaction. The overall reaction of manganese dioxide deposition on the anode is given by equation 1.6:

$$Mn^{2+} + 2H_2O \rightarrow MnO_2 + 4H^+ + 2e^- \,,\; E^\circ = 1.23V_{NHE} \qquad (1.6)$$

From equation 1.6 it is seen that the standard potential for the deposition of MnO_2 is the same as for oxygen evolution. Because of the deposition of MnO_2 on the anode surface, the anodes must be cleaned periodically (every 14 days) to remove the deposit, which may otherwise cause increased ohmic resistance and short-circuiting between the anode and cathode. The lead anodes undergo corrosion during anodic polarization as will be described in section 1.1.1. The formation of manganese dioxide is beneficial for the lead anodes because it reduces the corrosion rate of the lead [7], but it also causes an increase in energy consumption because of increased resistance in the deposit layer.

1.1.1 Lead anodes and alternative anode materials

All zinc producers are using lead anodes in their process today. There are some disadvantages connected to the use of lead anodes. They are not dimensionally stable because of low mechanical strength, and they are not inert to the sulphuric acid electrolyte. If small quantities of silver (Ag) (0.3-0.8%) is alloyed with the lead, the mechanical strength and electronic conductivity is improved and the corrosion rate of the lead anode is decreased. Most of the lead anodes used in metal electrowinning are alloyed with different elements (Ag, Sb or Ca). The lead anodes alloyed with silver have lower overvoltage for oxygen evolution than pure lead anodes, but the overvoltage is still high (800 mV). After 2-3 years the anodes must be replaced with new anodes. The periodic cleaning of the anodes also reduces the life-time because of rough mechanical treatment. In addition, lead is a hazardous material to work with, and it may cause environmental contamination.

During anodic polarization in sulphuric acid, a $PbSO_4$ layer is formed on the anode surface as described by equation 1.7 [8]. Lead monoxide (PbO) is also formed simultaneously as $PbSO_4$, and is converted into PbO_2 at higher potentials as given by equations 1.8 and 1.9 respectively [8]. The $PbSO_4$ layer is poorly conducting and is converted into lead dioxide (PbO_2) at higher anodic potentials as given by equation 1.10 [8]. The PbO_2 layer is conducting and protects the lead against attack by the acid, so the corrosion rate is lowered. But still some lead is oxidized to Pb^{2+} ions (equation 1.11), which may dissolve in the electrolyte or combine with SO_4^{2-} to form solid $PbSO_4$ [9].

$$Pb + H_2SO_4 \rightleftharpoons PbSO_4 + 2H^+ + 2e^- \tag{1.7}$$

$$Pb + H_2O \rightleftharpoons PbO + 2H^+ + 2e^- \tag{1.8}$$

$$PbO + H_2O \rightleftharpoons PbO_2 + 2H^+ + 2e^- \tag{1.9}$$

$$PbSO_4 + 2H_2O \rightleftharpoons PbO_2 + H_2SO_4 + 2H^+ + 2e^- \tag{1.10}$$

$$Pb \rightarrow Pb^{2+} + 2e^- \tag{1.11}$$

The dissolved lead ions in the electrolyte may be reduced on the cathode and contaminate the zinc metal. Small quantities (30 ppm $\leq$) of lead in the zinc metal reduce the quality of zinc, and make the zinc metal unsuitable for die-casting applications because of problems associated with inter-granular corrosion [10].

Since the lead anodes have the disadvantages mentioned above, alternative anode materials have been tested in zinc electrolysis. The requirements the alternative anode materials have to satisfy are [11]:

- High surface area
- High electrical conduction
- Good electrocatalytical properties
- Long-term mechanical and chemical stability at the support/active layer and at the active layer/solution interface
- Minimized gas bubble problems
- Enhanced selectivity
- Availability and low cost
- Health safety

Several scientists [12, 13, 14, 15, 16, 17, 18, 19] have studied various dimensionally stable anodes (DSA®) for oxygen evolution in acid solutions with promising results. The materials tested have been different metal oxides (RuO_2, IrO_2, MnO_2, Ta_2O_5 etc.) on Ti substrate. The main problem by using alternative anode materials in zinc electrowinning, is the presence of Mn^{2+} ions in the electrolyte. When Mn^{2+} ions are present in the electrolyte, they will oxidize on the anode and deposit as described by equation 1.6. Kulandaisamy et al. [20] observed a slight increase in anode potential in manganese-containing electrolyte, due to blocking of catalytic sites by the deposition of MnO_2. Figures 1.3 and 1.4 show Scanning Electron Microscopy (SEM) images of the surface of a new IrO_2 - Ta_2O_5 coating on titanium substrate, and the same coating used as anode in electrolysis for 10 hours in 2M sulphuric acid containing Mn^{2+} concentrations in the same range as the industrial electrolyte ($c(Mn^{2+}) = 10$ g/l) respectively.

The bright particles in figure 1.3 are IrO_2, which are the electroactive sites for oxygen evolution. The dark phase is mainly Ta_2O_5, which is non-conducting and

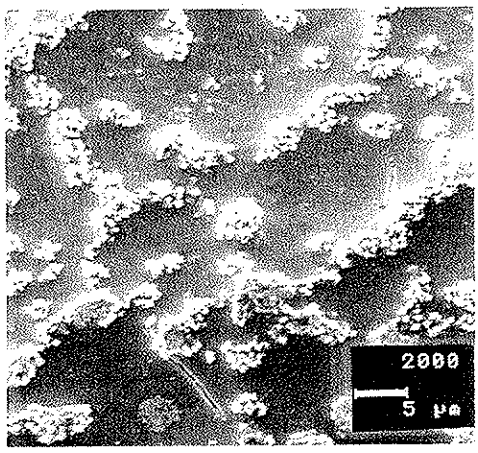

Figure 1.3: *SEM image of a new Ti/IrO_2 - Ta_2O_5 electrode surface. 2000X SE.*

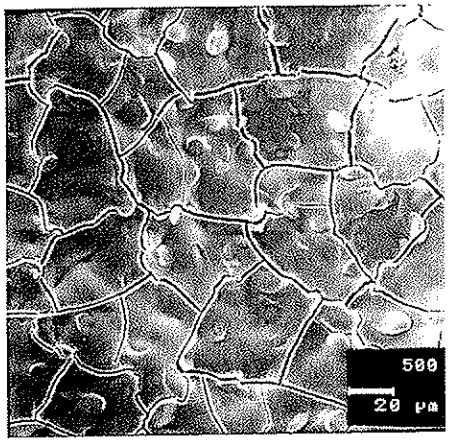

Figure 1.4: *SEM image of MnO_2 deposit on Ti/IrO_2 - Ta_2O_5 electrode. 500X SE.*

works as chemical stabilizer for IrO_2. Figure 1.4 shows deposited MnO_2 on the anode surface. The active sites (IrO_2 particles) are completely covered, and the anode has been working as an MnO_2 electrode from one hour after electrolysis start. The problems related to the deposition of MnO_2 on the IrO_2/Ta_2O_5 anode in zinc electrowinning, have not been much investigated and reported earlier. Nidola et al. [21] described in a US patent in 1998, a new electrocatalytic coating on Ti, which was suitable for oxygen evolution from acid electrolytes containing manganese and fluorides. The coating consisted of Ru and Ir as major components, while Sn, Co, Ti and Ta was in minor and intermediate concentrations [21]. The overpotential for oxygen evolution was decreased such that MnO_2 was spontaneously removed from the anode surface [21]. It is not known if the coating described by Nidola et al. [21], is produced commercially and used in zinc electrowinning today.

1.2 Scope of the present work

The objective of this work was to investigate electrocatalytic coatings (IrO_2 - Ta_2O_5) on titanium substrate in sulphuric acid where manganese species are present. The mechanisms of the deposition and reduction of manganese dioxide, and ways to remove the deposited manganese dioxide electrochemically or chemically from the anode surface, have been investigated.

Chapter 2

Literature review

2.1 Oxygen - evolving anodes: Ti/IrO_2 - Ta_2O_5

The disadvantages of the lead anodes in acid solutions was mentioned in section 1.1.1. The motivation to find an anode material which is dimensionally stable, does not dissolve in the electrolyte and has low oxygen overpotential, has led to a numerous scientific publications during the past 20 years.

Dimensionally stable anodes (DSA®) are widely used in the electrochemical industry such as in chlorine and chlorate production, metal electrowinning from chloride electrolytes, electro-organic synthesis and electroplating [22]. The operating environment may vary from mild (acid-water electrolysis) to very severe conditions at high current densities such as fast electroplating processes. In general, DSA® electrodes are characterized by a thin active coating of a few microns thickness, deposited on a base metal (Ti, Zr, Ta or Nb) [14]. The DSA® concept is normally associated with a RuO_2 coating on a Ti substrate, used in chlorine and chlorate production.

2.1.1 Preparation of Ti/IrO_2 - Ta_2O_5 anodes and their properties

Vercesi et al. [23] investigated several metals (stainless steel, Ti, Al, Ni, Zr and Ta) to study the influence of the base metal on the coating morphology and electrocatalytic activity. Ti was found to be the best choice of substrate metal

for technical and economical reasons [14, 22], because of its low density and price compared to Ta, which is more stable in acid solutions [18, 24].

Some metal oxides exhibit metallic conductivity, but they are seldom used alone in practical applications [11]. Usually they are more or less heavily doped or mixed with less active oxides of higher chemical stability [11]. The oxides can be prepared anodically or thermally. The stability of anodically grown oxides is poorer than that of oxides prepared by thermal decomposition of appropriate precursors [11]. IrO_2 posesses metallic conductivity [17] and is a good electrocatalyst for oxygen evolution [25]. The electrochemical stability sequence of the conducting components is given by [14]: $IrO_2 > Pt > RuO_2$.

The oxygen evolving electrodes are prepared as follows:

1. The Ti base is roughened by sandblasting and etching in boiling oxalic acid [26, 27] or hot concentrated HCl [15, 24, 27].
2. The coating solutions are prepared by dissolution of the coating compounds in the form of soluble salts (H_2IrCl_6, $TaCl_5$) in a suitable solvent such as n-butanol and concentrated HCl [26, 28], concentrated HCl and ethanol [29] or isopropyl alcohol [20].
3. Repeated application of the coating solution on the pretreated base metal by brush [14] or spray.
4. Evaporation of the solvent at low temperature (80°C [20, 23] -120°C [26]).
5. Finally thermal decomposition of the metal-containing salts into the corresponding oxide phases at high temperatures (350-950°C [20, 23, 30]) in air.

For oxygen evolution in acid solutions, the best coating would be Ti/RuO_2 - TiO_2, which has a Tafel slope of 40 mV/decade against 60 mV/decade for Ti/IrO_2 - Ta_2O_5 when taking into account only the best catalytic activity [22]. However, the RuO_2-based coating is unstable for oxygen evolution and may oxidize according to reaction 2.1 forming RuO_4, which is volatile [31].

$$RuO_2 + 2H_2O \rightarrow RuO_4 + 4H^+ + 4e^- \tag{2.1}$$

In the IrO_2 - Ta_2O_5 coating on Ti substrate, IrO_2 is the catalytic and conducting component, while Ta_2O_5 behaves as a stabilizer and dispersant of the catalyst [22].

Otogawa et al. [26] observed the surface morphology of the IrO_2/Ta_2O_5 coating to be heterogeneous. The layer consisted of cracks, smooth areas containing Ir_2O_5 and Ta_2O_5, and aggregate particles of pure IrO_2 [26]. At the smooth areas innumerable micro-cracks were observed under high magnification [26]. It was also observed that the IrO_2 crystallites aggregated and grew perpendicular to the base surface [26]. The growth of IrO_2 crystallites occurred not only on the outermost surface, but also on the underlying phase of the coating [26]. Cross sections of the coating showed that no cracks were found to penetrate into the base metal [26].

Several other scientists observed the "mud-crack" structure as shown in figure 2.1 [17, 22, 23, 28, 32]. According to Vercesi et al. [23], the cracks were believed to result from mechanical tensions which were not compensated for by the plasticity of the coating, and were due to the difference in thermal expansion coefficient between the base metal and the coating. Krysa et al. [29] observed that the morphology of the IrO_2-Ta_2O_5 active layer (0.32-0.39 mg/cm^2 Ir) depended strongly on the pretreatment of the Ti base metal, and that an increase in surface roughness led to longer service life time, and a lower rate of steady state dissolution of the coating.

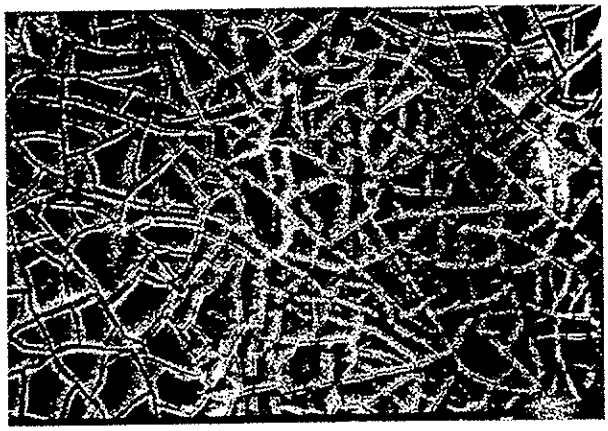

Figure 2.1: *SEM image of the surface of a Ti/IrO_2 electrode exhibiting the "mud-crack" structure [28].*

Roginskaya et al. [32] observed that coatings with x < 30 mol% IrO_2 contents, contained crystalline IrO_2 and two additional rutile structure phases with very diffuse XRD lines, as well as amorphous Ta_2O_5. According to Mraz and Krysa [30] surface enrichment appeared to be a result of low homogenization of the

mixed oxides. A lower degree of crystallinity in the coatings was obtained from non-aqueous solutions by Roginskaya [32], while Vercesi et al. [23] observed that IrO_2 needles were formed when an organic solvent was used, but not in aqueous solvents.

The temperature of 350°C was found to be too low for proper oxidation of the applied material: no IrO_2 agglomerates appeared and only a few cracks were formed. Lodi et al. [33] observed the existence of a relatively well defined IrO_2 rutile phase after heating a powder at 350°C in oxygen for 6 hours. At 750°C and 950°C the number of IrO_2 crystals on the surface was increased considerably, while the number of cracks tended to decrease, and eventually disappeared [23]. It was suggested that increasing the annealing temperature caused a general deterioration of the conducting properties [33].

Foti et al. [34] prepared Ir-based coatings on Ti base by rapid thermal decomposition of $H_2IrCl_6 \cdot 6H_2O$ precursor by using electromagnetic induction heating. When using a pulse heating technique by induction at an apparent temperature below 250°C, a smooth amorphous surface was obtained [34]. For samples prepared at T$\geq$300°C, highly crystalline coatings were obtained [34]. In acid solution, a progressive activation was observed upon cycling the potential between 0.2 and 1.5 V vs. Mercury Sulphate Electrode (MSE) [34].

Vukovic [16] prepared an activated IrO_2 film by polarizing the electrode, which was an Ir wire, with square wave pulses from -0.25 to +0.25 V vs. SCE and treated the oxide film at 200°C afterwards. The Tafel slopes at the low current densities were 40 mV/decade for the activated electrodes, and it increased to 55 mV/decade after heat treatment at 200 °C. A Tafel slope of 160 mV/decade was measured at high current densities. It was observed that stabilization of the IrO_2 surface was achieved by heat treatment of the film [16]. Vukovic [16] observed a shift in the voltammetric charge towards more positive potentials in voltammograms recorded after 5 hours of polarization. The explanation for such a voltammetric profile was suggested to be a change in the stoichiometry of the IrO_2 to a higher oxidation state of Ir, its surface becoming more effective absorbent of OH^- intermediates taking part in the oxygen evolution reaction.

Martelli et al. [22] found the average of the Tafel coefficient for new electrodes to be 60 mV/decade and 120 mV/decade at low and high current densities respectively. Passivated/deactivated electrodes showed an average Tafel slope of 80-100 mV/decade at low current density, and 120 mV/decade at high current density [22].

The oxygen overpotential was observed to increase slightly with the calcination temperature, and the service life was sufficiently long for a calcination temperature of 450°C [30]. The activity of IrO_2 for O_2 evolution decreases as the temperature of preparation is increased [11]. For higher current densities, the oxygen overpotential was observed to decrease with increasing Ir content, and it rapidly decreased with increasing coating thickness up to ~0.4 mg/cm^2 [29]. For a coating thickness of 1.0-1.2 mg/cm^2 the oxygen overpotential was almost constant [29].

Martelli et al. [22] found the best coating for oxygen evolution in acid solutions to be:

Ti/IrO_2 (70 mol%) - Ta_2O_5 (30 mol%)

Also Mraz and Krysa [30] found that the values of service life were at maximum for coating compositions of 65-70% IrO_2 and 30-35% Ta_2O_5 on Ti base in acid solution. The real service life was estimated to be from 5 to 10 years based on accelerated electrolysis tests at a current density of i = 2 A/cm^2 [30].

2.1.2 Deactivation and passivation of the Ti/IrO_2 - Ta_2O_5 anodes

Although the Ti/IrO_2 - Ta_2O_5 anodes are dimensionally stable, electrochemically and chemically stable, the service life is limited. The stability of the coating depends mainly on the anodic stability of the conducting oxide and the stability of the non-conducting oxide and its ability to protect the base metal [14]. The end of the service life for a given electrode was determined by the time at which the anode potential increased significantly [14]. For a IrO_2 - Ta_2O_5 electrode, the relationship between the total amount of coating and the service life was not found to be linear [14]. By calculating the efficiencies in Ah/mol of conducting oxide, a maximum occurred for a 1.5 μm thick coating [14]. Krysa et al. [29] observed that for an Ir content of 0.45-1.2 mg/cm^2, the service life was proportional to the Ir content in the coating.

Martelli et al. [22] classified the deactivation mechanisms into:

- passivation of the metal base
- coating consumption
- coating detachment
- mechanical damages
- mixed mechanisms

The deactivation occurs with a sudden increase in the electrode potential, that rapidly reaches high values, signifying a complete electrochemical failure because of formation of an insulating layer of stochiometric TiO_2 at the interface between the metallic base and the active coating [18, 20, 22]. Passivation can be induced by penetration of acid solutions through cracks and pores into the Ti substrate [18]. The service life was found to be influenced slightly by the acid concentration, but variations in the electrolyte temperature was thought to play an important role [22].

According to Comninellis and Vercesi [14], IrO_2 is sufficiently stable and the deactivation occurs through dissolution of the substrate or building up of a non-conducting layer between the coating and the base metal. Mraz and Krysa [30] detected Ti^{4+} ions in the electrolyte during the accelerated life test, due to corrosion of the Ti substrate. They also found that the slowly changing steady-state rate of dissolution of the IrO_2 active layer was reached after 600-700 hours. Interruption of electrolysis for more than 1 hour increased the dissolution rate of Ir [30]. Also Kulandaisamy et al. [20] suggested anodic dissolution during oxygen evolution, which occurred at the catalyst/electrolyte interface, as a possible deactivating mechanism.

Otogawa et al. [26] studied the variation of a Ti/IrO_2 - Ta_2O_5 anode during electrolysis at high current densities (3 A/cm^2) by SEM, EDX, XRF and XPS. They observed that some parts of the smooth area (Ta_2O_5) peeled off during electrolysis and the number of cracks increased. Mapping images showed that

IrO_2 disappeared/selectively decreased in the outermost layer, while the distribution of Ta_2O_5 was almost uniform. Variation in the relative intensity, I_{Ir}/I_{Ta}, suggested that Ir on the coating surface was gradually lost into the electrolytic solution during the first stage (0-250 h) of electrolysis. During the second stage (250-1450 h) the relative intensity of Ir gradually increased.

Gottesfeld and Srinivasan [35] prepared a thick oxide layer on Ir in 0.5M H_2SO_4 by a potential multi cycling treatment, and suggested that the loss of activity may actually be due to some restructuring mechanisms, occurring mainly at the oxide-electrolyte interface such as loss of active area. Mraz and Krysa [30] suggested that the reason for the increase in the overpotential is the fact that the electrochemical active surface area changes during electrolysis.

Passivation may be promoted by several sources such as impurities (inorganic and organic) in the electrolyte giving precipitation on the anode surface of insoluble $SrSO_4$, α-MnO_2 or β-PbO_2, according to Martelli et al. [22], who concluded that the only possible source of passivation, internal to the coating, was a loss of catalytic sites or conductivity. In addition, phosphates or chromates in the electrolyte can react preferentially with the Ta component [22]. Oxidation and dissolution of noble metal oxides are possible when high potentials are reached by the electrode [22].

Krysa et al. [29] observed that the increase in the oxygen overpotential and reduction in the electrode capacity during accelerated life tests, were in accord with the Ir dissolution, and could be divided into three periods. The three periods were described by:

- First period: A slight increase in oxygen overpotential was caused by the change in the ratio Ir:Ta in the coating during dissolution of Ir.
- Second period: With the steady state Ir dissolution, which is achieved at the end of the first period; the oxygen overpotential was almost constant.
- In the third period, an increase in the Ir dissolution rate was typical and it was connected with rapid increase in the oxygen overpotential.

2.2 Manganese dioxide

2.2.1 Properties of manganese dioxide

Manganese is the most abundant of the heavy metals in the earth's crust apart from iron [36]. The steel industry is the main consumer of manganese (90 % of the total production), the remainder is shared between alloys, chemicals and battery industries [37]. Manganese oxides have many different applications because of the several oxidation states of manganese, which exhibit oxidation states of +1, +2, +3, +4, +5, +6 and +7 in its compounds [36].

Manganese dioxide, MnO_2, exhibits six different polymorphic modifications, depending on the preparation procedure. The six modifications are; $\alpha-$, $\beta-$, $\gamma-$, $\delta-$, $\varepsilon-$ and ϱ-MnO_2 [38]. Only the β form is stoichiometric and tetragonal with rutile structure (a = 4.4 Å, c = 2.87 Å) [36, 37, 38]. The coordination number of manganese in MnO_2 is six with respect to oxygen [36, 39]. β-MnO_2 is found in ores under the name of pyrolysite [36]. The XRD patterns are very sharp and well defined for β-MnO_2 [37]. The upper limit of oxidation is n = 1.98 for β-MnO_2 and combined water is usually not present, which leads to almost complete absence of ion-exchange properties [37]. The true density of manganese dioxide is difficult to determine because of the porous nature of the material [37]. The reduction of β-MnO_2 proceeds in a heterogeneous phase where γ-MnOOH is the reduction product, being similar to the mineral manganite [37].

γ-MnO_2 is orthorhombic (were a = 4.52 Å, b = 9.27 Å and c = 2.86 Å [37]), non-stochiometric [38], and contains a variety of defects [40]. The non-stoichiometry occurs because OH^- ions replace a portion of the O^{2-} ions, and in that way stabilize the substitution of Mn^{3+} ions for Mn^{4+} [36, 39]. The non-stoichiometry may also be present because a fraction of the Mn^{4+} is missing, producing Mn^{4+} vacancies [39]. Each empty Mn^{4+} site is coordinated to four protons present in form of OH^- [39]. The protons associated with Mn^{3+} are mobile [39]. γ-MnO_2 may be described as $MnO_{1.9-1.96}(xH_2O)$, where x represents about 4 % combined water [37]. γ-MnO_2 is bright, hard and grey to grey black in colour [36, 40] .

The XRD patterns show relatively few lines, and some of them are very diffuse and broad [37]. γ-MnO_2 is being produced electrolytically, from 0.5-0.7 M $MnSO_4$ dissolved in 0.2-0.7 M H_2SO_4 at high temperatures (90-98°C) and current densities of 2-12 mA/cm^2 [37, 38, 41], on inert anode substrates such as Ti or graphite/carbon [40, 42].

At temperatures T = 350-400°C the transition $\gamma \rightarrow \beta$ becomes complete and dehydration of the lattice occurs [38]. Remy [36] described that MnO_2 cannot give up any oxygen without destruction of its crystal lattice. When MnO_2 is heated above 530°C in air, it starts to loose oxygen [36]. The reduction of γ-MnO_2 proceeds in a homogeneous phase down to n = 1.5, and the phase limit corresponds to α-MnOOH being similar to the mineral groutite [37].

Both β- and γ-MnO_2 exhibit semiconducting properties (n-type) [39, 43] because the electrons can pass through the lattice, by being transferred between different Mn-atoms in different states of oxidation, but at equivalent positions in the crystal lattice [44]. Both β- and γ-MnO_2 may be used as electrodes at high anodic current densities [38]. γ-MnO_2 or EMD (electrolytic manganese dioxide), is mostly used as cathode material in dry batteries [40]. Hydrated MnO_2 behaves as an amphoteric substance [36, 37] as shown in figure 2.2. In acid solutions manganese dioxide behaves as a weak acid.

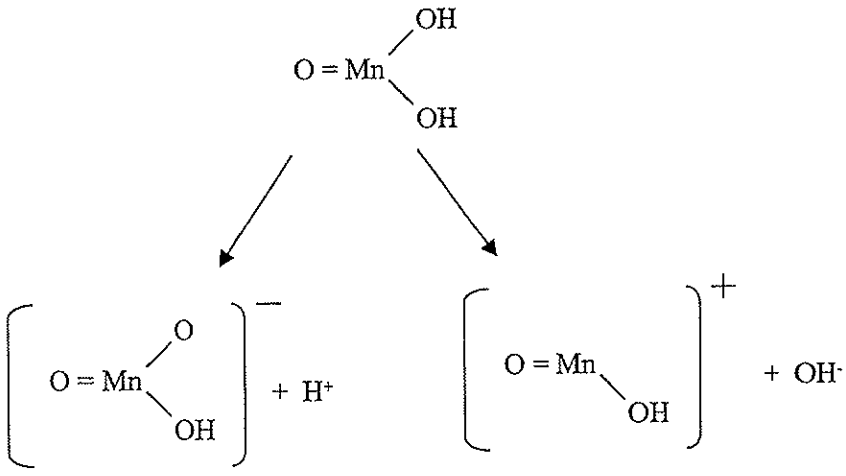

Figure 2.2: *Amphoteric behaviour of hydrated manganese dioxide [37].*

2.2.2 Deposition of manganese dioxide

In the battery literature, numerous results on the electrolytic deposition and reduction of γ-MnO_2 are presented. Several mechanisms are proposed for oxidation

of Mn^{2+} and deposition of manganese dioxide at different electrode materials in acidic solutions. As mentioned in section 2.2.1, γ-manganese dioxide is deposited from a sulphuric acid electrolyte with manganese sulphate at high temperatures. Most of the literature referred to here, describes deposition of MnO_2 of battery quality. Only a few papers treat the deposition of MnO_2 during zinc electrowinning, which is of interest in this thesis. It is assumed that parallels can be drawn between the deposition mechanisms for battery grade MnO_2, and MnO_2 deposited during zinc electrowinning, at higher acid concentrations, lower Mn^{2+} concentrations and low temperature (35°C).

Fleischmann et al. [45] found that nucleation of manganese dioxide occurred at preferred sites, and the centres formed grew in two or three dimensions. Kao et al. [42] also observed that the growth of MnO_2 proceeded three dimensionally on a platinum anode. The overall reaction for deposition of manganese dioxide is given by equation 2.2 [37]:

$$Mn^{2+} + 2H_2O \rightarrow MnO_2 + 4H^+ + 2e^- \tag{2.2}$$

It is not likely that reaction 2.2 occurs in one step. Kao et al. [42] and Welsh [46] suggested that a precursor of MnO_2 such as the Mn^{3+} ion could be the initial oxidation product (given by equation 2.3), because Mn^{4+} is not stable in the solution and is less likely to be the initial oxidation product. The nucleation of MnO_2 at a clean platinum surface was suggested to occur as described by equation 2.4 [46].

$$Mn^{2+} \rightarrow Mn^{3+} + e^- \tag{2.3}$$

$$2Mn^{3+} + 2H_2O \rightleftharpoons MnO_2 + Mn^{2+} + 4H^+ \tag{2.4}$$

The equilibrium (equation 2.4) is approached rapidly from right to left and it is quite slow from left to right [46]. As the temperature is increased, the equilibrium shifts to the right because the decomposition rate of Mn^{3+} ion is markedly influenced by the temperature [46]. Experiments carried out on a ring-disc electrode, showed a static ring current during growth of MnO_2, which indicates constant concentration of the oxidized intermediate product [42]. Diffusion of Mn^{2+} was found to be the factor controlling the growth of MnO_2 [9, 42].

Petitpierre et al. [47] have studied the oxidation of Mn^{2+} in sulphuric acid by cyclic voltammetry on a platinum working electrode, and suggested an ECE (Electrochemical-Chemical-Electrochemical) mechanism for deposition of EMD as given by equations 2.3, 2.5 and 2.6:

$$Mn^{3+} + 2H_2O \rightarrow MnOOH + 3H^+ \tag{2.5}$$

$$MnOOH \rightarrow MnO_2 + H^+ + e^- \tag{2.6}$$

Petitpierre et al. [47] also studied the effect of acid concentration, temperature and manganese concentration in the electrolyte. They found that the system was quasi reversible when $c(H_2SO_4)$> 60 wt% and only one anodic peak and one cathodic peak were observed. At $c(H_2SO_4)$= 30 wt% the electrolyte was coloured in the end of the anodic sweep and an extra cathodic peak was observed. At $c(H_2SO_4) < 30$ wt% a brown black deposit was observed at the electrode surface during the anodic peak. When the temperature was increased from 20°C to 80°C, the intensity of the anodic peak increased and the oxidation potential became more anodic. At T > 40 °C the anodic peak split into two peaks, and a compact γ-MnO_2 was observed on the anode surface.

According to experiments carried out by Welsh [46], manganese dioxide may be suspended in the bulk electrolyte instead of being deposited on the anode surface. Typical process conditions were [46]:

- Low temperature in the electrolyte (T = 20°C)
- High current density (i = 37.2 A/m^2)
- Sulphuric acid concentration 200 g/l
- Manganese sulphate concentration 20 g/l
- Intensive agitation of the electrolyte.

If the current density is raised to a high level (at least 27.9 A/m^2) so that O_2 gas is evolved on the anode, disturbance caused by the gas evolution may prevent MnO_2 from depositing on the electrode [46]. According to Welsh [46], formation of new MnO_2 nuclei occurs mainly in the immediate vicinity of the anode surface

where the Mn^{3+} concentration is highest. When the conditions of temperature, acid concentration and current density are such that the rate of decomposition of manganic ion (Mn^{3+}) to its equilibrium value is equal to or greater than its rate of formation on the anode, formation of a dense MnO_2 deposit occurs on the anode surface [46].

Rodrigues et al. [48] also studied manganese dioxide formation during zinc electrowinning in a slurry cell with agitation so that Mn^{3+} formed on the anode surface, was moved away and disproportionated in the bulk electrolyte. They used lead anodes and observed that no MnO_2 was formed on the surface of new anodes at a temperature of 34°C. As the anodes aged, MnO_2 formed more easily on the anode surface, and it deposited more prominently in corroded regions of the anodes. The effect of acid concentration on the manganese dioxide deposition was found to be as follows [48]:

- $c(H_2SO_4) < 120$ g/l $\Rightarrow$ anodes were covered with MnO_2.
- $c(H_2SO_4) = 146$ g/l $\Rightarrow$ less MnO_2 on the anode surface.
- $c(H_2SO_4) = 188$ g/l $\Rightarrow$ minor amounts of MnO_2 on the anode surface.
- $c(H_2SO_4) = 224$ g/l $\Rightarrow$ no evidence of MnO_2 deposit on the anode surface.

It was concluded that to limit MnO_2 deposition on the anode, the acid concentration should remain higher than 200 g/l and the cell temperature should not exceed 33°C [48]. High current densities decreased the current efficiency for MnO_2 deposition, because larger amounts of oxygen were evolved. MnO_2 produced during zinc electrolysis (T = 33°C) was found to be γ-MnO_2 from XRD-analysis [48]. Bodoardo et al. [49] also observed that MnO_2 deposit obtained at room temperature was γ-MnO_2, but it was poorly crystallized.

Kao et al. [40] observed a phase transformation from γ-MnO_2 to β-MnO_2 during deposition of EMD. β-MnO_2 started to form on the EMD surface and gradually propagated into the core of the particles/deposit. The formation and growth of β-MnO_2 was suggested to be assisted by Mn^{2+} ions in the electrolyte, and protons in the EMD lattice during deposition of EMD. Temperature was also found to be an important parameter for the "betafication".

Paul et al. [50] suggested that Mn^{2+} ions diffused through a porous layer of an intermediate product (MnOOH, Mn_2O_3, $Mn(OH)_4$), and became oxidized on the interface of deposited manganese dioxide and the intermediate product. They

also assumed that diffusion of protons produced in the overall reaction at the reaction interface, was much faster than diffusion of Mn^{3+} ions. When a rotating ring-disc electrode was used (the ring potential was kept at -0.1 vs. calomel to reduce possible Mn^{3+} ions formed), significant amounts of Mn^{3+} ions leaving the disc were detected at the ring, indicating that the first oxidation step includes oxidation of Mn^{2+} to Mn^{3+} [50].

According to Davies [51], the Mn^{3+} ions are very unstable at low acid concentrations and will disproportionate as described by equation 2.7. Disproportionation of Mn^{3+} is strongly affected by temperature and acid concentration in the electrolyte. The disproportionation rate increases with increasing temperature and decreasing acid concentration [48]. Mn^{3+} can be stabilized by: increasing the acid concentration, increase of Mn^{2+} concentration and complex formation [51]. The Mn^{4+} ions formed in reaction 2.7 are very unstable and will immediately react with water to produce manganese dioxide and release protons, as given by equation 2.8.

$$2Mn^{3+} \rightleftharpoons Mn^{2+} + Mn^{4+} \tag{2.7}$$

$$Mn^{4+} + 2H_2O \rightleftharpoons MnO_2 + 4H^+ \tag{2.8}$$

Jorgensen [43] observed that growth of manganese dioxide deposit occurred at the deposit/electrolyte interface. A composition gradient through the deposited material was observed, where n in MnO_n decreased from 1.95 near the interface substrate/deposit to 1.90 at the electrolyte interface [43]. Also Welsh [46] observed that MnO_2 production proceeded on the MnO_2 particle surface. A study of the effect of Fe^{2+} ions on the deposition of EMD provided results that strongly supported the concept of an intermediate layer formed between the growing MnO_2 deposit and the electrolyte [52].

Rodrigues et al. [53] have made cyclic voltammetry studies in 0.5 M $MnSO_4$ dissolved in 0.5 M H_2SO_4 at T = 80°C with a platinum working electrode. They observed that the anodic peak current for oxidizing Mn^{2+} to MnO_2 was proportional to the square root of the Mn^{2+} ion concentration and independent of the acid concentration. Rodrigues et al. [53] suggested the following mechanism for deposition of MnO_2 on a platinum electrode as given by equations 2.9 - 2.14:

$$Mn^{2+}_{bulk} \rightarrow Mn^{2+}_{surface} \tag{2.9}$$

$$Mn^{2+}_{surface} \rightarrow Mn^{3+}_{ads} + e^- \tag{2.10}$$

$$H_2O \rightarrow OH_{ads} + H^+ + e^- \tag{2.11}$$

$$2Mn^{3+}_{ads} \rightarrow Mn^{2+}_{ads} + Mn^{4+}_{ads} \tag{2.12}$$

$$Mn^{2+}_{ads} + 2OH_{ads} \rightarrow MnO_2 + 2H^+ \tag{2.13}$$

$$Mn^{4+}_{ads} + 2H_2O \rightarrow MnO_2 + 4H^+ \tag{2.14}$$

According to Rodrigues et al. [53], deposition and reduction of manganese dioxide is an irreversible process because the anodic and cathodic peak potentials are separated by several hundred millivolts and the peak potentials change with scan rate. During the anode reaction, the electrode surface turned black due to deposition of MnO_2. The peak current plotted as a function of the square root of scan rate showed linear relationship, and the oxidation reaction was suggested to be diffusion controlled. Since the anodic peak current was found to be proportional to the square root of Mn^{2+} concentration, it was suggested that the anodic deposition of MnO_2 involved a complex mechanism.

Velayutham et al. [54] investigated the effect of the Mn^{2+} concentration and the acid concentration on the deposition of MnO_2, and observed that the peak current for oxidation of Mn^{2+} increased linearly with Mn^{2+} concentration and the square root of scan rate ($c(Mn^{2+}) > 40$ mM, 8M H_2SO_4). They concluded that Mn^{2+} oxidation proceeds via a quasi reversible diffusion controlled process. An adsorption and blocking effect was noticed because neither plots of the peak current as a function of Mn^{2+} concentration, nor the square root of the scan rate passed through the origin. Furthermore the $i_p/c(Mn^{2+})$ values decreased continuously with increased Mn^{2+} concentration. The anodic peak current increased substantially with decreasing acid concentration at low scan rates (5 mV/s) because H_2O catalyses the disproportionation reaction 2.7 [54]. The apparent number of

electrons in the oxidation step increased with decreasing acid concentration (n = 1.6 in 4M H_2SO_4). Paul et al. [52] observed that the crystallinity of the MnO_2 increased with decreasing acid concentration (20-40 g/l), and the smooth deposit adhered strongly to the electrode surface.

2.2.3 Reduction of manganese dioxide

Electrochemical reduction of manganese dioxde has been widely studied in alkaline and acidic electrolytes. In the present work, it will be referred only to reduction of manganese dioxde at various concentrations of sulphuric acid. Most of the literature is taken from the dry battery literature where discharge and reduction of EMD is important.

Lee et al. [55, 56] and Maskell [57] deposited manganese dioxde on glassy carbon, platinum and gold and investigated the reduction of manganese dioxde by linear sweep voltammetry, at various concentrations of sulphuric acid. At acid concentrations below 3.75 M (0.0125-3.75 M) Lee et al. [55, 56] observed two cathodic peaks (peak 1: 0.75 V vs. MSE and peak 2: -0.2 V vs. MSE) while at concentrations higher than 3.75 M, three reduction peaks were observed (peak 3 between peaks 1 and 2 at 0.1 V vs. MSE) [57]. It was suggested that peaks 1 and 2 could be explained by a reduction reaction given by equation 2.15. In addition to reaction 2.15, a chemical equilibrium given by equation 2.16 was reported in acidic solutions [55].

$$MnO_2 + H^+ + e^- \rightarrow MnOOH \tag{2.15}$$

$$MnO_2 + Mn^{2+} + 2H_2O \rightarrow 2MnOOH + 2H^+ \tag{2.16}$$

The overall reduction reaction was given by equation 2.17 [55].

$$MnO_2 + 4H^+ + 2e^- \rightarrow Mn^{2+} + 2H_2O \tag{2.17}$$

Peak 1 was found to be independent of the electrode material and electrode rotation, and it was suggested that the first reduction step (peak 1) occurred at the deposit/electrolyte interface. Formation of a poorly conducting layer caused

a sharp reduction in current after peak 1. Scanning Electron Microscope (SEM) images of the deposit taken before and after the reduction peak 1, showed that sharp dendritic features were absent after the reduction. The bulk density was observed to be greatly reduced (25% of the original value), and it was suggested that direct reduction to Mn^{2+} was unlikely to be the primary reduction reaction. With increasing equilibrium time, Lee et al. [55] observed that the charge needed in the first reducing peak decreased. XRD-analysis of the deposit after reduction peak 1 showed still the presence of γ-MnO_2, and no substantial changes in crystallite size were observed. Peak 1 shifted to more negative potentials with decreasing acid concentrations (0.0125-3.75), because lower acid concentrations may induce higher MnOOH activity according to equation 2.16 [55].

While peak 1 was found to be independent of electrode material, peak 2 was markedly influenced by the choice of electrode material [55]. The reduction process during peak 2 was suggested to occur at the substrate/deposit interface, by formation of a Schottky-type barrier at the interface substrate-semiconductor (MnO_2 deposit) between peaks 1 and 2. Like peak 1, peak 2 was unaffected by electrode rotation, suggesting that species in the solution were not involved in the reduction process [57].

At high acid concentrations (3.75-7.5 M) a third reduction peak was observed by Lee et al. [56] between peaks 1 and 2 at a potential of 0.1 V vs. MSE. The mechanism of the third reduction peak may be explained by equations 2.18 and 2.19. The charge-transfer reaction occurs principally on the substrate [56]. Red colour was discernible in the solution immediately adjacent to the electrode. When the acid concentration was increased, peak 3 shifted to more positive values and led to the disappearance of peak 2.

$$\frac{1}{2}\,MnO_2 + \frac{1}{2}\,Mn^{2+} + 2\,H^+ \rightarrow Mn^{3+} + H_2O \tag{2.18}$$

$$Mn^{3+} + e^- \rightarrow Mn^{2+} \tag{2.19}$$

Formation of Mn^{3+} may also occur as described by equation 2.20 [56]:

$$MnOOH + 3\,H^+ \rightarrow Mn^{3+} + 2\,H_2O \tag{2.20}$$

Petitpierre et al. [47] also observed three cathodic peaks (on a Pt electrode)

at temperatures above 60°C, where peak 1 was observed at 740 mV, peak 2 at 525 mV and peak 3 at 340 mV vs. MSE. Petitpierre et al. [47] described the first reduction peak as reduction of Mn^{3+} near the electrode surface as given by equation 2.19, because at low temperatures (20°C) no MnO_2 was formed, but the first cathodic peak was observed. The second and third cathodic peaks had merged and the reduction reactions were given by equations 2.15 and 2.18 as described by Lee et al. [55].

Rodrigues et al. [53] observed two cathodic peaks (0.9 and 0.375 V vs. SCE) at high temperature (80°C) in 0.5 M $MnSO_4$, 0.4 M H_2SO_4 on a Pt electrode, and suggested the following mechanism, given by equations 2.21 and 2.22:

$$MnO_2 + H^+ + e^- \rightarrow MnOOH \tag{2.21}$$

$$MnOOH + 3\ H^+ + e^- \rightarrow Mn^{2+} + 2H_2O \tag{2.22}$$

The cathodic peak 1 remained the same for all holding times of the potential, and it was suggested that the appearance of the first reduction peak was not due to reduction of intermediate species as described by Petitpierre et al. [47] (eq. 2.19) but reduction of MnO_2. Some black deposit was found on the electrode surface after peak 1. It was also observed that the reduction charge was less than the oxidation charge for all scan rates [53].

Bodoardo et al. [49] investigated deposition and reduction of manganese dioxide on a Pt electrode by cyclic voltammetry with varying pH. Two cathodic peaks were observed at room temperature (T = 25°C) at 650 and 0 mV vs. MSE. It was suggested that during the first reduction peak a passivating layer (MnOOH) was formed on the MnO_2 surface. The second reduction peak occurred due to cracks in the passive layer, because the deposit was formed under non-stationary conditions. The reduction mechanism for the second reduction peak was suggested to be the same as for peak 1 [49]. The anodic area corresponded very well to the sum of the areas of the cathodic peaks, which indicated that all the deposited dioxide was reduced during the cathodic scan [49].

When the temperature was increased to 90°C, the second reduction peak disappeared and the deposit was not completely reduced (only 30 % of the deposited material was reduced) [49]. According to Bodoardo et al. [49] the disproportionation reaction 2.23 is important in the reduction of MnO_2, and it depends both on the pH of the solution and the Mn^{2+} concentration. Low pH and high Mn^{2+}

concentration caused rapid formation of the passive layer. When reduction of MnO_2 was carried out in an electrolyte containing 0.5 M Mn^{2+}, the intensity of the first cathodic peak decreased. Bodoardo et al. [49] found that MnO_2 produced by the disproportionation reaction given by equation 2.23, was scarcely reducible compared to electrochemically deposited manganese dioxde.

$$2\ MnOOH + 2\ H^+ \rightleftharpoons MnO_2 + Mn^{2+} + 2\ H_2O \tag{2.23}$$

According to Ruetschi [39], who presented a cation-vacancy model for MnO_2, γ-MnO_2 is highly reactive and may undergo electrochemical reduction at high rates. Reduction of γ-MnO_2 may involve introduction of protons into the crystal lattice and proceed as given by equation 2.24, where aq and c designate aqueous solution and crystalline phase respectively.

$$Mn^{4+}(c)\ +\ H^+(aq) + O^{2-}(c)\ +\ e^-\ \rightarrow\ Mn^{3+}(c)\ + OH^-(c) \tag{2.24}$$

In a review by Kordesch [37] it is concluded that during reduction of MnO_2, electron absorption occurs in the solid phase, where Mn^{4+} is reduced to Mn^{3+}, inducing an increase in volume. The electrode potential was found to be dependent of the concentration of MnOOH at the oxide/electrolyte phase boundary. The removal of MnOOH (eq. 2.23) from the electrode surface may be regarded to be the rate determining step in the overall electrochemical reaction (eq 2.17).

Cahoon [58] observed that a solution of Mn^{2+} diffused into the pores of MnO_2 particles to a considerable degree and deposited MnOOH there. Formation of MnOOH was suggested to occur on the external surface of the particle where MnO_2 and Mn^{2+} meet. Further reaction of Mn^{2+} in the solution with the unreacted core of MnO_2 particles, was thought to occur by diffusion of Mn^{2+} through the coating of MnOOH already formed on the external surface. The MnOOH particles were larger in diameter compared to the electrolytic MnO_2.

According to Voshburgh [44], electrons are available anywhere within the MnO_2 deposit. The reduction reaction may take place where the protons and electrons meet. The meeting place for the first reduction of MnO_2 was suggested to be the MnO_2 exposed to the solution [44]. The first reduction step was suggested to be reduction of MnO_2 to MnOOH as given by equation 2.15. During the discharge, protons may penetrate the oxide layer and meet the electrons in the interior. Mn^{3+} is the first reduction product of Mn^{4+} because simultaneous transfer of two electrons to the Mn^{4+} ion is highly improbable. When enough MnOOH had

accumulated on the surface, it was further reduced according to reaction 2.25. At pH 5 MnOOH may react further to produce Mn^{2+} as given by equation 2.26 [44].

$$MnOOH + H^+ + e^- \rightarrow Mn(OH)_2 \tag{2.25}$$

$$2MnOOH + 2H^+ \rightarrow MnO_2 + Mn^{2+} + 2H_2O \tag{2.26}$$

Chapter 3

Theory

3.1 Electron transfer

Usually in electrochemical processes, electron transfer occurs at the interface electrode surface/electrolyte. A simple reversible electron transfer is given by equation 3.1:

$$O + ne^- \rightleftharpoons R \tag{3.1}$$

The reversible potential for reaction 3.1 is described by Nernst equation:

$$E^{rev} = E^\circ - \frac{RT}{nF} ln \frac{a_R}{a_O} \tag{3.2}$$

where E^{rev} is the reversible potential, E° is the standard potential, R is the gas constant, T is the temperature in Kelvin, n is the number of electrons transferred, F is the Faraday constant, a_R and a_O are the activities of R and O respectively.

At the reversible potential, E^{rev}, the sum of the anodic and cathodic current densities is zero and the magnitude of the anodic and cathodic partial current densities is equal to the exchange current density, i_o which gives:

$$| \overrightarrow{i} | = | \overleftarrow{i} | = \mathrm{i}_o \tag{3.3}$$

Non-equilibrium is usually the reality for most electrochemists, and the reversible potential is mostly used as a reference potential to define the overpotential, η, which represents the extra energy the reaction needs to proceed. The overpotential is defined by equation 3.4:

$$\eta = \mathrm{E} - \mathrm{E}^{rev} \tag{3.4}$$

For a charge transfer controlled reaction, the net current in the system can be expressed by the Butler-Volmer equation:

$$\mathrm{i} = \overrightarrow{i} + \overleftarrow{i} = \mathrm{i}_o[\exp\left(\frac{\alpha_a n F \eta_a}{RT}\right) - \exp\left(-\frac{\alpha_c n F \eta_c}{RT}\right)] \tag{3.5}$$

For large overpotentials, anodic or cathodic, the smaller term in equation 3.5 can be neglected, and the Tafel equations may be expressed by equations 3.6 and 3.7 derived from equation 3.5 for anodic and cathodic overpotentials respectively:

$$\eta_a = -\frac{2.3RT}{\alpha_a n F}\log \mathrm{i}_o + \frac{2.3RT}{\alpha_a n F}\log|\mathrm{i}| \tag{3.6}$$

$$\eta_c = \frac{2.3RT}{\alpha_c n F}\log \mathrm{i}_o - \frac{2.3RT}{\alpha_c n F}\log|\mathrm{i}| \tag{3.7}$$

The Tafel approximation is generally used for $|\eta| \geq 70/\mathrm{n}$ mV [59]. A more convenient form of the Tafel equation is:

$$\eta = \mathrm{a} + \mathrm{b} \cdot \log|\mathrm{i}| \tag{3.8}$$

3.2 Mass transfer

In electrochemical systems, three types of mass transfer may be present: diffusion, migration and convection. Usually electrochemical experiments are carried out in unstirred solutions or by using forced convection. Diffusion is movement of a species down a concentration gradient, whenever there is a potential change at the electrode surface [59]. The concentration profile of a reduced species R, which is oxidized on the electrode surface, is shown in figure 3.1 as a function of the distance from the electrode surface and time.

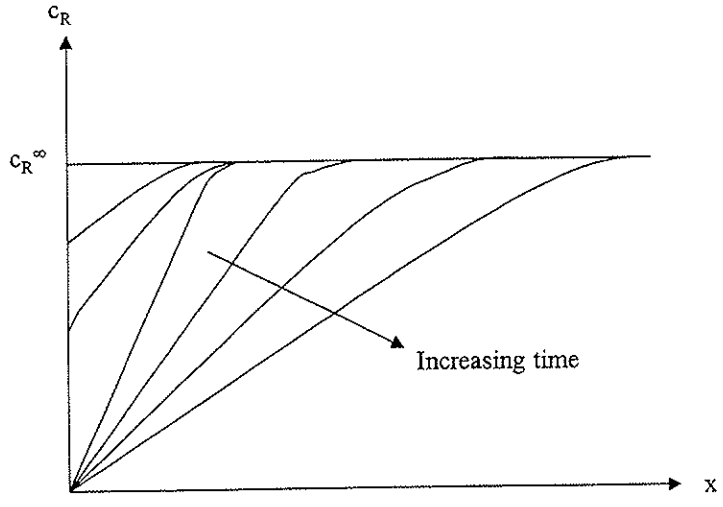

Figure 3.1: *Concentration gradients of a species R in the Nernst diffusion layer as a function of the distance from the electrode surface during cyclic voltammetry.* $c_R{}^\infty$ *is the bulk concentration of species R and x is the distance from the electrode surface.*

Linear diffusion normal to a plain electrode, may be characterized by Fick's first law, where the flux of a species (R) through a plane parallel to the electrode surface is given by equation 3.9, where J is the flux, D_R is the diffusion coefficient, and $\frac{\partial c_R}{\partial x}$ is the concentration gradient of species R.

$$J = -D_R \frac{\partial c_R}{\partial x} \tag{3.9}$$

At the electrode surface (x = 0), the current of the electrochemical reaction may

be related to Fick's first law as described by equation 3.10.

$$\frac{i}{nF} = -D_R \left(\frac{\partial c_R}{\partial x}\right)_{x=0} \tag{3.10}$$

3.3 Cyclic voltammetry

Potential sweep techniques and cyclic voltammetry (CV) are widely applied in mechanistic investigations in electrochemistry. Linear sweep voltammetry (LSV) is the simplest technique, where the electrode potential is swept between two limiting potentials E_1 and E_2 at a scan rate, v, often denoted in millivolts per second. The relationship between potential and scan rate is given by equation 3.11.

$$E = E_1 \pm vt \quad \text{for} \quad 0 < t < \lambda \tag{3.11}$$

Cyclic voltammetry is more widely applied than linear voltammetry, and the scan is reversed back to the starting potential so that reverse reactions may be detected. In both sweep techniques, the cell current is recorded as a function of the applied potential. The potential-time wave and current-potential curve for sweep measurements are shown in figures 3.2 and 3.3 respectively.

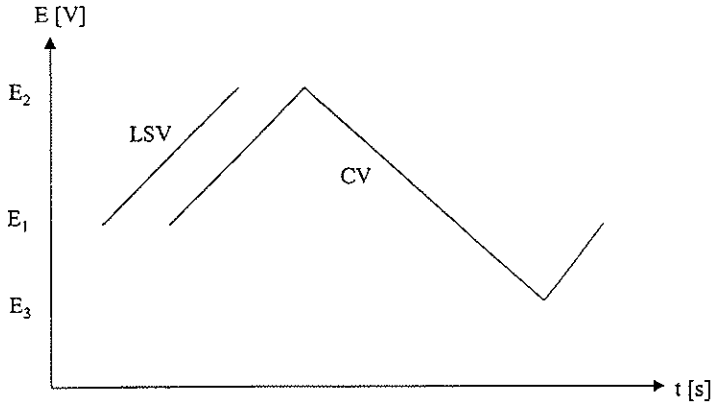

Figure 3.2: *Potential-time profiles for linear and cyclic voltammetry.*

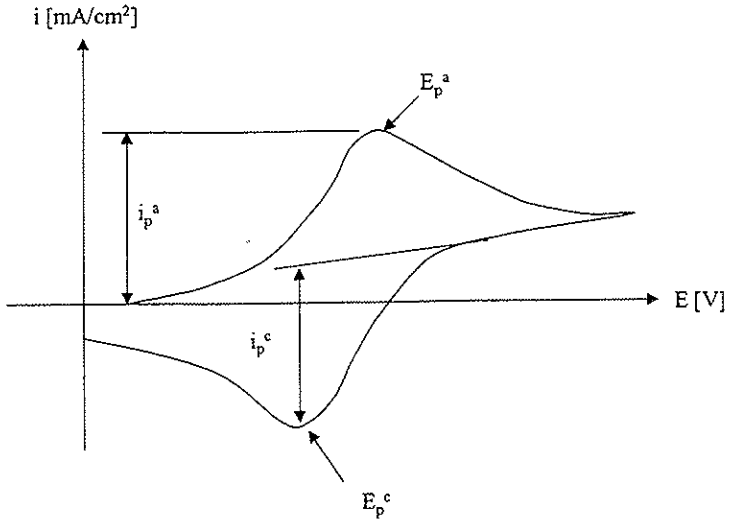

Figure 3.3: *Cyclic voltammogram for a reversible process, $O + ne^- = R$ (only R is initially present), where both reactant and product are soluble in the electrolyte. Peak potentials (E_p^a, E_p^c) and peak current densities (i_p^a, i_p^c) are indicated on the figure.*

A number of diagnostic test for different reaction mechanisms exist for electrochemical reactions as [59];

- reversible reaction
- irreversible reaction
- quasi reversible reaction
- coupled mechanism, chemical-electrohemical (ce)
- coupled mechanism, electrochemical-chemical (ec)
- coupled mechanism, electrochemical-chemical-electrochemical (ece)
- catalytic mechanism and coupled chemical reactions.

Only a few of these diagnostic tests will be presented in the present work.

3.3.1 Reversible reactions

A simple reversible reaction is given by equation 3.12, where only R is initially present in the electrolyte.

$$O + ne^- \rightleftharpoons R \tag{3.12}$$

At very low scan rates, the steady state current is recorded. When the scan rate is increased, an anodic peak with increasing intensity is observed [59]. This occurs because of larger concentration gradients in the Nernst diffusion layer as shown in figure 3.1. When the concentration of R at the electrode surface is zero, the concentration gradient starts to decrease because of the relaxation. The concentration gradient will increase with increasing scan rate, leading to an increase in anodic current according to equation 3.10.

The oxidized product, being soluble in the electrolyte, near the electrode surface will be reduced in the reversed scan when E^{rev} is reached. Some of the oxidized product may diffuse into the bulk electrolyte, giving a lower peak current for the reverse peak. For planar diffusion to the electrode surface, the relationship between peak current, concentration, diffusion coefficient and scan rate is given by the Randles-Sevčik equation:

$$i_p = -0.4463nF\left(\frac{nF}{RT}\right)^{1/2} c_R^{\infty} D^{1/2} v^{1/2} \tag{3.13}$$

Table 3.1: *Diagnostic tests for cyclic voltammograms of reversible reactions at 25° C with soluble product [59].*

1.	$\Delta E_p = \lvert E_p^a - E_p^c \rvert = 59/n$ mV
2.	$\lvert E_p - E_{p/2} \rvert = 59/n$ mV
3.	$\lvert i_p^a / i_p^c \rvert = 1$
4.	$i_p \propto v^{1/2}$
5.	E_p is independent of v
6.	at potentials beyond E_p, $i \propto t^{-1/2}$

For reversible reactions the electron transfer process is assumed to be significantly faster than the rate of mass transfer. Some diagnostic tests for reversible reactions

are given in table 3.1.

3.3.2 Irreversible and quasi-reversible reactions

For totally irreversible systems an increase in peak separation is observed when the scan rate is increased. This is because mass transfer becomes comparable to the rate of electron transfer at high scan rates. Some diagnostic tests for totally irreversible reactions are given in table 3.2.

Table 3.2: *Diagnostic tests for cyclic voltammograms of totally irreversible reactions at 25° C [59].*

1.	no reverse peak
2.	$i_p^a \propto v^{1/2}$
3.	E_p^a shifts $\frac{30}{\alpha_c n_\alpha}$ for each decade increase in v
4.	$\lvert E_p - E_{p/2} \rvert = \frac{48}{\alpha_c n_\alpha}$

Some processes are reversible at low scan rates but become irreversible at high scan rates after passing through a quasi-reversible region at intermediate scan rate values. This phenomenon occurs when the relative rate of electron transfer with respect to the rate of mass transport, is insufficient to maintain Nernstian equilibrium at the electrode surface. Diagnostic tests for quasi-reversible reactions are given in table 3.3.

Table 3.3: *Diagnostic tests for cyclic voltammograms of quasi-reversible reactions at 25° C [59].*

1.	$\lvert i_p \rvert$ increases with $v^{1/2}$ but not proportional to it
2.	$\lvert i_p^c / i_p^a \rvert = 1$ provided $\alpha_a = \alpha_c = 0.5$
3.	ΔE_p is greater than $\frac{59}{n}$ mV and increases with increasing v
4.	E_p^a shifts positively with increasing v

3.3.3 The ECE mechanism

An ECE mechanism includes three reaction steps, where the first step is electrochemical, the second is chemical and the third is electrochemical. Reactions 3.14,

3.15 and 3.16 describe an ECE mechanism where only R is initially present in the electrolyte.

$$O'' + ne^- \rightleftharpoons R \tag{3.14}$$

$$O'' \xrightarrow{k} O' \tag{3.15}$$

$$O + ne^- \rightleftharpoons O' \tag{3.16}$$

The ECE mechanism is common in multi-electron transfer processes (electro-organic synthesis) where it is assumed that the electron transfer is reversible and the chemical reaction is irreversible. Table 3.4 shows some diagnostic tests for ECE reactions.

Table 3.4: *Diagnostic tests for cyclic voltammograms of ECE reactions at 25° C [59].*

1.	$\lvert i_p^a\rvert/v^{1/2}$ varies with scan rate but may reach limiting values at high and low scan rates $\lvert i_p^a\rvert/v^{1/2}$ (low v) > $\lvert i_p^a\rvert/v^{1/2}$ (high v)
2.	$\lvert i_p^c/i_p^a\rvert$ increases with scan rate and approaches unity at high scan rates

3.3.4 Electrocrystallization and deposition processes

In electrochemical systems, metals and other phases can deposit from the solution onto the electrode surface via electrochemical steps or coupled mechanisms (electrochemical and chemical steps). The distinct steps in the electrocrystallization process are given by [59]:

1. diffusion of ions in solution to the electrode surface
2. electron transfer
3. partial or complete loss of the solvation sheath, resulting in the formation of ad-atoms

4. surface diffusion of ad-atoms
5. clustering of ad-atoms to form critical nuclei on a perfectly smooth surface or in a foreign substrate
6. incorporation of ad-atoms at lattice sites
7. development of crystallographic and morphological characteristics of the deposit.

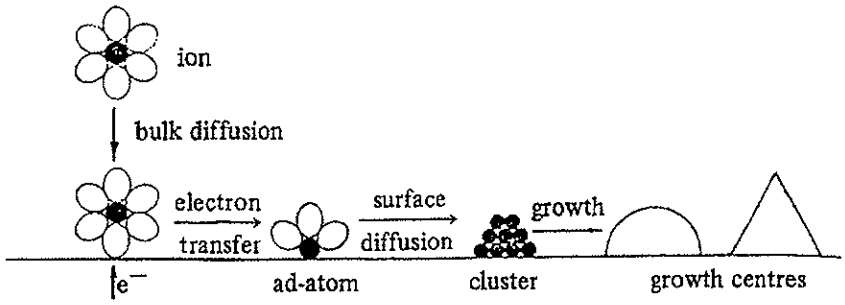

Figure 3.4: *Some of the steps involved in the electrocrystallization of a metal on a substrate of a different material [59].*

Figure 3.4 shows the steps involved in the electrocrysatallisation of a metal on a substrate [59]. A cyclic voltammogram for a deposition reaction is shown in figure 3.5. The leading edge in the forward scan is slightly steeper than for a process involving soluble species [59]. The reverse scan differs substantially from systems with soluble species. The current trace crosses the forward scan and the reverse peak is sharp. The cross-over phenomenon occurs because of the nucleation overpotential in the forward scan [59], or because of an increase in the electrode surface area. The area under the reverse peak corresponds to the amount of material deposited during the forward scan [59].

3.3.5 Passivation

Passivation films on metals protect the metal surfaces from further corrosion. Linear voltammetry measurents can be used to see when or if a passive film is

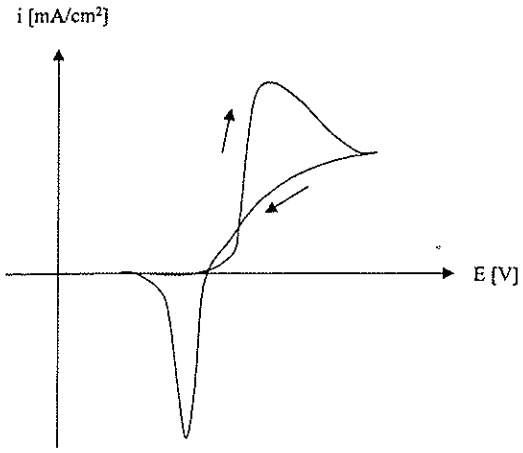

Figure 3.5: *A cyclic voltammogram for a deposition reaction exhibiting nucleation overpotential or change in the electrode surface area.*

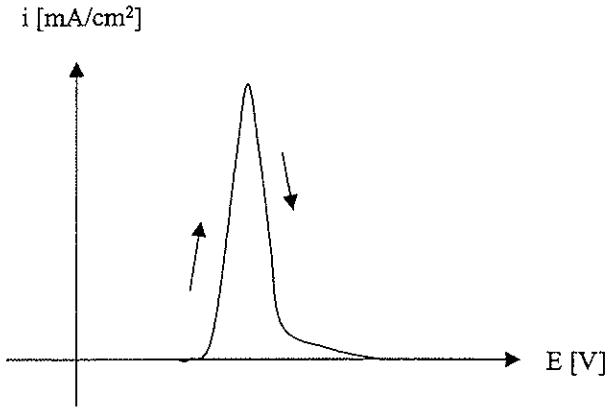

Figure 3.6: *Linear voltammetry on a metal exhibiting passivation.*

formed on the metal surface in various solutions. Cyclic voltammetry can be used to find if the passivating film may be reduced in the reverse scan or not. Figure 3.6 shows the formation of a passive film on a metal surface. The current density rises as the passive film grows across the surface, and falls rapidly as the surface is passivated [59].

3.4 Electrocatalysis

Catalysts are often used in chemical industry to increase the rate of a chemical reaction, which does not proceed by itself at a significant rate. The principal idea with a catalyst is that it is not consumed during the reaction, but is renewed when the reaction is completed. The catalyst may be homogeneous or heterogeneous.

The term electrocatalysis is applied to systems where the oxidation or reduction requires band formation, or at least a strong interaction to the reactant, intermediates, or the product with the electrode surface [59]. In electrochemical systems, a catalyst which constitutes the electrode material itself, is used to decrease the overpotential of a desired electrode reaction. The activity of a good electrocatalyst is expressed by the Tafel slope, and the i_o value measures the intrinsic ability of the solid surface to catalyze the reaction at $\eta = 0$ [19]. A good electrocatalyst has low overpotential (low Tafel slope) and high exchange current density for an electrode reaction, but long term stability is more important than low overpotential in practical/industrial applications [25].

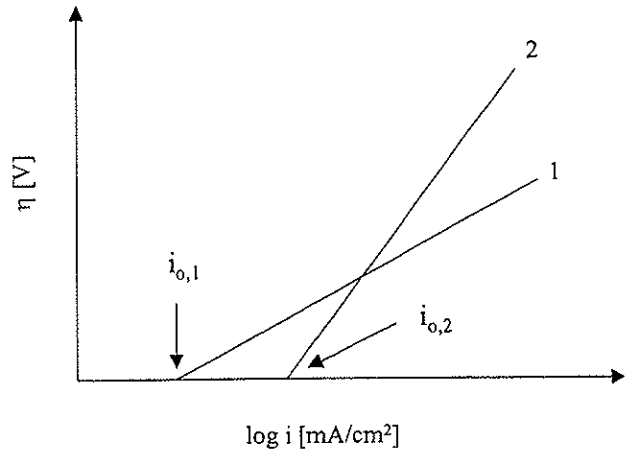

Figure 3.7: *Sketch of the related importance of the exchange current density, $i_{o,1}$ and $i_{o,2}$, and Tafel slopes showing the relative electrocatalyic properties of two electrodes.*

The relationship between overpotential and current density, is given by the Tafel equations 3.6 and 3.7 for anodic and cathodic reactions respectively. Figure 3.7 presents a sketch of the overpotential as a function of the logarithm of the current density, showing that the highest exchange current density value does not

necessarily give the best electrocatalytic electrode material. The best electrocatalyst may be found by comparing the overpotential as a function of time, when constant current density is applied.

There are many different electrocatalysts in use in electrolysis processes today, but DSA® (Ti/RuO_2) in the chlor-alkali industry is the best known. Oxygen evolving electrodes will be described in more detail in section 3.5. When investigating different electrode materials, i - E characteristics for the various materials are compared [59]. The steady state current density is measured as a function of potential at very low scan rates, such that mass transfer is not the rate determining step. Some characteristics for electrocatalysts are [59]:

- The exchange current density, i_o, varies with the electrode material.
- The Tafel slope is commonly not $b = \frac{\alpha nF}{2.3RT}$ but values of $\frac{b}{2}, \frac{b}{3} and \frac{b}{4}$ are common.
- The Tafel slope may depend on the electrode material, which indicates a change in reaction mechanism.
- The temperature dependence of the Tafel slope may not be straightforward.

In an electrocatalytic process, the measured current density depends on both the catalytic activity of the surface and the real surface area, because the rate determining step is a surface reaction. For a mass transport controlled reaction the current density is independent of the surface roughness if this is small compared to the diffusion layer thickness ($\sim 10^{-2}$ cm) [59].

3.4.1 The oxygen evolution reaction in acid solutions

Mechanisms for oxygen evolution are widely reviewed. Trasatti [25] has collected the following mechanisms for oxygen evolution in acid solutions (S is the active site which may be a metal oxide):

- Electrochemical oxide path (Bockris):
  a) $S + H_2O \rightarrow S\text{-}OH + H^+ + e^-$
  b) $S\text{-}OH \rightarrow S\text{-}O + H^+ + e^-$
  c) $2S\text{-}O \rightarrow 2S + O_2$

- Oxide path (Bockris):
  a) $S + H_2O \rightarrow S\text{-}OH + H^+ + e^-$
  b) $2S\text{-}OH \rightarrow S\text{-}O + S + H_2O$
  c) $2S\text{-}O \rightarrow 2S + O_2$

- Krasil'schihikov path:
  a) $S + H_2O \rightarrow S\text{-}OH + H^+ + e^-$
  b) $S\text{-}OH \rightarrow S\text{-}O^- + H^+$
  c) $S\text{-}O^- \rightarrow S\text{-}O + e^-$
  d) $2S\text{-}O \rightarrow 2S + O_2$

An oxide with a high catalytic activity for the oxygen evolution reaction should, besides having acceptable electronic conductivity, show a high affinity for absorbed OH intermediates [35]. For an oxide layer with a low surface affinity for oxygen intermediates, the first reaction step in the Krasil'schihikov path is rate determining (giving a high Tafel slope) [35]. If equilibrium coverage of OH intermediates is achieved due to a fast rate of OH electrosorption on the surface of the oxide, the second step may become rate determining, resulting in a lower Tafel slope, which is typical for good electrocatalysts [35].

The observed Tafel slope for oxygen evolution varies between 0.04 V and 0.12 V, but 0.03 V has also been reported [25]. Break in the Tafel line when going from low to high overpotentials may occur because of the following reasons [25]:

1) Change in reaction mechanism.
2) Transition from $\Theta_B \simeq 0$ to $\Theta_B \simeq 1$ takes place while the mechanism is unchanged. Θ_B is the fraction of catalyst surface covered by the intermediate.
3) Change in the rate determining step of the same mechanism.

Experimental kinetic parameters for the oxygen evolution reaction on various anode materials are given in table 3.5 [25].

Table 3.5: *Tafel slopes for various anode materials in acid solution [25].*

Electrode material	Solution	T [°C]	b [V]
β-MnO_2	0.5M H_2SO_4	30	0.11
Ir	1M H_2SO_4	25	0.052-0.112
IrO_x	0.5M H_2SO_4	25	0.05
Ti-IrO_2	0.5M H_2SO_4	30	0.056
PbO_2	2.2M H_2SO_4	30	0.051 (α)-0.121 (β)

3.5 Properties of inert anodes

Lead and lead alloys (Ag/Sb) are widely used for oxygen evolution in acid solutions. As mentioned in section 1.1.1, lead alloys are not dimensionally stable because they slowly dissolve in the electrolyte, leading to problems such as changes in the gap between the anode and cathode, and contamination of the product. According to Jeon et al. [60] the conventional Pb or Pb alloy anodes can easily be replaced with catalytic electrodes, which show excellent corrosion resistance, no contamination of the electrolyte and lower energy consumption. Jeon et al. [60] observed that the overpotential was reduced by 30-40% in the zinc electrowinning process when catalytic anodes were used instead of lead alloy anodes.

DSA®-type oxygen-evolving anodes can be operated in corrosive electrolytes at high current densities [27]. The good electrocatalytic activity of the DSA®-type oxygen-evolving anodes, must be coupled with long-term stability with no significant loss of material and/or poisoning [61]. The oxides used in DSA®-coatings are expensive materials (especially IrO_2), and their price is rather similar to the price of platinum when taking into account the required catalyst loading in each case [61].

In general, DSA®-type electrodes are characterized by a thin active coating of a few microns, deposited on a base metal (Ti, Zr, Ta or Nb). The coating enables the electric charge transport between the base metal and the electrode/electrolyte interface, and is chosen for its high chemical and electrochemical stability, and its ability to catalyse the desired electrochemical reaction [14]. The coating is usually a binary mixture of oxides, one which is conductive and the other non-conductive: the general form is Me/AO_x-BO_y where Me is the base metal, AO_x

is the conducting oxide and BO_y the non-conducting oxide of the coating [14].

Some metal oxides exhibit metallic conductivity because of non-stoichiometry or partly filled d-bands. Figure 3.8 shows the overpotential as a function of the logarithm of the current density (log i) for oxygen evolution on various metal oxides from acid solution. As can be seen from figure 3.8, RuO_2 and IrO_2 are the best electrocatalysts for oxygen evolution.

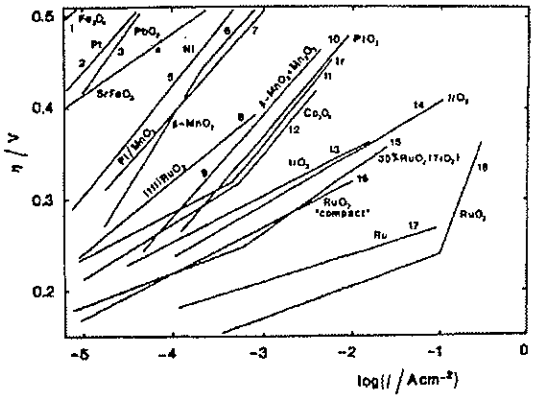

Figure 3.8: *The overpotential as a function of log(i) for various oxygen-evolving anode materials [25].*

3.5.1 The Ti/IrO_2-Ta_2O_5 electrode

As described in section 2.1, Ti/IrO_2 - Ta_2O_5 is the best anode for oxygen evolution in acid solutions. IrO_2 is a relatively good electrocatalyst, but it is poorer than RuO_2 because of higher Tafel slope and overpotential for oxygen evolution [25]. IrO_2 is more stable than RuO_2 during oxygen evolution, as mentioned earlier (section 2.1). Figure 3.9 presents an outline of the preparation procedure of Ti/IrO_2 - Ta_2O_5 electrodes as described by De Nora et al. [62].

Vercesi et al. [23] studied the influence of the base metal on the coating morphology and electrocatalytic properties. From the calculated activation energies, the valve metals and their alloys can be classified in the following sequence as regards oxygen affinity [27].

Ti < Zr < Ta < Nb < Ta-40% Nb

The valve metals have a critical temperature in air. Above this temperature,

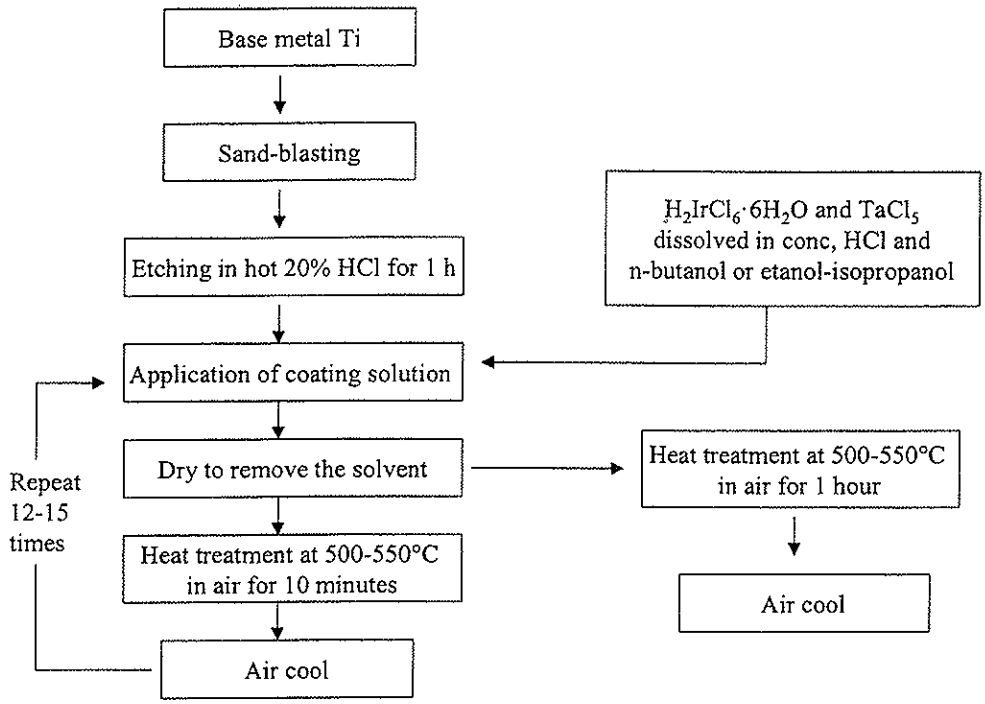

Figure 3.9: *Outline of the preparation procedure of Ti/IrO_2 - Ta_2O_5 electrode [23, 26, 62].*

the oxidation rate of the valve metals increases considerably [27]. During the preparation of the coating on the base metal, the sample was heated at high temperatures (500-550°C) in the presence of oxygen. Under these conditions, surface oxidation of the base metal (M) occurs with the formation of an oxide (MO_x) as given by equation 3.17:

$$M + xO \rightarrow MO_x \tag{3.17}$$

The build-up of an oxide layer between the coating and the base metal can have deleterious effects, such as exfoliation of the coating, or formation of an insulating layer between the base metal and the coating. The temperature required for the coating deposition should, therefore, never be above the critical temperature for the base metal [27]. The critical oxidation temperature for Ta is 350°C while it is 550°C for Ti [23]. The IrO_2 - Ta_2O_5 coatings are prepared by heating the

coating solution at 500-550°C, and that is why Ti is used instead of Ta.

The increase in surface roughness of the base metal during sand-blasting and etching, leads to higher service life and lower steady state dissolution rate of the coating [29]. Vercesi et al. [23] observed that the quality of the base pretreatment, was even more important for the coating morphology than the nature of the base metal itself. To increase the surface roughness, the Ti is sand-blasted and etched in concentrated HCl for 1 hour. The reaction between HCl and Ti metal is described by equations 3.18, 3.19 and 3.20 [27]. The surface of Ti after pretreatment in HCl has an appropriate degree of roughness, caused by pitting corrosion. If Ti is pretreated in oxalic acid, the surface appears to be a little smoother compared with HCl etching, but it is sufficiently rough for coating adhesion [27].

$$TiO_2 + 4HCl \rightarrow TiCl_4 + 2H_2O \tag{3.18}$$

$$Ti + 3HCl \rightarrow TiCl_3 + \frac{3}{2}H_2 \qquad \text{main reaction} \tag{3.19}$$

$$Ti + \frac{x}{2}H_2 \rightarrow TiH_x \tag{3.20}$$

The coating solution can be prepared by dissolving appropriate amounts of $H_2IrCl_6 \cdot 6H_2O$ and $TaCl_5$ in an ethanol-isopropanol mixture or n-butanol in HCl, to form the painting solution [23, 26]. The solution is applied by brush or spray onto the pretreated base metal in 12-15 sequential coatings. The brush is used to minimize the loss of active material [14]. The decomposition of the coating agents into the corresponding oxides occurs above 500°C (with high yields, >94%, [63]) according to the following equations (3.21, 3.22 and 3.23):

$$H_2IrCl_6 \cdot 6H_2O \xrightarrow{150°C} IrCl_4 + 6H_2O + 2HCl \tag{3.21}$$

$$IrCl_4 + 2H_2O \xrightarrow{500°C} IrO_2 + 4HCl \tag{3.22}$$

$$2TaCl_5 + 5H_2O \xrightarrow{500°C} Ta_2O_5 + 10HCl \tag{3.23}$$

In the Ti/IrO_2 - Ta_2O_5 anode, IrO_2 represents the active sites where the oxygen evolution takes place, and Ta_2O_5 is the chemical stabilizer for IrO_2. It was observed that IrO_2 appeared as crystalline clusters on the amorphous phase of Ta_2O_5 [26]. The crystal structure of IrO_2 is tetragonal as the TiO_2 [64], while Ta_2O_5 possesses rhombic crystal structure for 700°C $\leq$ T [65]. In order to be electrochemically active, a cluster of conducting oxide must be connected to the base metal, and at the same time, it must be in contact with the electrolyte [14]. The most probable reactions in the case of IrO_2 occurring at the interface between the electrocatalyst and the electrolyte are given by equations 3.24 - 3.26 [20].

$$IrO_2 + H_2O \rightarrow IrO_3 + 2H^+ + 2e^- \tag{3.24}$$

$$IrO_3 \rightarrow IrO_2 + O_{ads} \tag{3.25}$$

$$2O_{ads} \rightarrow O_2 \tag{3.26}$$

According to De Nora et al. [62], the IrO_2-Ta_2O_5 coating is a n-type semiconductor. By addition of the doping metal oxides of Ca, Mg, Ba, Co, Fe, Ni, Cr, Mo or Mn, the conductivity may be reversed from n-type to p-type, which improves the anodic process by producing electronic holes [62]. The catalytic activity of the doped coatings was increased because a lower anode potential was observed compared to the undoped anodes [62].

3.6 Manganese dioxide

As mentioned in section 2.2.1, MnO_2 is mainly used as cathode in dry cells, but it is also used as anode for oxygen evolution although its performance is less satisfactory than that of noble metals [25]. Oxygen evolution proceeds on MnO_2 with a Tafel slope of 0.12 V in acid solution where primary discharge of H_2O is the rate determining step. The catalytic properties are maximized if β-MnO_2 is thermally treated at around 480°C where partial conversion of MnO_2 to Mn_2O_3 occurs and makes a solid redox couple. Excess Mn_2O_3 decreases the catalytic properties. Figure 3.10 shows the Pourbaix diagram for the manganese species at T = 25°C.

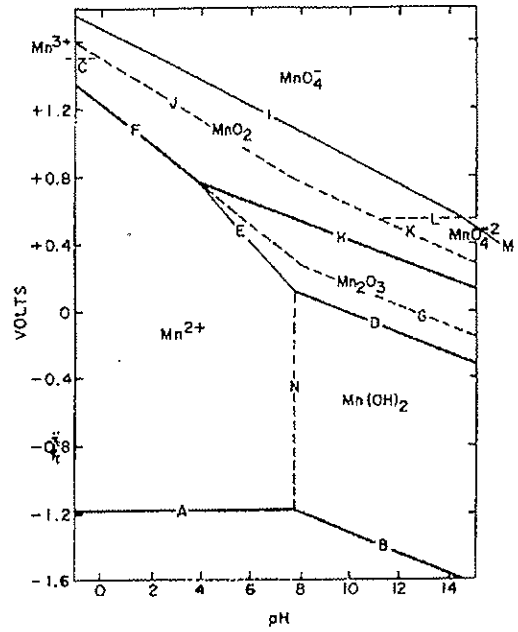

Figure 3.10: *The pH-potential diagram of the manganese system at $T = 25°C$ [66].*

3.6.1 Deposition of manganese dioxide

Deposition of MnO_2 on the anode from zinc electrolyte containing $MnSO_4$, occurs as a parasitic reaction to the oxygen evolution. The deposition mechanism was reviewed in section 2.2.2, and only a short summary will be given here. It is likely that deposition of MnO_2 from Mn^{2+} occurs as an ECE mechanism (equation 3.27, 3.28 and 3.29) as suggested by Petitpierre et al. [47].

$$Mn^{2+} \rightarrow Mn^{3+} + e^- \tag{3.27}$$

$$Mn^{3+} + 2H_2O \rightarrow MnOOH + 3H^+ \tag{3.28}$$

$$MnOOH \rightarrow MnO_2 + H^+ + e^- \tag{3.29}$$

At high oxidation potentials, Mn^{2+} may oxidize directly to permanganate (MnO_4^-) as given by equation 3.30 [7, 67].

$$Mn^{2+} + 4H_2O \rightarrow MnO_4^- + 8H^+ + 5e^- \qquad E^\circ = 1.51V_{NHE} \tag{3.30}$$

The permanganate ions, which are good oxidation agents, may react with the Mn^{2+} ions in the electrolyte, and form Mn^{4+} according to equation 3.31 [7]. The Mn^{4+} ions can hydrolyze and form dispersed MnO_2 in the bulk as described by equation 3.32.

$$2MnO_4^- + 3Mn^{2+} + 16H^+ \rightarrow 5Mn^{4+} + 8H_2O \tag{3.31}$$

$$Mn^{4+} + 2H_2O \rightleftharpoons MnO_2 + 4H^+ \tag{3.32}$$

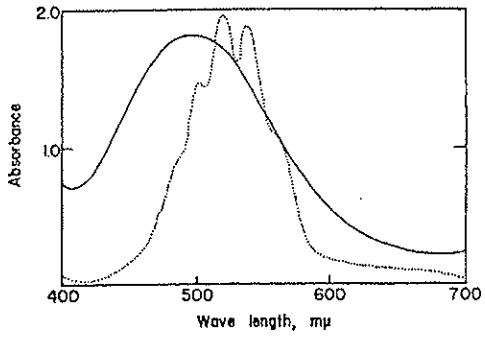

Figure 3.11: *Absorption spectra of $0.87{\cdot}10^{-3}$ M MnO_4^- in 1M H_2SO_4 (dotted curve), and Mn^{3+} in 7M H_2SO_4 (solid curve), prepared from 0.2 M $MnSO_4$ in 7M H_2SO_4 for ~97 minutes at current 24.8 A [68].*

The colour of the Mn^{3+} ions is quite similar to that of MnO_4^- ions, which is red-violet. To distinguish between the two species, an absorption spectrum of the electrolyte may be taken, and compared to the absorption spectra of the two species. Figure 3.11 shows the absorption spectra for $0.87{\cdot}10^{-3}$ M MnO_4^- in 1M H_2SO_4 and Mn^{3+} in 7M H_2SO_4. The MnO_4^- ions have two absorption peaks (525 and 550 nm), while Mn^{3+} has only one round absorption peak at ~500 nm.

3.6.2 Reduction and dissolution of manganese dioxide

Reduction of MnO_2 is believed to take place via electrochemical as well as by chemical reactions. It is suggested that the first reduction step takes place in the interior of the deposit where the electrons and protons meet forming MnOOH, which is the initial product of the cathodic reactions as described by equation 3.33 [66, 69].

$$MnO_2 + H^+ + e^- \rightarrow MnOOH \tag{3.33}$$

In acid solutions MnOOH can react with the protons to form Mn^{3+} according to reaction 3.34 [56].

$$MnOOH + 3\ H^+ \rightarrow Mn^{3+} + 2\ H_2O \tag{3.34}$$

In addition, Mn^{2+} ions in the electrolyte may attack the deposited MnO_2 as described by the chemical reaction 3.35.

$$1/2\ MnO_2 + 1/2\ Mn^{2+} + 2\ H^+ \rightarrow Mn^{3+} + H_2O \tag{3.35}$$

The Mn^{3+} ions present near the electrode surface may be reduced to Mn^{2+} as given by equation 3.36.

$$Mn^{3+} + e^- \rightarrow Mn^{2+} \tag{3.36}$$

From the literature review in section 2.2.3 and the reactions described above, it is seen that deposited MnO_2 can be reduced electrochemically. Deposition of MnO_2 is difficult to avoid if Mn^{2+} ions are present in the electrolyte. The one way to avoid deposition of MnO_2 on the anode surface, is to use strong agitation in the electrolyte, and in that way remove the Mn^{3+} from the anode surface into the bulk electrolyte, so that formation of the MnO_2 takes place in the bulk electrolyte [48].

Velayutham et al. [54] found that phosphoric acid, H_3PO_4, stabilized the Mn^{3+} ions in the electrolyte, and the anodic peak current decreased compared to electrolyte with only H_2SO_4. Small additions of H_3PO_4 to the sulphuric acid may

diminish the deposition of MnO_2 on the anode surface during oxygen evolution. One problem by adding H_3PO_4 to the electrolyte when Ti/IrO_2 - Ta_2O_5 anodes are used, is that the phosphate can react preferentially with the Ta component [22].

If the oxidation of water is replaced with oxidation of a "fuel" that is compatible with the cathodic process, a reduction of the energy consumption in the process can be achieved [60]. The use of Fe^{2+}, depolarized the anodic reaction and reduced the overvoltage by 30-40% compared to the existing zinc electrowinning process with lead alloy anodes [60]. The cell arrangement is more complex when Fe^{2+} ions are present in the electrolyte, because the anolyte and catholyte must be separated with a membrane. Fe^{2+} is a good reducing agent in acid solution and can reduce the deposited MnO_2 as described by equation 3.37 [41].

$$MnO_2 + 2Fe^{2+} + 4H^+ \rightarrow Mn^{2+} + 2Fe^{3+} + 2H_2O \tag{3.37}$$

Manganese dioxide is not attacked by cold concentrated sulphuric acid, but if it is heated to 110°C, oxygen is evolved and manganese sulphate is formed, as described by equation 3.38 [36].

$$MnO_2 + H_2SO_4(\text{conc.}) \overset{T=110°C}{\rightleftharpoons} MnSO_4 + H_2O + \frac{1}{2}O_2 \tag{3.38}$$

If concentrated HCl is added to MnO_2, chlorine is evolved upon heating as given in equations 3.39 - 3.41 [36]. Some chlorine evolution takes place in the zinc electrowinning process today, but it is in very small quantities. If HCl should be used to dissolve the deposited MnO_2 on the anodes, it should be done in a closed chamber outside the cell.

$$MnO_2 + 4HCl \rightarrow MnCl_4 + 2H_2O \tag{3.39}$$

$$MnCl_4 \rightarrow MnCl_3 + \frac{1}{2}Cl_2 \tag{3.40}$$

$$MnCl_3 \rightarrow MnCl_2 + \frac{1}{2}Cl_2 \tag{3.41}$$

Sulphur dioxide (SO_2) can be used to reduce MnO_2 in sulphuric acid solution by dissolving the gas in the electrolyte. The main reaction is formation of manganese sulphate, which is soluble in H_2SO_4, as described by equation 3.42. The main drawback with this process is that SO_2 is a very poisonous gas, and should be handled with care.

$$MnO_2 + SO_2 \rightarrow MnSO_4 \tag{3.42}$$

Hydrogen peroxide (H_2O_2) can act as a strong reducing agent in the presence of dilute acids. MnO_2 is reduced to $MnSO_4$ in the presence of H_2O_2 as described in equation 3.43 [36]. In addition, H_2O_2 may reduce Mn^{3+} ions to Mn^{2+} according to equation 3.44 [70]. Compared to the chemicals described above, H_2O_2 is easy to handle, and can be added to the electrolyte without any changes in the existing electrowinning cell. Dominguez et al. [70] removed deposited MnO_2 from the lead alloy anode during the electrowinning process, and observed that 12 kg of H_2O_2 (100%) per ton of Zn produced was required in an electrolyte with Mn^{2+} concentration of 2 g/l.

$$MnO_2 + H_2O_2 + H_2SO_4 \rightarrow MnSO_4 + 2H_2O + O_2 \tag{3.43}$$

$$Mn^{3+} + H_2O_2 \rightarrow 2Mn^{2+} + 2H^+ + O_2 \tag{3.44}$$

If deposition of MnO_2 is avoided by addition of reducing agents, accumulation of Mn^{2+} ions in the electrolyte will occur. Fussi et al. [71] described a method for removing manganese from zinc blends with high manganese contents (more than 0.5%). The manganese concentration in the electrolyte was reduced through a cold electrolytic demanganization process, prior to the standard zinc electrowinning.

Chapter 4

Experimental

The experiments in this thesis are divided into 4 major parts as follows:

- Kinetic measurements (cyclic voltammetry and linear voltammetry).
- Galvanostatic electrolysis experiments.
- Pulse (potential) experiments.
- Scanning Electron Microscopy (SEM) with element analysis.

4.1 Apparatus and chemicals

The cell used in the various experiments was the same when planar electrodes were used. An outline of the cell is shown in figure 4.1. The anode materials used in the experiments are described in section 4.2.

Some experiments were performed by using rotating cylinder electrodes. The base metal was Ti, and the electrode was prepared in the same way as the standard coating Ti/IrO_2 - Ta_2O_5 (described in section 4.2). Three electrodes were bolted onto a threaded bolt of copper, to ensure good electronic contact. Soft rings of Teflon were placed between two anodes to eliminate the edge effect on the anode in the middle. The rest of the threaded bolt was covered by Teflon. Figure 4.2 presents a sketch of the rotating cylinder electrodes on the electrode holder of

stainless steel. The cathode was a concentric cylindrical sheet of aluminium, and the distance between the anode and the cathode was ~3 cm.

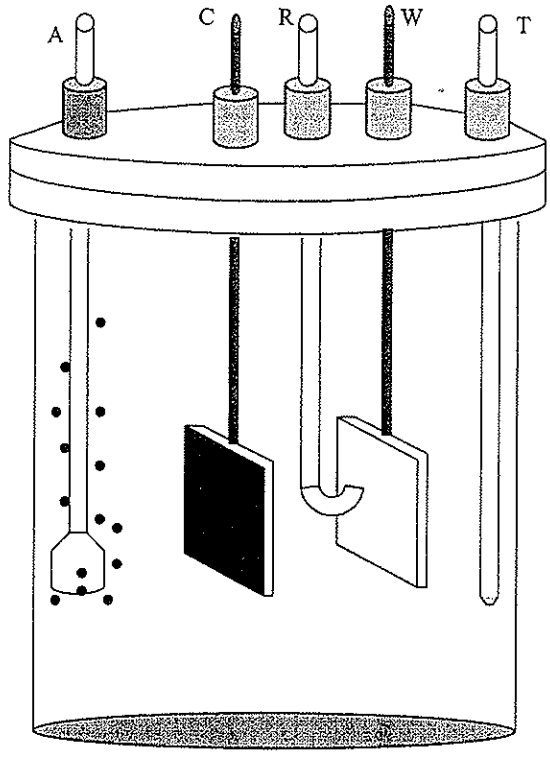

Figure 4.1: *Outline of the cell used in the present work. A: inlet of air. C: counter electrode. R: luggin capillary to the reference electrode (Hg/Hg_2SO_4 (2M H_2SO_4)). W: working electrode. T: thermometer. The electrolyte volume was 1l, and the distance between the working electrode and the counter electrode was ~3 cm.*

The cell was placed in a water-bath with a thermostat, where the temperature was held constant. The cyclic voltammetry measurements were obtained by an EG & G Princeton PAR potentiostat, model 236A, with ancillary software. Linear voltammetry and AC impedance measurements were obtained with an Autolab potentiostat (PGSTAT20). A direct current supply (Hewlett Packard 6032A) was used in the galvanostatic experiments, and a multimeter (Keithley 2000) was used to measure the potential between anode and the reference electrode (Hg/Hg_2SO_4 (2 M H_2SO_4), Ref 601, Radiometer). The mercury sulphate electrode, MSE, (Hg/Hg_2SO_4 (2 M H_2SO_4)) served as reference electrode in all experiments. A

rotator (EG&G Parc Model 616 RDE) was used to rotate the cylinder electrodes. A Personal Computer (486) was used to log the potential and current data during the measurements.

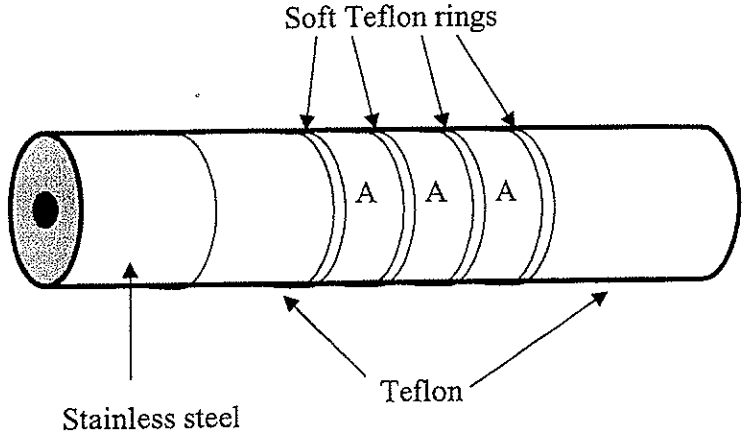

Figure 4.2: *Schematic drawing of the cylinder electrodes on the electrode holder. A = electrodes with IrO_2 - Ta_2O_5 coating (described in section 4.2) with d_o = 2 cm (outer diameter) and h = 0.8 cm (high).*

Table 4.1 shows the chemicals used in the experiments. It was desided to carry out the experiments in H_2SO_4 containing only Mn^{2+}, to eliminate the effect of other metal ions which are present in the zinc electrolyte ($ZnSO_4$ etc.). The chemicals were of pro analysi quality and were used as received.

Table 4.1: *The chemicals used in the experiments.*

Chemicals	Producer
Manganese sulphate hydrate, $MnSO_4 \cdot H_2O$	Merck
Sulphuric acid, H_2SO_4 (96-98%)	Merck
Hydrogen peroxide, H_2O_2 30 %	Merck

4.2 Anode materials

Table 4.2 contains all the anode materials tested in the present work. All the oxygen-evolving electrodes with catalytic coating were produced by Permascand AB in Ljungaverk, Sweden. The Ti/IrO_2 - Ta_2O_5 electrode, which is the standard

oxygen-evolving anode, was a Ti sheet (2x3 cm, sand-blasted and etched in HCl) coated with IrO_2 - Ta_2O_5 as described by De Nora et al. [62]. The modified coatings were prepared with the IrO_2 - Ta_2O_5 coating (US patent 3,926,751 [62]) as the starting material. The IrO_2 content was held constant for all the modified coatings. Addition of MnO_2 was introduced by replacing the Ta_2O_5 content (in mol%), to see if the MnO_2 content in the coating had any effect on the catalytic properties of the coating in electrolytes containing Mn^{2+} ions. The MnO_2 content in the catalytic coatings is written as MnO_x, because the crystal structure is not known. The x value is assumed to be less than 2. The electrode surface was investigated by SEM before and after the electrochemical experiments.

Table 4.2: *Anode materials studied in the experiments.*

Material	Description
Pt	Rolled
Pb/Ag	Lead alloyed with 0.5 wt% Ag
IrO_2 - Ta_2O_5	the standard IrO_2 - Ta_2O_5 coating on Ti
IrO_2top	the standard IrO_2 - Ta_2O_5 with three outer layers of IrO_2
IrO_2	pure IrO_2 coating on Ti
IrTaMnO_x5	IrO_2/ Ta_2O_5/5 mol% MnO_x on Ti
IrTaMnO_x50	IrO_2/ Ta_2O_5/50 mol% MnO_x on Ti
IrTaMnO_x75	IrO_2/ Ta_2O_5/75 mol% MnO_x on Ti
IrMnO_x	IrO_2/100 mol% MnO_x on Ti

4.3 Experimental procedures

4.3.1 Cyclic voltammetry

The cyclic voltammetry measurements were performed in sulphuric acid containing Mn^{2+} ions, on the various anode materials (table 4.2) in a cell as described in figure 4.1. The counter electrode was of Pt. An overview of the parameters in the cyclic voltammetry are given in table 4.3. The scan was started at the open circuit potential, and reversed before the oxygen evolution started, and run in the cathodic direction until 0 mV vs. MSE, and ended at the initial potential. The geometrical area of the working electrode was 1 cm^2.

Table 4.3: *Parameters in the cyclic voltammetry measurements. The temperature was held constant at 35° C.*

Working electrode	Scan interval [mV]	SR [mV/s]	c(Mn^{2+}) [g/l]	c(H_2SO_4) [M]
Pt	300 → 1200 → 0 → 300	0.5-100	1-40	0.5-6
IrO_2 - Ta_2O_5	250 → 950 → 0 → 250	1-100	0-10	2
IrO_2top	250 → 950 → 0 → 250	1-5	10	2
IrO_2	250 → 950 → 0 → 250	1-5	10	2
$IrTaMnO_x5$	250 → 950 → 0 → 250	1-5	10	2
$IrTaMnO_x50$	250 → 950 → 0 → 250	1-5	10	2
$IrTaMnO_x75$	250 → 950 → 0 → 250	1-5	10	2
$IrMnO_x$	250 → 950 → 0 → 250	1-5	10	2

The effect of the Mn^{2+} concentration and the scan rate

In these experiments, the acid concentration was held constant (2M H_2SO_4) while the Mn^{2+} concentration and scan rate were varied. The temperature was 35°C for all the experiments and no forced convection was used. The working electrode was Pt. Table 4.4 presents an overview of the different parameters.

Table 4.4: *Parameters in cyclic voltammetry where the effect of Mn^{2+} concentration and scan rate was to be studied on Pt as working electrode.*

c(H_2SO_4) [M]	T [°C]	c(Mn^{2+}) [g/l]	Scan rate [mV/s]
2	35	1, 2, 5, 10, 20, 30, 40	1
2	35	10	10
2	35	10	100

The effect of acid concentration

The Mn^{2+} concentration was constant (10 g/l) in these experiments, while the sulphuric acid concentration was varied as follows: 0.5, 1, 2, 4 and 6 M. The scan rate was 1 mV/s and steady state conditions were assumed. The temperature was 35°C and no forced convection was used. Platinum served as working electrode.

The effect of temperature and convection

These experiments were carried out in 2M H_2SO_4 containing $c(Mn^{2+})$ = 10 g/l with Pt and Ti/IrO_2 - Ta_2O_5 as working electrode. The convection was introduced mechanically. Table 4.5 shows the parameters used in these experiments.

Table 4.5: *The parameters in cyclic voltammetry where the effect of temperature and convection was studied on Pt and Ti/IrO_2 - Ta_2O_5 as working electrodes. The geometric area of the working electrodes was 1 cm^2.*

$c(H_2SO_4)$ [M]	$c(Mn^{2+})$ [g/l]	Temperature [°C]	Stirring	SR [mV/s]
2	10	35	no	1
2	10	35	yes	1
2	10	21	no	1
2	10	21	yes	1

4.3.2 Linear voltammetry

The linear voltammetry measurements (by Autolab potentiostat (PGSTAT20)) was used to record E-i curves on IrO_2 - Ta_2O_5 and on the modified coatings (table 4.2) in pure 2M H_2SO_4 at 35°C, and in 2M H_2SO_4 containing Mn^{2+} ions (10 g/l). The potential interval was 0-1500 mV vs. MSE and the scan rate was 1 mV/s. The geometrical area of the working electrodes was 0.25 cm^2 and no forced convection was applied in these experiments. No corrections were used for the ohmic drop between the capillary tip and the electrode surface.

4.3.3 AC Impedance measurements

AC Impedance measurements were carried out on Ti/IrO_2 - Ta_2O_5 electrodes in pure 2M H_2SO_4 at 35°C, and no forced convection was applied to the cell. Various potentials were applied to the working electrode (OCP, 0.5 V, 1.0 V and 2.0 V vs. MSE) during the impedance measurement, to see if the ohmic drop between the capillary tip and the working electrode surface increased for the high potentials.The Autolab potentiostat (PGSTAT20) was used in these experiments, and the frequency interval was 10-100 kHz.

4.3.4 Galvanostatic electrolysis

The electrolysis experiments were carried out in a cell as described in figure 4.1. A direct current supply (Hewlett Packard 6032A) was used to impose the wanted current through the circuit, and a multimeter (Keithley 2000) was used to measure the anode potential vs. MSE. The cathode was of aluminium, and only hydrogen evolution was expected to take place on the cathode. Evaporated electrolyte was replaced by distilled water. Table 4.6 shows the parameters for the electrolysis experiments.

Table 4.6: *The parameters used in the galvanostatic electrolysis.*

Anode material	c(H_2SO_4) [M]	c(Mn^{2+}) [g/l]	i [A/cm^2]	T [°C]
Pb/Ag	2	10	0.05	35
Pt	2	10	0.05	35
IrO_2 - Ta_2O_5	2	0.01, 5, 10	0.05	35
IrO_2 - Ta_2O_5	2	0	0.05, 0.5, 1	35
IrO_2top	2	10	0.05	35
IrO_2	2	10	0.05	35
$IrTaMnO_x5$	2	10	0.05	35
$IrTaMnO_x50$	2	10	0.05	35
$IrTaMnO_x75$	2	10	0.05	35
$IrMnO_x$	2	10	0.05	35

Electrolysis on rotating cylinder electrode

Three rotating cylinder electrodes with IrO_2 - Ta_2O_5 coating (d = 2 cm, h = 0.8 cm) (fig. 4.2) were used as anodes for electrolysis in 2M H_2SO_4 with c(Mn^{2+}) = 10 g/l at T = 35°C and various rotating velocities (0, 50, 300 and 3000 rpm = 0 - 3.0 m/s). The applied current density was 0.05 A/cm^2, and it was assumed that all three electrodes had the same electronic contact. The current was not switched off until the anodes were taken out of the cell after 10 hours. The cylinder electrode in the middle was assumed to obtain uniform current distribution, and was investigated in the SEM after being washed in distilled water, cast in epoxy and polished.

Use of H_2O_2 as reducing agent

It was tried to suppress the deposition of MnO_2 during oxygen evolution on the anode, by addition of H_2O_2. In all these experiments, Ti/IrO_2 - Ta_2O_5 served as anode material in 2M H_2SO_4 with $c(Mn^{2+}) = 10$ g/l. The temperature was 35°C, and the current density was 0.05 A/cm^2. An injection pump was used to add H_2O_2 dropwise to the electrolyte with a velocity of 8-9 ml/hour. The quantities of H_2O_2 added to the electrolyte per hour were: 0.9 g, 1.19 g, 1.79 g and 3.57 g. Air was bubbled through the electrolyte to mix the H_2O_2 in the electrolyte. The electrolysis time was 100 hours.

4.3.5 Potential pulses

The pulse experiments were accomplished to see if the deposited MnO_2 could be reduced on the anode by reversing the electrode potential in the cathodic direction (relative to the oxidation potential) for a short time. Figure 4.3 shows the different potential pulses applied to the working electrode (Ti/IrO_2 - Ta_2O_5). Air was bubbled through the electrolyte to remove the reduced species from the anode surface. The experiments were conducted for 100 hours.

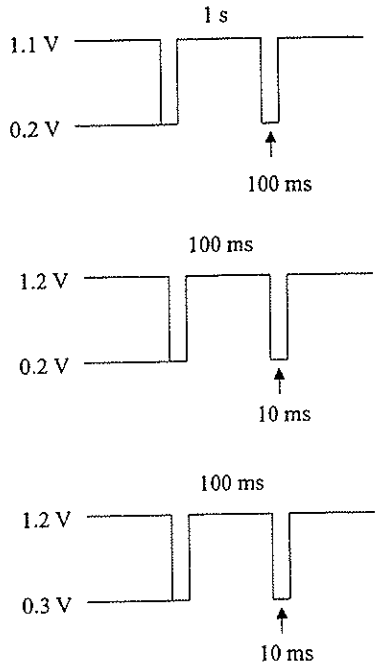

Figure 4.3: *The potential pulses applied to the* Ti/IrO_2 - Ta_2O_5 *electrode in 2M* H_2SO_4 *with* $c(Mn^{2+})$= *10 g/l at* $T = 35°C$. *The anode area was 1* cm^2.

Chapter 5

Results and discussion

5.1 SEM images of oxygen-evolving coatings on Ti

The oxygen-evolving coatings studied in present work, were produced by Permascand AB in Ljungaverk (Sweden) according to the procedure described by De Nora et al. [62]. The electrodes were studied by SEM (secondary electron mode, SE) with element analysis (EDS) to view the morphology and the element distribution in the coatings. Figures 5.2 - 5.8 show the SEM images of the various coatings: IrO_2 - Ta_2O_5, IrO_2top, IrO_2, $IrTaMnO_x5$, $IrTaMnO_x50$, $IrTaMnO_x75$ and $IrMnO_x$. The description of the coatings is given in table 4.2 in section 4.2.

Figure 5.1 shows the morphology of the Ti substrate after sand-blasting and etching in hot HCl. The surface had a high degree of roughness, which should increase the adherence of the coating to the base metal. The surface of the standard IrO_2 - Ta_2O_5 coating (10 layers) is shown in figure 5.2. As mentioned in section 2.1, several scientists observed a mud-crack structure for the IrO_2 - Ta_2O_5 coating [17, 22, 23, 28, 32]. A few cracks were observed on the IrO_2 - Ta_2O_5 coating, but no mud-crack structure. The bright crystallite particles consisted of IrO_2, while the dark and smooth phase consisted of Ta_2O_5 and IrO_2. Otogawa et al. [26] observed the same morphology as in figure 5.2, but the Ta_2O_5 rich phase consisted of more macro cracks than is seen in figure 5.2.

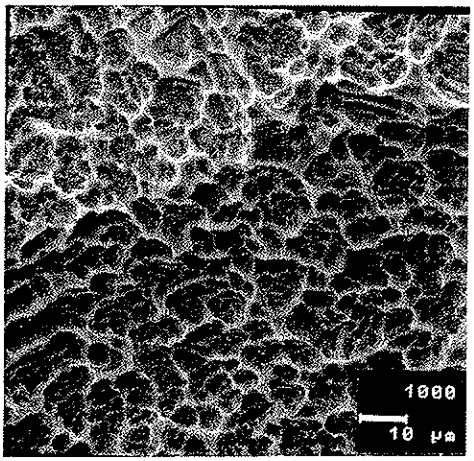

Figure 5.1: *Surface of sandblasted and etched (in HCl) Ti. 1000X.*

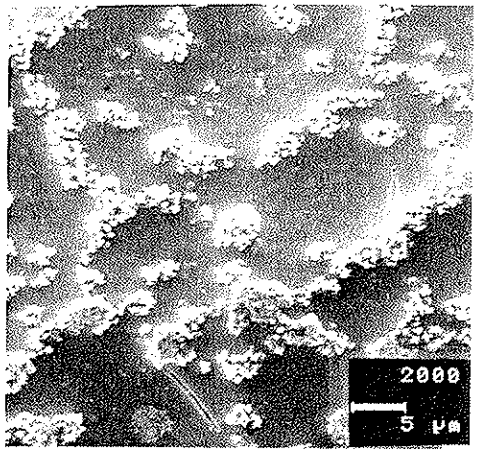

Figure 5.2: *Surface of the IrO_2 - Ta_2O_5 coating. 2000X.*

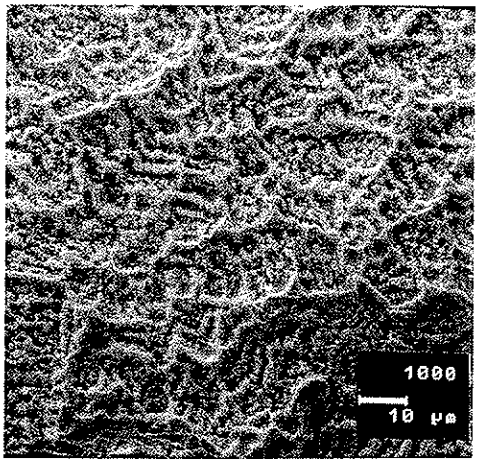

Figure 5.3: *Surface of the IrO_2top coating. 1000X.*

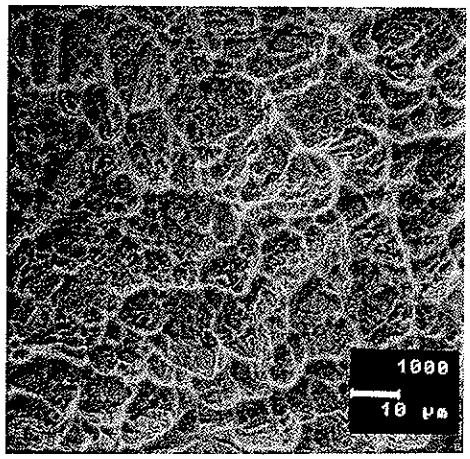

Figure 5.4: *Surface of the IrO_2 coating. 1000X.*

When the three outer layers consisted of pure IrO_2 on top of the IrO_2 - Ta_2O_5 coating, as presented in figure 5.3, the IrO_2 crystallites were more uniformly distributed on the Ta_2O_5 surface. But still some chained agglomerates were observed. The catalytic surface area was expected to increase for this coating because of higher quantities of IrO_2 on the coating surface. Figure 5.4 shows the surface of pure IrO_2 coating. The IrO_2 crystallites were distributed over the entire surface, but the morphology of the etched Ti base metal was visible (compare figures 5.1 and 5.4), which indicates that the coating was very thin. Relatively high quantities of Ti were detected (in the element analysis) compared to the standard IrO_2 - Ta_2O_5 coating. The appearance of Ti in the IrO_2 coating, may be due to a very thin or porous coating.

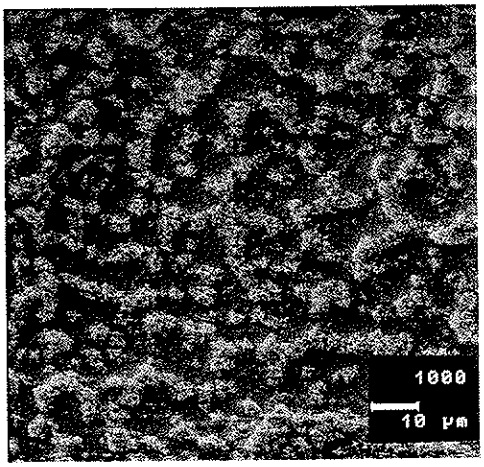

Figure 5.5: *Surface of the $IrTaMnO_x5$ coating. 1000X.*

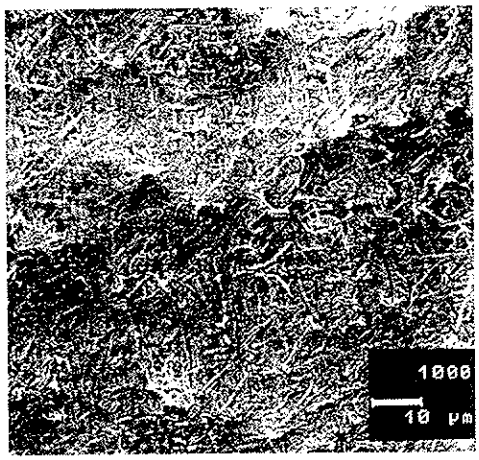

Figure 5.6: *Surface of the $IrTaMnO_x50$ coating. 1000X.*

The IrO_2 - Ta_2O_5 coating was doped with small quantities of MnO_x (5 mol%) by reducing the equivalent quantities of the Ta_2O_5 content. The SEM image of the coating surface is shown in figure 5.5. The outlook of this coating was very similar to the standard IrO_2 - Ta_2O_5 coating, and it contained only a few cracks. The smooth Ta_2O_5 phase contained MnO_x, while the agglomerates mainly consisted of IrO_2. When the MnO_x content was increased to 50 mol%, the morphology of the coating surface changed markedly (see figure 5.6). No IrO_2 agglomerates were observed, as for IrO_2 - Ta_2O_5. Instead the IrO_2, Ta_2O_5 and MnO_x existed in apparently one phase.

The coating consisted of bar-shaped crystallites, and cracks. Small quantities of Ti were detected in the element analysis, due to cracks and pores.

Figures 5.7 and 5.8 show the surface of the $IrTaMnO_x75$ and $IrMnO_x$ coating respectively. The morphology of the $IrTaMnO_x75$ coating consisted of flakes with many cracks, and no agglomerates of IrO_2 were observed. The same was observed for the $IrMnO_x$ coating, but some areas of the coating had higher quantities of IrO_2 and MnO_x than others. This coating was smoother and had less cracks than the $IrTaMnO_x75$ coating.

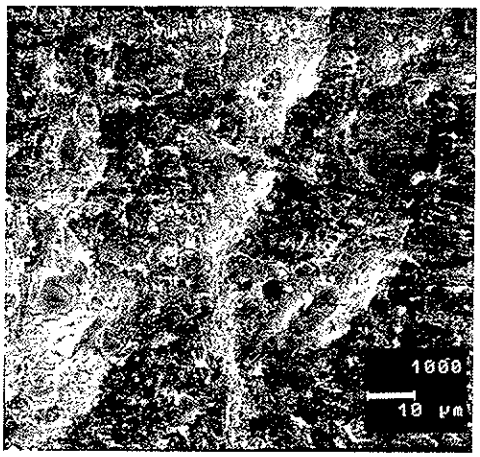

Figure 5.7: *Surface of the $IrTaMnO_x75$ coating. 2000X.*

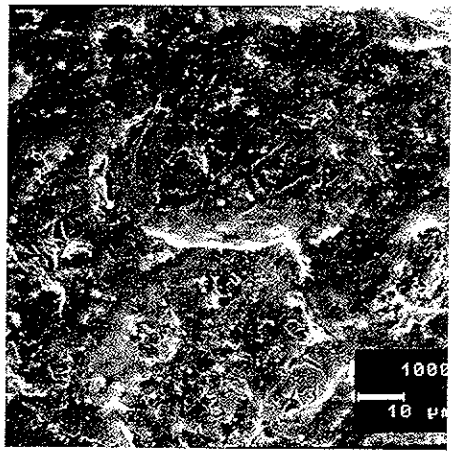

Figure 5.8: *Surface of the $IrMnO_x$ coating. 1000X.*

The crystal structure of the compounds (IrO_2, Ta_2O_5 and MnO_x) in the various coatings presented in figures 5.2 - 5.8 was studied by XRD (X-ray Diffraction). The coating was very thin (1-10 μm), and the X-ray beam went through the coating and detected only the Ti substrate. Powder analysis of the coatings is a better method to study the crystal structure of the coating compounds by XRD, than the coating on the base metal.

As described above, there was a marked change in the morphology of the coatings, when the MnO_x concentration was raised above 5 mol%. The increasing number of cracks for these coatings compared to the IrO_2 - Ta_2O_5 coating, may be caused by greater difference in the thermal expansion coefficient between MnO_x and the Ti base metal, than between Ti and Ta_2O_5. The IrO_2 content was the same in all the coatings, so the electrocatalytic activity should not change markedly

from one coating to the other. However, the catalytic surface area may not be the same for all the coatings. The IrO_2top coating, where the three outer layers were pure IrO_2, should have the highest catalytic surface area. The formation of the agglomerates of IrO_2 in the IrO_2-Ta_2O5 coating was thought to be caused by the calcinating temperature [22]. The results described above show that the composition of the coating, by addition of MnO_x, may cause changes in the morphology.

5.2 Cyclic voltammetry in sulphuric acid containing Mn^{2+} ions

In the present experiments a mercury sulphate electrode (MSE) (Hg/Hg_2SO_4 with 2M H_2SO_4) served as reference electrode, while platinum was used as counter electrode, as described in figure 4.1 in section 4.1. Both Pt and Ti/IrO_2 - Ta_2O_5 were used as working electrodes. The scan was started at the open circuit potential, and reversed before visible oxygen evolution started. The purpose of these experiments was to study the mechanisms for oxidation of Mn^{2+} to form manganese dioxide (MnO_2), and reduction of the deposited manganese dioxide.

A diploma work was performed by Bjørnarå [72] in connection with the present work. I was co-supervisor for Bjørnarå, and will therefore include the absorption curves for Mn^{3+}, and refer to his diploma work. The rest are my results, if nothing else is mentioned.

5.2.1 Platinum as working electrode

Platinum was used as working electrode because of its high oxygen overvoltage. It was expected that the oxidation peak current caused by oxidation of Mn^{2+}, and the current caused by oxygen evolution could be separated also at high scan rates with Pt as working electrode.

Effects of Mn^{2+} concentration and scan rate

In these experiments 2M H_2SO_4 was used as supporting electrolyte, and the concentration of Mn^{2+} was varied as follows: 1, 5, 10, and 40 g/l. The temperature

was held constant at 35°C, which is close to the temperature for industrial zinc electrowinning. Figure 5.9 shows cyclic voltammograms where the manganese concentration was varied from 1 to 40 g/l. No mechanical stirring was used in these experiments. The scan was very slow (SR = 1 mV/s), so that steady state conditions could be assumed.

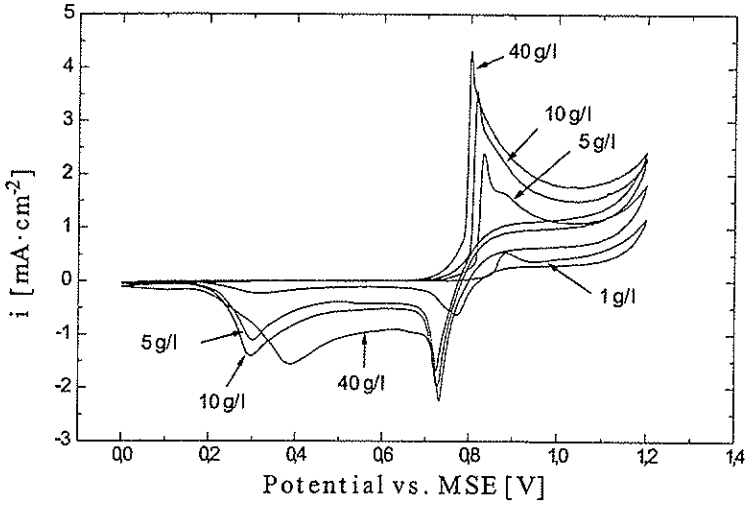

Figure 5.9: *Cyclic voltammetry on a Pt electrode in 2M H_2SO_4 with varying Mn^{2+} concentration (1-40 g/l), scan rate 1 mV/s, T= 35° C.*

During the anodic scan, two anodic peaks were visible, where the first peak was very sharp and the second one was smaller. Since two anodic peaks were observed, the oxidation of Mn^{2+} to MnO_2 may occur in two electrochemical steps as described by equations 3.27 and 3.29 in section 3.6.1. When the Mn^{2+} concentration was increased, the first oxidation peak became sharper while the second one was less pronounced. The reduction in current density after the first peak may be due the formation of an insulating intermediate, MnOOH, as suggested by Petitpierre et al. [47] and by Paul et al. [50] in equation 3.28. A brown deposit was observed on the electrode surface at the first oxidation peak. At higher oxidation potentials the electrode was covered by a black deposit.

A round oxidation peak was observed for the lowest Mn^{2+} concentration (1 g/l). The round form of the oxidation peak instead of a sharp peak, may be explained by only small amounts of the insulating intermediate formed on the electrode

surface, so that some of the active electrode surface may still have been active for further oxidation of Mn^{2+} to Mn^{3+}. At higher Mn^{2+} concentrations, formation of the insulating intermediate may have been dominating, covering the entire electrode surface, and passivating the electrode against further oxidation of Mn^{2+} to Mn^{3+}. The intermediate product may oxidize to MnO_2 at higher potentials according to equation 3.29.

Several scientists have suggested that the Mn^{3+} ion is not stable at low acid concentrations, and that it will disproportionate to Mn^{2+} and Mn^{4+} immediately, as given by equation 2.7 in section 2.2.2. The colour of the Mn^{3+} ions in sulphuric acid is very similar to that of permanganate (MnO_4^-), which is red-violet [68], and can be confused. UV absorption spectroscopy may be used to compare the absorption spectra of the MnO_4^- (two peaks at wave lengths 525 and 550 nm) and the Mn^{3+} ion (one round peak at ~500 nm).

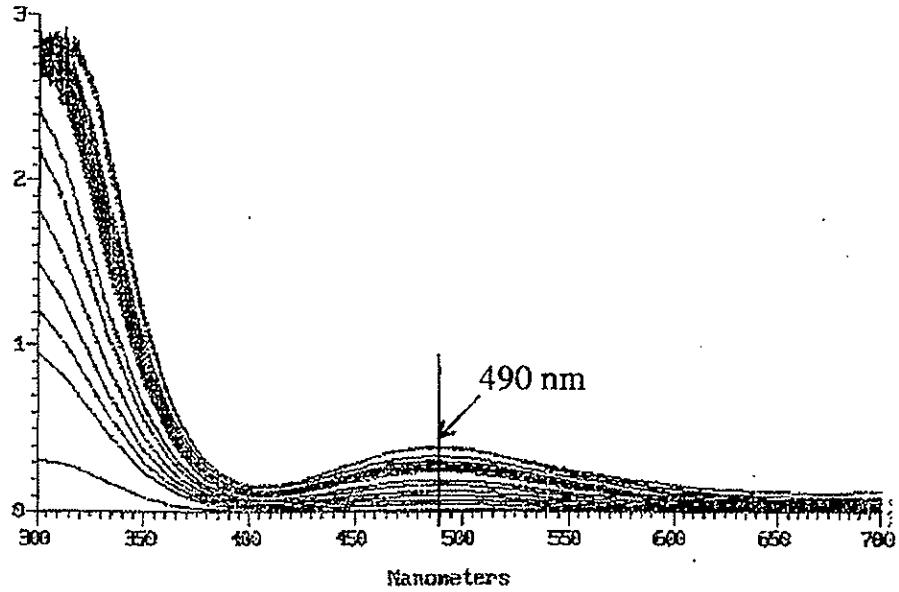

Figure 5.10: *Absorption spectra obtained during voltammetry measurement (interval 500-950 mV) in 2M H_2SO_4 containing c(Mn^{2+}) = 10 g/l at T = 35° C and scan rate 0.05 mV/s [72].*

It was decided to record absorption spectra of the electrolyte during the anodic scan on a Pt electrode. The scan was run from 500 to 950 mV in 2M H_2SO_4 containing c(Mn^{2+}) = 10 g/l at T = 35°C and scan rate 0.05 mV/s. Figure 5.10

shows that the intensity of the absorption spectra increased when the oxidation potential was increased. The peak was round and the maximum was observed at wave length 490 nm, and was very similar to the absorption spectrum for Mn^{3+} obtained by Selim and Lingane [68], presented in figure 3.11 in section 3.6.1. This observation indicates that Mn^{3+} ions may be present in 2M H_2SO_4, and that the first oxidation step in the oxidation of Mn^{2+} to MnO_2 could be described by equation 3.27.

During the cathodic scan three peaks were observed (figure 5.9), where the first peak was very sharp and appeared at 730-800 mV, the second was hardly seen (at ~600 mV), while the third one had a normal shape and appeared at 300-400 mV. After the first reduction peak, a current plateau was observed, before reduction peak number three appeared. From the voltammetry curves for c(Mn^{2+})= 5 and 10 g/l, a very small reduction peak can be observed at 550 mV. The current density on the plateau increased with increasing Mn^{2+} concentration in the electrolyte, because of larger quantities of reducible deposit on the electrode surface.

It is likely that an insulating layer of MnOOH was formed (equation 3.33) in the first reduction peak, as suggested by several scientists [44, 47, 49, 53, 55]. The first reduction peak became sharper when the Mn^{2+} concentration was increased. For the lowest Mn^{2+} concentration (1 g/l) only small amounts of MnO_2 were present on the electrode surface, leading to less formation of MnOOH which could deactivate further electron transfer through the deposit. For Mn^{2+} concentrations higher than 1 g/l, the current density decreased immediately and gave a very sharp peak. Black deposit was still present on the electrode surface after the first reduction peak.

According to Vosburgh [44], MnO_2 is a semiconductor where the electrons can pass through by being transferred between Mn^{4+} and Mn^{3+}. Upon discharge of the MnO_2 electrode, MnOOH is formed on the surface of the electrode [66]. Kordesch [37] and Ruetschi [39] suggested that reduction of MnO_2 may involve protons present in the lattice, and that absorption of electrons may take place in the solid phase. Lee et al. [55, 56] found that the first reduction step took place on the interface deposit/electrolyte, because dendrites present on the deposit surface before reduction peak 1, were absent after the reduction peak. Anyway, XRD analysis of the deposit surface after the first reduction peak did not show any new phase, but only γ-MnO_2.

When the Mn^{2+} concentration in the electrolyte was increased, more MnO_2 was expected to deposit on the electrode surface. If the first reduction step took

place at the interface deposit/electrolyte, the ohmic drop through the deposit layer should shift the reduction potential for the first reduction peak to more cathodic potentials for higher Mn^{2+} concentrations, because the MnO_2 deposit is a semiconductor [25]. The first reduction peak potential decreased 70 mV from c(Mn) = 1 g/l to c(Mn) = 40 g/l, and was nearly independent of the Mn^{2+} concentration for c>5 g/l. It is suggested that the first reduction step is determined by diffusion of protons and electrons in the MnO_2 lattice. Since the reduction peak potential was nearly independent of the amount of deposited MnO_2 on the electrode, it is suggested that the first reduction step takes place beneath the surface as the protons can penetrate the MnO_2 crystal lattice.

The reduction potential for the third reduction peak became dependent on the Mn^{2+} concentration for $c(Mn^{2+}) > 10$ g/l. Lee et al. [56] observed three reduction peaks in sulphuric acid solutions with concentrations 3.75-7.5M, and suggested that Mn^{3+}, produced by chemical dissolution of MnO_2 and MnOOH as described by equations 2.16 and 2.18, was reduced at potentials 0.1 V vs. MSE. The reduction potential for the third reduction peak shifted ~80 mV in the positive direction, when the Mn^{2+} concentration was increased 40 times. It is suggested that Mn^{3+} produced according to equations 3.34 and 3.35, was reduced during the third reduction peak as described by equation 3.36. The shift of the reduction potential for peak 3 to less cathodic potentials, may be explained by the Nernst equation 3.2 because of larger quantities of Mn^{3+} produced during the dissolution of MnO_2 and MnOOH.

Figure 5.11 shows cyclic voltammograms recorded on a platinum electrode for varying Mn^{2+} concentrations (1-10 g/l) at 10 mV/s. Compared to figure 5.9 the oxidation peak shifted to more anodic potentials when the scan rate increased for all manganese concentrations, indicating that the oxidation of Mn^{2+} to MnO_2 is an irreversible reaction. Rodrigues [53] observed the same for deposition of MnO_2 from 0.5M Mn_2SO_4 in 0.4M H_2SO_4 at 80°C, and suggested that the anodic deposition of MnO_2 involved a complex mechanism.

The oxidation peak was less sharp at 10 mV/s than at 1 mV/s, and only one oxidation peak was observed. This may be explained, as suggested by Petitpierre et al. [47], by less time for the chemical reaction (3.28) to occur and produce an insulating intermediate product (MnOOH), which could passivate the entire electrode surface. A current plateau was observed before the oxygen evolution started, and it is suggested that further oxidation of Mn^{2+} to MnO_2 occurred in this area.

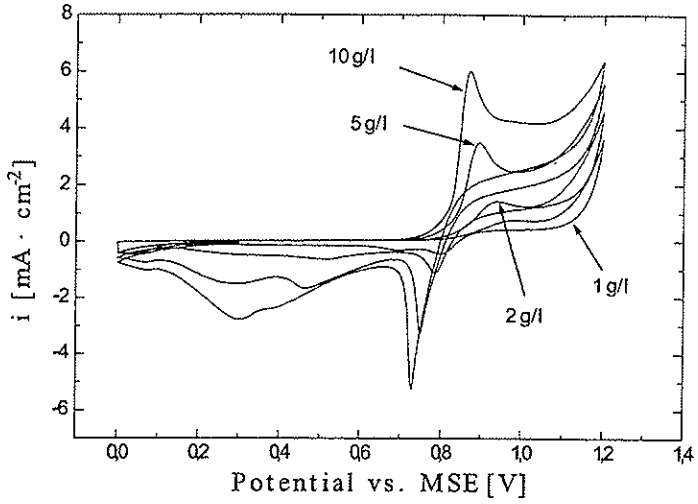

Figure 5.11: *Cyclic voltammetry on a Pt electrode in 2M H_2SO_4 with varying Mn^{2+} concentration (1-10 g/l), at scan rate 10 mV/s and T= 35° C.*

At 10 mV/s, the first reduction peak had the same shape as observed for 1 mV/s. The second reduction peak was clearly seen for Mn^{2+} concentrations 2, 5 and 10 g/l. For the lowest concentration (c(Mn^{2+})= 1 g/l) only two reduction peaks were observed at this scan rate, which may be due to small quantities of deposited MnO_2 on the electrode surface.

Maskell [57] observed two reduction peaks in acidic solutions with concentrations 0.0125-3.75 M, and suggested the same reduction reaction (3.33) for the two reduction peaks. Petitpierre et al. [47] observed three reduction peaks at 60°C in 0.5M Mn_2SO_4 and 3.8 M H_2SO_4. The results obtained in figure 5.11 show that three reduction steps may take place at lower Mn^{2+} concentrations (c(Mn^{2+}) $\geq$ 5 g/l $\approx$ 0.09M), lower temperatures (35°C) and lower acid concentrations (2M H_2SO_4). The reduction step during the second reduction peak is believed to be the same as for the first cathodic peak.

When the scan rate was increased to 100 mV/s (figure 5.12), no sharp oxidation peak was observed like for the lower scan rates described earlier, and the oxidation peak shifted to higher potentials (see also figure A.1 in Appendix A). A current plateau was observed before the oxygen evolution started as observed for scan rate 10 mV/s. This may be explained, as suggested by Petitpierre et al.[47], by

less time for the chemical reaction 3.28 to occur and produce an insulating layer of MnOOH, or a change in the deposition mechanism. The plot of the oxidation peak current is plotted as a function of the square root of the scan rate in figure A.2 in Appendix A, which may indicate a change in the deposition mechanism of MnO_2.

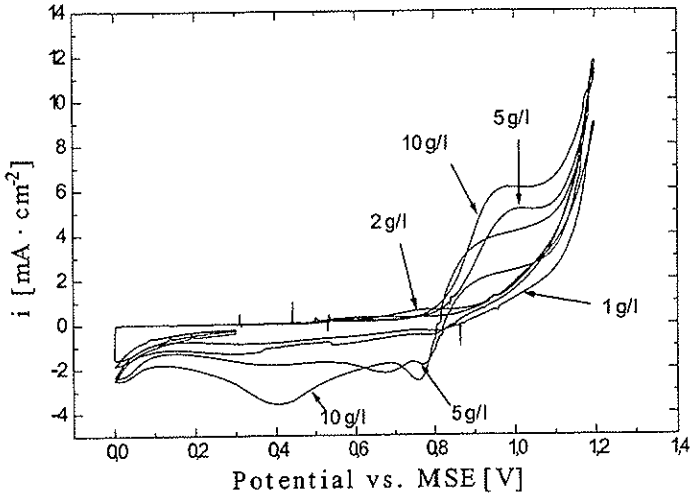

Figure 5.12: *Cyclic voltammetry on a Pt electrode in 2M H_2SO_4, at scan rate 100 mV/s and T= 35° C.*

Only two reduction peaks were observed for the highest Mn^{2+} concentrations (5 and 10 g/l). The first reduction peak was hardly seen for the low manganese concentrations, while it had a round form for Mn^{2+} concentrations 5 and 10 g/l. Compared to figures 5.9 and 5.11, it is seen that the intensity of the first reduction peak decreased when the scan rate was raised from 1 to 100 mV/s. It is likely that only small amounts of MnO_2 were formed at high scan rates because of less time for nucleation, so that parts of the electrode surface may still have been active, giving a round reduction peak instead of a sharp peak. Another explanation of the round reduction peak, may be that the scan was too fast for the entire interface to be passivated by MnOOH. The reduction peak observed at 400 mV for c(Mn^{2+}) = 10 g/l may be reduction of Mn^{3+} ions near the electrode surface.

Figure 5.13 presents the relationship between anodic (both oxidation peaks) and cathodic charge (all reduction peaks) consumed during the scan. The ratio was more than 1 for all concentrations, which indicates that not all of the oxidized species were deposited. Bodoardo et al. [49] observed that the anodic peak area corresponded well to the sum of the cathodic peaks, while Rodrigues et al. [53] observed the same as in the present work, that the cathodic charge was less than the anodic charge at any scan rate.

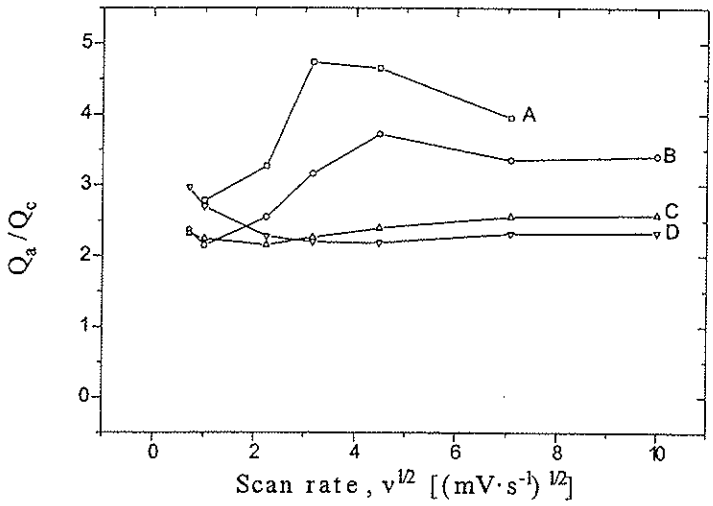

Figure 5.13: *Relationship between anodic and cathodic charge (Q_a/Q_c) used to deposit and reduce manganese dioxide on a Pt electrode in 2M H_2SO_4 with varying Mn^{2+} concentration, as a function of the square root of scan rate, T= 35° C. A; $c(Mn^{2+})$= 10 g/l, B; $c(Mn^{2+})$= 5 g/l, C; $c(Mn^{2+})$= 2 g/l and D; $c(Mn^{2+})$= 1 g/l.*

For the lowest Mn^{2+} concentrations, the relationship was nearly independent of the scan rate and Mn^{2+} concentration. When the Mn^{2+} concentration was increased to 5 and 10 g/l, the relationship between the anodic and cathodic charge increased, compared to the curves for 1 and 2 g/l. A maximum was also observed in the ratio between anodic and cathodic charge at scan rate 10 mV/s for $c(Mn^{2+})$ = 10 g/l and scan rate 20 mV/s for $c(Mn^{2+})$ = 5 g/l. In all these voltammetry measurements, it was observed that all the deposited manganese dioxide was reduced during the cathodic scan. The reduction in charge consumption during the cathodic scan for the highest Mn^{2+} concentrations compared to the anodic

charge, may be due to higher quantities of Mn^{2+} oxidized at the electrode surface, while the rate of the chemical reaction did not increase linearly with the amounts of Mn^{3+} at the electrode surface. It was assumed that oxygen evolution on the electrode could be neglected, but small amounts of oxygen evolved besides the deposition of MnO_2 may have contributed to the high ratio of Q_a/Q_c.

The effect of acid concentration

To study the effect of varying acid concentration on the deposition and reduction of MnO_2, the sulphuric acid concentration was varied as follows; 0.5, 1, 2, 4 and 6 M. The Mn^{2+} concentration was 10 g/l and the temperature was 35°C. No mechanical stirring was applied in these experiments. The oxidation peak shifted to higher potentials (+200 mV) when the acid concentration was increased from 0.5 to 6M (figure 5.14). This observation supports earlier studies for production of MnO_2, which state that low acid concentrations catalyze the MnO_2 deposition [37, 38, 41].

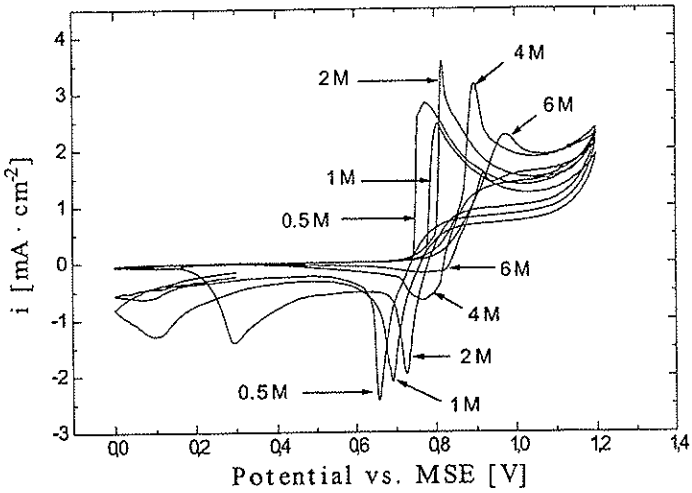

Figure 5.14: *Cyclic voltammetry on a Pt electrode in H_2SO_4 (0.5-6 M), c(Mn^{2+}) = 10 g/l, at scan rate 1 mV/s and T= 35° C.*

The oxidation peak current density was found to vary with the acid concentration, which is contrary to what was found by Rodrigues et al. [53]. They found that the oxidation peak current density was independent of the acid concentration. Petitpierre et al. [47] observed that the oxidation peak became sharper when the acid concentration decreased from 88 wt% to 10 wt%, and the intensity of the oxidation peak current density increased. The oxidation peaks for acid concentrations 2 and 4M were the sharpest, while it was round for the lowest concentrations (0.5 and 1M) and the highest concentration (6M). The round form for the oxidation peak of the lowest acid concentrations, may be due to no formation of an insulating intermediate (MnOOH), instead the Mn^{3+} ions may have disproportionated into Mn^{2+} and Mn^{4+} (equation 2.7) and formed MnO_2, which is a semiconductor. For the highest acid concentration (6M), it is believed that the Mn^{3+} ion was stabilized so that less amounts of MnOOH were formed, giving no sharp reduction in the current density, or that a change in the deposition mechanism occurred.

The reduction of deposited MnO_2 was observed to be very dependent on the acid concentration in the electrolyte. The reduction potential for the first reduction peak was shifted to more cathodic potential by 170 mV when the acid concentration was lowered from 6 M to 0.5 M (figure 5.14). This shift may occur because of lower mass transfer of protons to the interior of the MnO_2 deposit at low acidity. It was also observed that the peak current density for the first reduction peak increased with decreasing acid concentration, as observed by Petitpierre et al. [47], which indicates that larger quantities of MnO_2 were formed when the acid strength was reduced.

For acid concentrations 4 and 6 M, the first reduction peak was not sharp as observed for the lower acid concentrations, but rounded. This change may occur because of less deposited MnO_2 present on the electrode surface, so the electrode was only partly covered by an insulating MnOOH layer during the first reduction step. The reduction peak for 6 M acid was hardly visible, which may be explained by very small amounts of MnO_2 present on the electrode. Petitpierre et al. [47] suggested that the first reduction peak occurred due to reduction of Mn^{3+} to Mn^{2+} near the electrode surface according to equation 3.36. It has been established that Mn^{3+} is stable in solutions with high acid strength [51], and that sulphuric acid concentration of 6M was the most favourable for stabilizing the Mn^{3+} ion [68]. If Mn^{3+} is reduced during the first reduction peak, the peak current density should increase with increasing acid strength because of higher concentrations of Mn^{3+} present near the electrode surface. This was not observed in the present work.

For the lowest acid concentrations, it was observed that not all the deposited manganese dioxide had been reduced at the end of the scan, because some black deposit was still present on the electrode surface. Also the third reduction peak was shifted to more cathodic potentials for the lowest acid concentrations, which may have been due to low reaction rate for the chemical reactions producing Mn^{3+} ions. These results show that the acid strength has a pronounced effect on the deposition and reduction process of MnO_2, both in the chemical and the electrochemical reductions steps.

The effect of temperature and stirring

The voltammograms analysed earlier in this section, were carried out in 2M H_2SO_4 and at varying Mn^{2+} concentration in electrolyte with no stirring. The voltammograms presented in figure 5.15 show the effects of temperature and stirring.

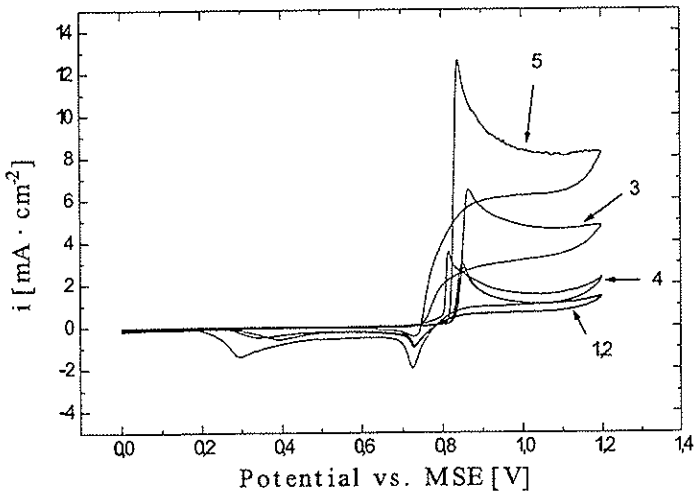

Figure 5.15: *Cyclic voltammetry on a Pt electrode in 2M H_2SO_4, $c(Mn^{2+}) = 10$ g/l, scan rate 1 mV/s, 1 and 2 ; $T = 21°C$ and no stirring, 3; $T = 21°C$ with stirring, 4; $T = 35°C$ and no stirring, 5; $T = 35°C$ with stirring.*

Scans 1 and 2 show that the system was quite reproducible, and that the electrode surface returned to the initial condition after the reduction of manganese dioxide. When the temperature was increased from 21 to 35°C, the oxidation potential was decreased by ~50 mV, but the change in the anodic peak current density was very small (0.5 mA/cm^2).

From the scans 1, 2 and 4 it was observed that an increase in temperature had an effect on the quantities of deposited MnO_2 on the anode surface, but no effect on the reduction potential for the first reduction peak. At 35°C more manganese dioxide was deposited compared to 21°C, because a higher value for the peak current density was observed for the first reduction peak, and higher quantities of cathodic charge were consumed to reduce the deposited MnO_2. When stirring was introduced to the system, the oxidation peak increased about 3 times at 21°C and 4 times at 35°C. This observation tells us that the combination of increased temperature and stirring, enhanced the oxidation rate of Mn^{2+} to Mn^{3+}. There was not observed any reduction peak for scan 3, because no MnO_2 may have been deposited on the electrode surface due to the high stirring rate. Scan 5 shows a reduction peak, but this one was much smaller than observed for scans 1, 2 and 4, because only small amounts of MnO_2 were deposited on the electrode surface.

The reverse scan crossed the forward scan for curves 3 and 5. This phenomenon was not observed in curves 1, 2 and 4. The cross-over phenomenon may be due to nucleation overpotential in the forward scan (as described in section 3.3.4), caused by the high stirring rate in the electrolyte.

The conclusion of this experiment is that high temperature and stirring enhance the oxidation of Mn^{2+} to Mn^{3+}, because of higher mass transfer of Mn^{2+} to the electrode surface. High stirring rate also inhibits deposition of manganese dioxide on the electrode surface at low temperatures (21°C), but at 35°C small quantities of deposit occurred on the electrode surface even when the stirring rate was very high. It is suggested that the oxidation of Mn^{2+} to Mn^{3+} is diffusion controlled, because of higher intensity of the oxidation peak when stirring was introduced. Since the reduction potential for the first reduction peak was independent of temperature and stirring, and thereby independent of the mass transfer of protons to the interface deposit/electrolyte, it is suggested that the reduction of the deposited MnO_2 occurs in the interior of the deposit, and not at the interface deposit/electrolyte, as suggested by Lee et al. [55].

5.2.2 Ti/IrO_2 - Ta_2O_5 as working electrode

In section 5.2.1 we have seen cyclic voltammograms on platinum as working electrode in sulphuric acid as a function of varying Mn^{2+} concentration, scan rate, acid concentration, temperature and stirring. In the following experiments presented in this section, the scan rates were low, and steady state current was assumed. The mechanisms for deposition and reduction of manganese dioxide are already suggested in section 5.2.1.

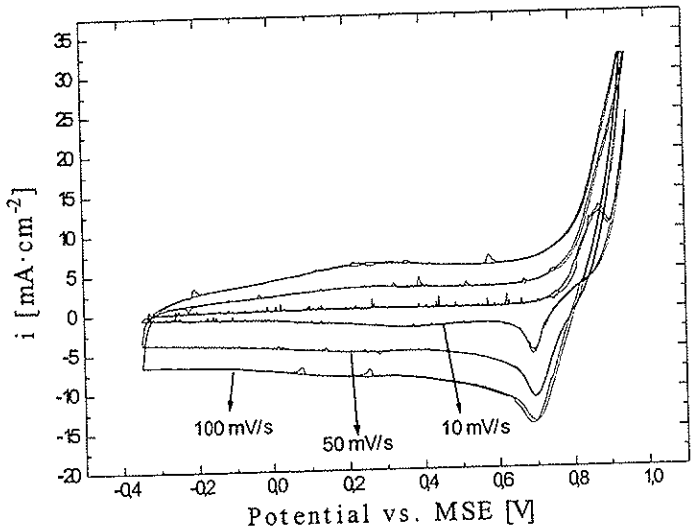

Figure 5.16: *Cyclic voltammetry on a Ti/IrO_2 - Ta_2O_5 electrode in 2M H_2SO_4 containing c(Mn^{2+}) = 10 g/l at T = 35° C and varying scan rate 10-100 mV/s. Scan interval: -350 mV → 950 mV → -350 mV.*

Figure 5.16 presents a cyclic voltammogram on a Ti/IrO_2 - Ta_2O_5 electrode in 2M H_2SO_4 containing c(Mn^{2+}) = 10 g/l at T =35°C and varying scan rates (10-100 mV/s). An oxidation peak was observed only at 10 mV/s. Voltammograms presented in figure 5.11 also showed only one oxidation peak on the Pt electrode at scan rate 10 mV/s. At higher scan rates the oxidation peak disappeared into the oxygen evolution at 950 mV, because Ti/IrO_2 - Ta_2O_5 has lower overvoltage for oxygen evolution compared to Pt. Only one cathodic peak was observed for these scan rates, and the reduction potential was nearly independent of the scan rate, as observed on the Pt electrodes. The broad oxidation and reduction bands at 200 mV are due to oxidation and reduction of iridium dioxide, as observed by

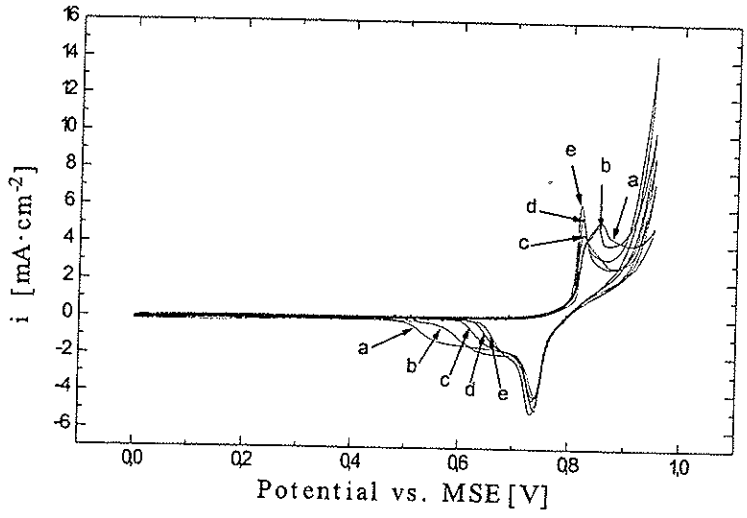

Figure 5.19: *Cyclic voltammetry on various coatings in 2M H_2SO_4, $c(Mn^{2+})$ = 10 g/l, T = 35° C and scan rate 1 mV/s. a; IrO_2 - Ta_2O_5. b; $IrTaMnO_x5$. c; $IrTaMnO_x50$. d; $IrTaMnO_x75$. e; $IrMnO_x$.*

During the cathodic scan, no large differences were observed in the reduction potential for the first reduction peak. This observation supports the suggestion that reduction of MnO_2 is dependent on diffusion of protons to the interior of the deposit, and not on the electronic properties of the electrode material. Lee et al. [55] also observed in their studies of reduction of MnO_2 on different electrode materials (Glassy Carbon, Pt and Au), that the first reduction peak was independent of the electrode material.

Figure 5.19 presents cyclic voltammograms recorded on coatings of IrO_2 - Ta_2O_5 where some of the Ta_2O_5 was replaced by MnO_x (5-100 mol%) as described in table 4.2 in section 4.2. The cyclic voltammogram for IrO_2 - Ta_2O_5 is included for comparison with the coatings containing manganese oxide. The oxidation peak for IrO_2 - Ta_2O_5 and coating $IrTaMnO_x5$ consisted of two peaks, leading to a broad oxidation peak. For the other coatings containing more MnO_x (50-100 mol%), a sharp oxidation peak was observed as with Pt, which indicates passivation of the electrode surface. The oxidation potential was 30 mV lower for coatings containing large quantities of MnO_x. The difference is not very large and it might be due to small differences in electronic properties between the various

coatings.

The first reduction peak was independent of the composition of the coatings and occurred at the same reduction potential (740 mV vs. MSE). Table 5.1 presents the reduction interval (start of the cathodic scan at i = 0 to the end i = 0 after the cathodic peaks) and the reduction charge in the same interval for the various coatings studied in figures 5.18 and 5.19.

Table 5.1: *Reduction intervals and consumed charge during the reduction interval for reduction of MnO_2 deposited, during the anodic scan in 2M H_2SO_4 containing $c(Mn^{2+})$=10 g/l at T=35° C and scan rate 1 mV/s for various coatings on Ti.*

Coating	Reduction interval [mV]		Reduction charge [mC]
IrO_2 - Ta_2O_5	~770-495	$\Delta U = 275$	591.6
IrO_2top	~770-480	$\Delta U = 290$	551.8
IrO_2	~770-450	$\Delta U = 320$	389.4
$IrTaMnO_x5$	~770-550	$\Delta U = 220$	332.7
$IrTaMnO_x50$	~780-610	$\Delta U = 170$	98.08
$IrTaMnO_x75$	~780-630	$\Delta U = 150$	107.7
$IrMnO_x$	~780-640	$\Delta U = 140$	111.3

After the first reduction peak it was observed that coatings with large quantities of MnO_x, needed more narrow potential ranges in the cathodic scan, before all the manganese dioxide deposit was reduced. The difference in the reduction potential interval between standard IrO_2 - Ta_2O_5 and the coating where all the Ta_2O_5 was replaced by MnO_x, was 160 mV. The reason for the more narrow reduction interval, may be that smaller quantities of MnO_2 had deposited on the modified coatings. Table 5.1 shows that the reduction charge decreased from 591.6 mC for IrO_2 - Ta_2O_5, to 98.08 mC for the coating with 50 mol% MnO_x. From figure 5.19 it can be observed that the oxidation current density increased abruptly at ~900 mV, caused by the start of oxygen evolution for coatings containing MnO_x. The oxygen evolution may have detached some of the deposited MnO_2 or Mn^{3+} ions from the electrode surface, giving less deposited MnO_2 to be reduced in the cathodic scan.

In figures 5.18 and 5.19 a small "shoulder" was observed before the main oxidation peak on IrO_2 - Ta_2O_5 and $IrTaMnO_x5$ coatings, indicating that the electron transfer occurred in two steps. A scan rate of 5 mV/s was used to separate the two oxidation peaks. Figure 5.20 shows two oxidation peaks on coating with pure IrO_2. On the other voltammograms, a shoulder was seen before the main

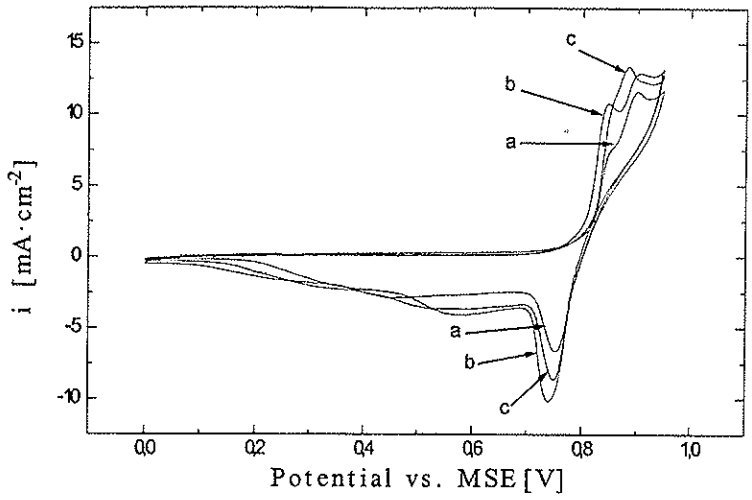

Figure 5.20: *Cyclic voltammetry on various coatings in 2M H_2SO_4, c(Mn^{2+}) = 10 g/l, T = 35 °C and scan rate 5 mV/s. a; IrO_2 - Ta_2O_5. b; IrO_2. c; IrO_2top.*

oxidation peak. No large differences were observed in the cathodic area, except that the electrode surface was not regenerated until the potential reached 0 mV, compared to 500 mV at scan rate 1 mV/s. These results correspond to the results obtained on the Pt electrode in section 5.2.1, and show that the diffusion steps and the chemical dissolution reactions are controlling the reduction process of MnO_2.

Deposition and reduction of MnO_2 during cyclic voltammetry

Figure 5.21 shows cyclic voltammograms on four Ti/IrO_2 - Ta_2O_5 electrodes. The voltammograms show that there were no large differences between the electrodes used, indicating that the electrode surfaces could be assumed to be approximately identical. To visualize the deposition and reduction of MnO_2 on the Ti/IrO_2 - Ta_2O_5 electrode surface, the cyclic voltammetry scan was interrupted in four positions; the oxidation peak (850 mV), just before the oxygen evolution (950 mV), after the first reduction peak (700 mV), and after the "tail" (400 mV) in the cathodic scan when a current plateau was reached, as shown in figure 5.22. After the scan was interrupted, the electrode was taken out of the electrolyte and washed with distilled water and dried in air. The surfaces of the dry electrodes were studied by SEM with element analysis.

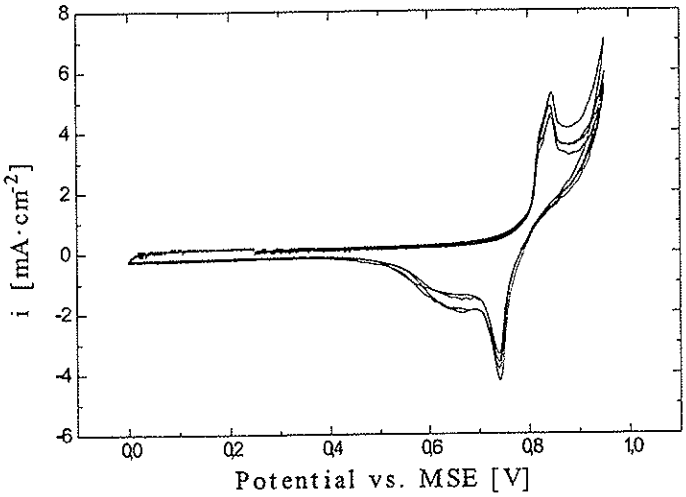

Figure 5.21: *Cyclic voltammetry on a Ti/IrO_2 - Ta_2O_5 electrode in 2M H_2SO_4, $c(Mn^{2+}) = 10$ g/l, $T = 35°C$ and scan rate 1 mV/s.*

SEM images of the electrode surface during cyclic voltammetry scans are shown in figures 5.23-5.26. The bright particles consisted mainly of IrO_2, and the dark phase was rich in Ta_2O_5. Earlier in this project, it was believed that manganese dioxide deposited only on Ta_2O_5-rich areas, but element analysis of the surface when the scan was interrupted at the oxidation peak, showed the presence of manganese and oxygen over the entire surface (figure 5.23). It is difficult to see

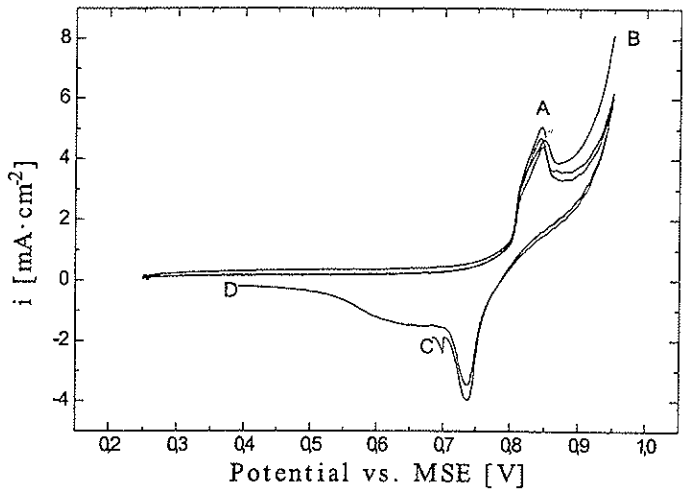

Figure 5.22: *Cyclic and linear voltammetry on a Ti/IrO_2 - Ta_2O_5 electrode in 2M H_2SO_4, $c(Mn^{2+})$ = 10 g/l, T = 35 °C, scan rate 1 mV/s. A; Scan interrupted at anodic peak (interval 250-850 mV). B; Scan interrupted at 950 mV before the oxygen evolution started (interval 250-950 mV). C; Scan interrupted after the first reduction peak (interval 250-950-700 mV). D; Scan interrupted after the "tail" (interval 250-950-400 mV).*

from the SEM image that manganese oxide species covered the entire surface, but it can be noticed that the IrO_2 particles look larger than on a clean Ti/IrO_2 - Ta_2O_5 electrode (figure 1.3 in section 1.1.1). When the scan was interrupted at 950 mV (figure 5.24), it was observed that the size of the IrO_2-particles looked bigger, and no large cracks were observed.

The surface of the deposit after the first reduction peak, is presented in figure 5.25. The electrode surface was completely covered by manganese oxide, and the apparent size of the IrO_2-particles had increased even more. A large amount of cracks was observed at this time. The cracks may have occurred because of stresses when the deposit thickness increased. The surface of the deposit did not seem to be more porous, as Lee et. al [55] had observed. They may have used higher magnification than in the present work.

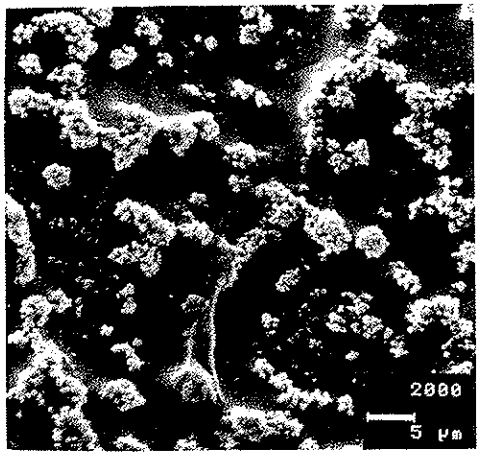

Figure 5.23: *Interval 250-850 mV. Interruption at the oxidation peak. 2000X.*

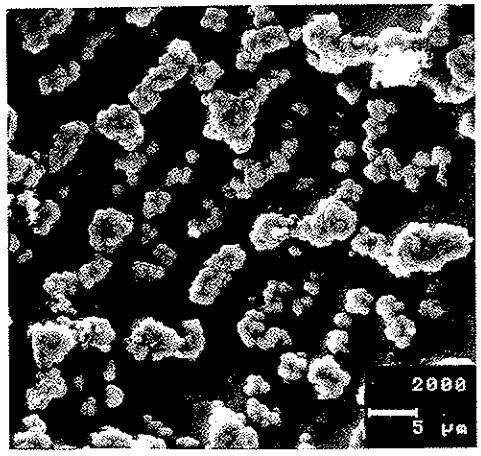

Figure 5.24: *Interval 250-950 mV. Interruption before full oxygen evolution. 2000X.*

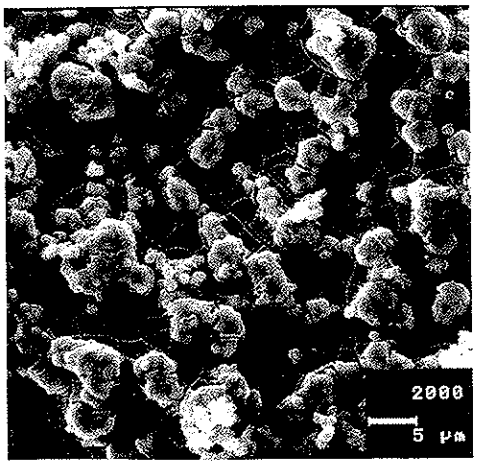

Figure 5.25: *Interval 250-950-700 mV. Interruption after first reduction peak. 2000X.*

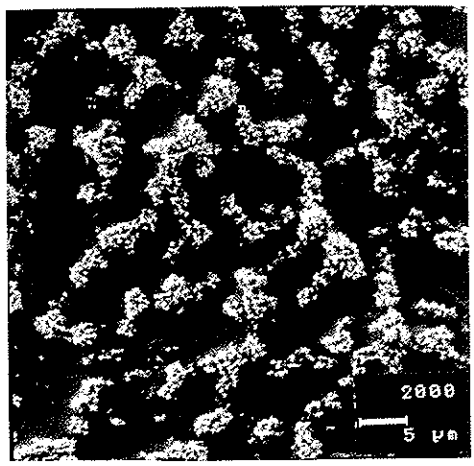

Figure 5.26: *Interval 250-950-400 mV. Interruption after the "tail". 2000X.*

From these results it seems that the first reduction peak is caused by reduction of manganese dioxide in the interior of the MnO_2 deposit, because no large changes were observed on the deposit surface. After the reduction "tail" (figure 5.26), where a current density plateau was observed, the electrode surface was regenerated and all the deposited manganese dioxide was reduced. The element analysis did not show any prints of manganese oxides on the surface after ~0 current density was obtained. This experiment shows that deposited manganese dioxide may be reduced electrochemically.

Reduction of deposited manganese dioxide

This experiment was performed to see if the reduction curve changed when different quantities of deposited manganese dioxide were to be reduced electrochemically. One Ti/IrO_2 - Ta_2O_5 electrode was used in these experiments. The electrode was polarized anodically at 850 mV (oxidation peak potential for MnO_2) for different time intervals (1-15 minutes). No oxygen evolution was observed on the electrode surface. The sequence of the experiments was random. After the polarization at 850 mV, the deposited manganese dioxide was reduced by linear voltammetry from 850 mV to 0 mV vs. MSE at scan rate 1 mV/s.

Figure 5.27 shows the linear voltammograms for reduction of deposited MnO_2. The initial current density got lower and lower when the polarization time increased. The reduction in the initial current density may have appeared because the deposition of MnO_2 occurs at the interface deposit/electrolyte as described by Jorgensen [43]. Increasing polarization time gives a thicker layer of deposit, which leads to higher ohmic resistance in the deposit and thereby lower current density.

The peak potential for the first reduction step increased by 20 mV when the polarization time was increased from 1 minute to 15 minutes, which may occur because of larger quantities of MnO_2 available on the electrode surface for reduction. The first reduction peak was very sharp as observed on the platinum electrodes, which may indicate passivation due to MnOOH formation. A second reduction peak was observed, which moved to more cathodic potentials when the polarization time increased, and it took longer time before the current approached zero, because larger amounts of deposited manganese dioxide were present on the electrode surface. This experiment shows that if large quantities of deposit is present on the electrode surface, the system needs longer time to reduce all the deposited MnO_2.

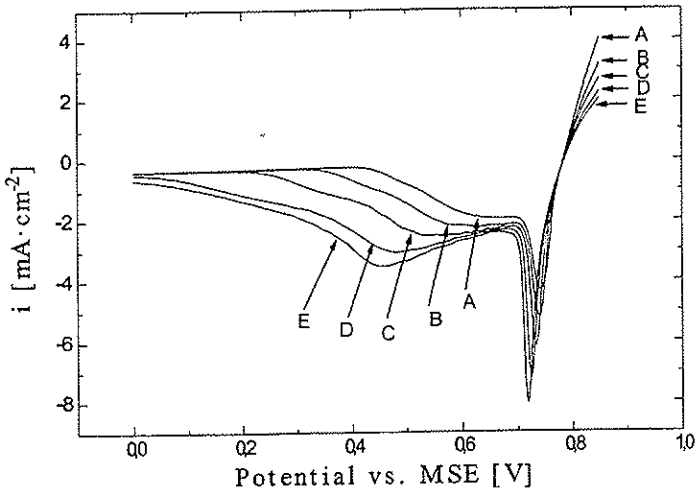

Figure 5.27: *Reduction of MnO_2 deposited on a Ti/IrO_2 - Ta_2O_5 electrode during different polarization times at 850 mV in 2M H_2SO_4, $c(Mn^{2+})$ = 10 g/l, T = 35° C, scan rate 1 mV/s and interval 850-0 mV. Polarization time: A; 1 minute. B; 2.5 minutes. C; 5 minutes. D; 10 minutes. E; 15 minutes.*

5.3 Linear sweep voltammetry

Polarization curves on various coatings in sulphuric acid

Polarization curves were recorded in pure 2M H_2SO_4 and in 2M H_2SO_4 containing $c(Mn^{2+})$ = 10 g/l. The various coatings used in these experiments (Ti/IrO_2 - Ta_2O_5, IrO_2top, IrO_2, $IrTaMnO_x5$, $IrTaMnO_x50$, $IrTaMnO_x75$ and $IrMnO_x$) are described in table 4.2, and the experimental procedure is described in section 4.3.2. The motivation for these experiments was to study the activity (the current density at a specific potential) of the various coatings in pure sulphuric acid and in electrolyte containing Mn^{2+} ions, and to compare the polarization curves (i as a function of applied potential).

Two polarization curves were recorded on each coating in 2M H_2SO_4, to see if the activity of the coatings had changed during the first experiment. The measured current densities were expected to be steady state values, and no correction was

applied for the ohmic drop between the capillary tip and the electrode surface. Nyquist diagrams described in Appendix B, showed that the electrolyte resistance between the capillary tip and the electrode surface, was 0.1 Ω and independent of the polarization potential applied to the working electrode. The electrolyte resistance did not have any large effect on the measured values in the potential range 0-1500 mV (see figure C.2 in Appendix C), which is of interest in the present work.

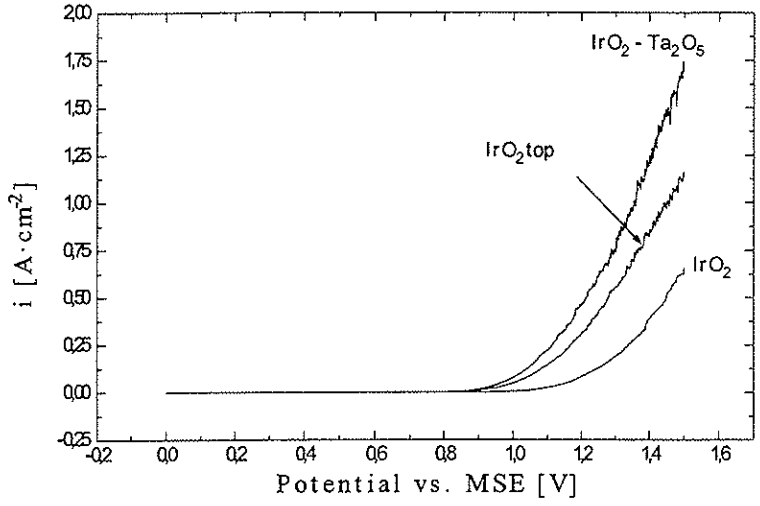

Figure 5.28: *Polarization curve on IrO_2 - Ta_2O_5, IrO_2top and IrO_2 coating in 2M H_2SO_4, T = 35° C, scan rate 1 mV/s and interval 0-1.5 V vs. MSE. First experiment.*

Figures 5.28 and 5.29 show the polarization curves obtained in 2M H_2SO_4 (first experiment) for the coatings IrO_2 - Ta_2O_5, IrO_2top, IrO_2 and IrO_2 - Ta_2O_5, $IrTaMnO_x5$, $IrTaMnO_x50$, $IrTaMnO_x75$ and $IrMnO_x$ respectively. The polarization curves for the second experiment are presented in figure C.1 in Appendix C.

Coating IrO_2 - Ta_2O_5 was observed to be the most active for all potentials (figure 5.28), which means that this coating exhibited the highest current density for a given potential. The electrode with pure IrO_2 coating was the least active. This may be because this coating did not cover the entire surface of the base metal. The Ti substrate may have been partially oksidized in contact with the electrolyte,

forming a nonconducting layer of TiO_2, as described by Martelli et al. [22] and Otogawa et al. [26].

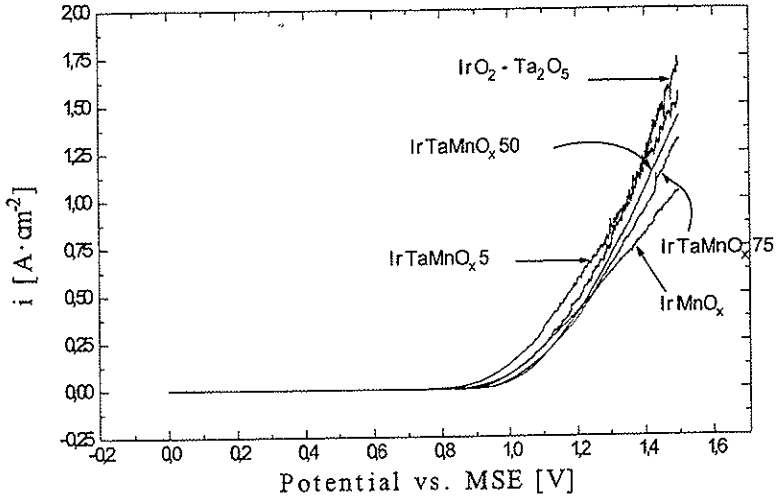

Figure 5.29: *Polarization curves on IrO_2 - Ta_2O_5, $IrTaMnO_x5$, $IrTaMnO_x50$, $IrTaMnO_x75$ and $IrMnO_x$ coatings in 2M H_2SO_4, T = 35° C, scan rate 1 mV/s and interval 0-1.5 V vs. MSE. First experiment.*

Also the IrO_2top coating was observed to be less active than IrO_2 - Ta_2O_5. From the SEM image of this coating (figure 5.3), no cracks or pores were observed, so the formation of an insulating layer of TiO_2 at the interface coating/base metal was unlikely. One might expect that this coating should show higher electrocatalytic activity than IrO_2 - Ta_2O_5, because it contained higher quantities of IrO_2 crystals on the coating surface, which should give a higher surface area of catalytic sites. As outlined in section 3.5.1, the Ta_2O_5 in the coating is not electrochemically active for oxygen evolution, and it only stabilizes IrO_2 chemically during anodic polarization. The reason why the IrO_2top coating was less active than IrO_2 - Ta_2O_5 is difficult to explain, and it needs further investigation.

Figure 5.29 presents the polarization curves for coatings IrO_2 - Ta_2O_5, $IrTaMnO_x5$, $IrTaMnO_x50$, $IrTaMnO_x75$ and $IrMnO_x$ in 2M H_2SO_4. The polarization curve of coating IrO_2 - Ta_2O_5 (the same curve as in figure 5.28) was included, to compare its electrocatalytic properties with the coatings where some of the Ta_2O_5 content was replaced by MnO_x. This figure shows that the coating

with 5 mol% MnO_x was the most active at low potentials. At potentials above 1.4 V vs. MSE, IrO_2 - Ta_2O_5 was the most active coating. At potentials above 1.2 V vs. MSE, increasing quantities of MnO_x (50 - 100%) in the coating, gave less electrocatalytic coatings.

From the SEM images (figures 5.6, 5.7 and 5.8) in section 5.1, it was observed that the coatings with high quantities of MnO_x (50 - 100%), consisted of cracks, and no agglomerates of IrO_2 were formed. The cracks may not have penetrated into the base metal, because some activity was observed although it was lower than for IrO_2 - Ta_2O_5 and $IrTaMnO_x5$.

Table 5.2: *Current densities for the various coatings in 2M H_2SO_4 and H_2SO_4 containing c(Mn^{2+}) = 10 g/l at T = 35° C at applied potential 1.1 V vs. MSE.*

Coating	i_1 [A/cm^2]	i_2 [A/cm^2]	$i_{Mn^{2+}}$ [A/cm^2]
IrO_2 - Ta_2O_5	0.22	0.35	0.11
IrO_2top	0.15	0.25	0.09
IrO_2	0.02	0.11	0.09
$IrTaMnO_x5$	0.31	0.46	0.13
$IrTaMnO_x50$	0.17	0.25	0.13
$IrTaMnO_x75$	0.17	0.23	0.10
$IrMnO_x$	0.22	0.23	0.10

Current density values for the various coatings at applied potential 1.1 V vs. MSE (where the oxygen evolution proceeded), are presented in Table 5.2. Higher current densities were observed in the second experiment than in the first experiment for all coatings. According to Comninellis and Vercesi [14], new DSA® electrodes go through an activation period, where the activity of the electrode increases until it reaches a maximum. The increase in the current densities may be due to this "activation" period. The $IrTaMnO_x5$ coating was the most active at potential 1.1 vs. MSE, exhibiting the highest current density. The pure IrO_2 coating was the least active for all potentials, indicating formation of small quantities of a passivating layer of TiO_2 at the interface base metal/coating, because it was observed an increased activation in the second experiment. The conclusion of these experiments is that IrO_2 - Ta_2O_5 and small amounts of MnO_x in the coating, give the most electrocatalytic coating.

These experiments were only performed for short times (30 minutes). It should be mentioned that the activity of the coatings may differ as a function of time and current density. It is also important to remember possible variations in the real surface area from one coating to another.

Polarization curves on oxygen-evolving coatings in sulphuric acid containing Mn^{2+} ions

Experiments with polarization curves in 2M H_2SO_4 containing Mn^{2+} ions, were performed to see how much the electrocatalytic activity of the coatings was reduced because of deposition of MnO_2 on the surface. Figures 5.30 and 5.31 show the polarization curves on the coatings IrO_2 - Ta_2O_5, IrO_2top, IrO_2, $IrTaMnO_x5$ and $IrTaMnO_x50$, $IrTaMnO_x75$, $IrMnO_x$ respectively.

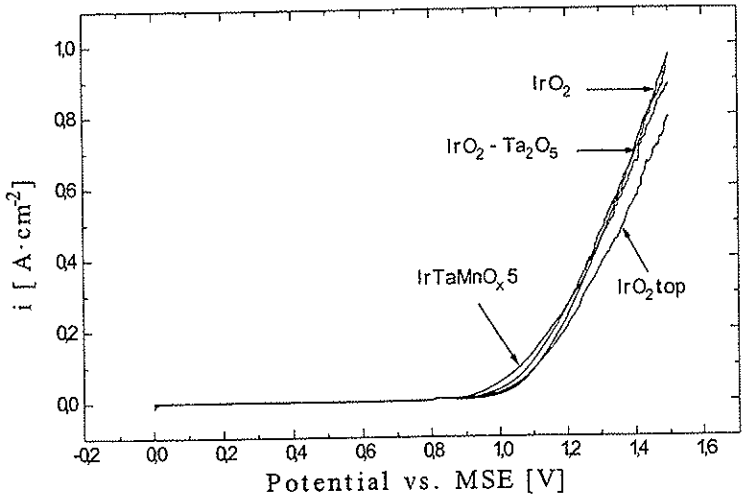

Figure 5.30: *Polarization curves on IrO_2 - Ta_2O_5, IrO_2top and IrO_2 in 2M H_2SO_4, c(Mn^{2+}) = 10 g/l, T = 35° C, interval 0-1.5 V vs. MSE and scan rate 1 mV/s.*

If figures 5.30 and 5.31 are compared to figures 5.28 and 5.29, it is obvious that deposition of MnO_2 blocked the electrocatalytic sites on the electrode surface to some extent. The current density at 1.5 V vs. MSE for the coatings in pure

H_2SO_4 was ~0,6 - 1,75 A/cm^2, while it was reduced to 0.5 - 0.95 A/cm^2 in 2M H_2SO_4 containing c(Mn^{2+}) = 10 g/l.

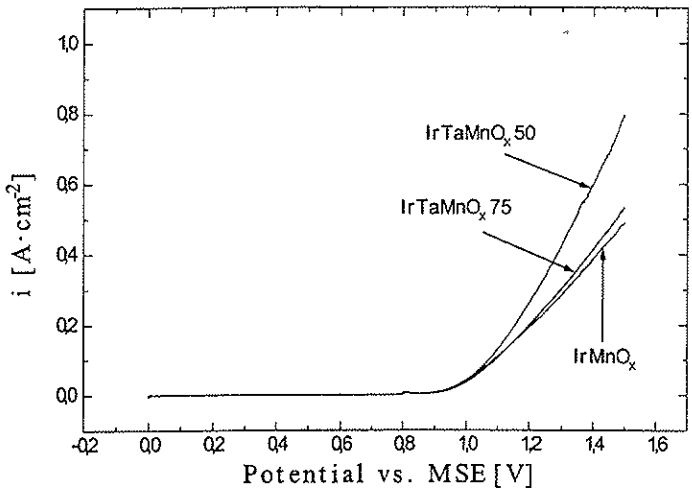

Figure 5.31: *Polarization curves on $IrTaMnO_x50$, $IrTaMnO_x75$ and $IrMnO_x$ coatings in 2M H_2SO_4, c(Mn^{2+}) = 10 g/l, T = 35° C, potential interval 0-1.5 V vs. MSE and scan rate 1 mV/s.*

The current densities for the various coatings, when potential 1.1 V vs. MSE was applied in 2M H_2SO_4 containing c(Mn^{2+}) = 10 g/l, are presented in table 5.2. These current densities seemed to be independent of the coating composition, which is opposite to the observations in 2M H_2SO_4, where the current density varied for the various coatings. The deposition of MnO_2 took place before the oxygen evolution started, as observed in section 5.2. The MnO_2 deposit may have caused approximately similar surface conditions for further oxygen evolution and oxidation of Mn^{2+} to MnO_2, giving nearly identical current densities.

5.4 Galvanostatic electrolysis

In this section, results of anode potential as a function of time will be presented. The main coating tested here was IrO_2 - Ta_2O_5, but the behaviour of the modified coatings in pure 2M H_2SO_4 will also be described as a function of current density.

The standard electrolysis parameters during the galvanostatic electrolysis tests were as follows; 2M H_2SO_4, c(Mn^{2+}) = 10 g/l, T = 35°C and i = 0.05 A/cm^2 (geometric). Experiments with a lead anode alloyed with silver (Pb/Ag) and Pt as anode material, were included to compare the electrode potential of the various anode materials, as a function of electrolysis time in sulphuric acid containing Mn^{2+} ions.

5.4.1 Effect of current density on modified coatings in sulphuric acid.

The coatings tested in this experiment were IrO_2 - Ta_2O_5, IrO_2top, IrO_2, $IrTaMnO_x5$, $IrTaMnO_x50$, $IrTaMnO_x75$ and $IrMnO_x$. The temperature was kept constant at 35°C, and the current densities were; 0.05, 0.5 and 1 A/cm^2, where each current density was kept constant for 10 hours. The anode potential vs. MSE in 2M H_2SO_4 as a function of the electrolysis time for the various coatings, is presented in figure 5.32.

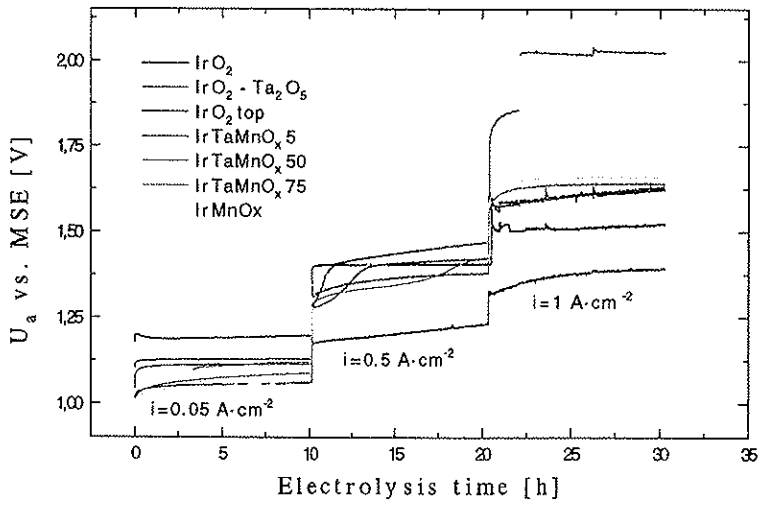

Figure 5.32: *Anode potential vs. MSE on IrO_2 - Ta_2O_5, IrO_2top, IrO_2, $IrTaMnO_x5$, $IrTaMnO_x50$, $IrTaMnO_x75$ and $IrMnO_x$ as a function of electrolysis time and current density in 2M H_2SO_4 at T = 35° C.*

For the lowest current density there was no large increase in the anode potential. The increase in anode potential in the first minutes of the experiments, may be due to lower surface area caused by oxygen gas filling pores and cracks. The difference between the lowest ($IrTaMnO_x5$) and highest (IrO_2) anode potentials was about 75 mV for the lowest current density (i = 0.05 A/cm^2) after electrolysis for 10 hours.

When the current density was increased ten times (to 0.5 A/cm^2), it was observed a slightly larger increase in the anode potential for all coatings. For some of the coatings (IrO_2 - Ta_2O_5, IrO_2top, $IrTaMnO_x50$ and $IrTaMnO_x75$) the increase in anode potential had an "s"-shape. The reason for this "s"-shape is not easily explained, but it might occur because of slow formation of insulating oxides or a change in the crystal structure and electron configuration of the coating components. The increase in anode potential varied from one coating to the other, and it occurred at different time intervals. The $IrTaMnO_x5$ coating had the lowest anode potential, while the IrO_2top coating had the highest value. The difference between the lowest and highest anode potential had increased to 240 mV after 20 hours of electrolysis.

At a current density of 1 A/cm^2 there was not observed any "s"-shaped increase in the anode potential for none of the coatings. Also at this current density the $IrTaMnO_x5$ coating had the lowest anode potential. The increase in anode potential was largest for this coating (90 mV), while it was insignificant for the other coatings. The large increase in anode potential for the $IrTaMnO_x50$ coating after 22 hours of electrolysis occurred because of an accidental movement of the capillary tip away from the electrode surface. The difference in anode potential between the lowest and the highest potential was 450 mV, if the potential increase for $IrTaMnO_x50$ is neglected.

After electrolysis for 30 hours, the electrodes were taken out and washed with distilled water and dried in air. The electrodes were weighed before and after electrolysis to see if there was any loss of coating during electrolysis at high current densities. Table 5.3 shows the weight difference for each coating. There were not observed any negative changes in weight during electrolysis. On the contrary, there was a slight increase in weight. The coatings IrO_2 and $IrMnO_x$ had the highest increase, 0.18 and 0.17 mg/cm^2 respectively. The positive change in weight may be explained by formation of higher valency oxides on the anode surface or formation of titanium dioxide at the interface substrate/coating.

SEM images of the electrode surface after electrolysis did not show any visible changes, which could indicate dissolution or breakdown of the coatings. The

Table 5.3: *Difference in weight before and after 30 hours of electrolysis in 2M H_2SO_4, T = 35° C and current densities; 0.05, 0.5 and 1 A/cm^2.*

Coating	Δm [mg/cm^2]
IrO_2 - Ta_2O_5	+0.15
IrO_2top	0
IrO_2	+0.18
$IrTaMnO_x5$	+0.1
$IrTaMnO_x50$	+0.13
$IrTaMnO_x75$	+0.15
$IrMnO_x$	+0.17

surface looked almost the same as before electrolysis. It was expected that the coatings might break down during the highest current density, but that did not happen. These experiments tell us that these coatings may be used at high current densities. However, it is not known whether the coatings will survive in long term electrolysis (months and years) at high current densities.

Potentiostatic electrolysis in sulphuric acid

In figure 5.32 it was observed that the anode potential increased in the beginning of the electrolysis experiments in pure 2M H_2SO_4. To study how the current density changed during the first minutes, an electrolysis experiment with constant applied potential (1.2 V vs. MSE) on a Ti/IrO_2 - Ta_2O_5 anode, was conducted in 2M H_2SO_4 at T = 35°C. The anode area was 1 cm^2.

Figure 5.33 shows the anodic current as a function of electrolysis time for 1 hour and 10 hours. The electrolysis was interrupted for 2 minutes after one hour, and then resumed for 10 hours with the same applied potential. It was observed from curves a and b that the anode current decreased rapidly in the beginning and thereafter decreased only insignificantly. When the electrolysis was restarted after the interruption, the current started at high current density and decreased immediately as was observed for curve a. These observations correspond to the increase in the anode potential in the beginning of galvanostatic electrolysis independent of Mn^{2+} ions in the electrolyte. The increase in the anode potential, and decrease in the anode current may be due to a decrease in the active surface area for oxygen evolution, caused by pores or cracks filled with oxygen gas. Krysa et al. [15] also observed that the anode potential was lower

after the interruption, but could not give any reasonable explanation for that observation.

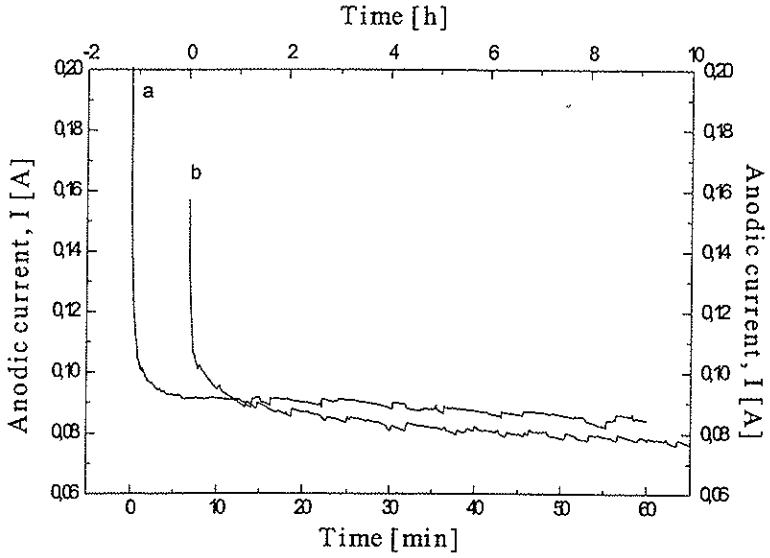

Figure 5.33: *Anodic current as a function of electrolysis time when a constant potential (1.2 V vs. MSE) was applied to a Ti/IrO_2 - Ta_2O_5 anode in 2M H_2SO_4 at T = 35° C. The anode area was 1 cm^2. a; anode current for the first hour. b; anode current for the next 10 hours.*

5.4.2 Electrolysis on Pb/Ag and Pt as anode materials

The lead anode (Pb/Ag) used in this experiment was polished, and electrolysis was conducted in 2M H_2SO_4 containing c(Mn^{2+}) = 10 g/l at T = 35°C and i = 0.05 A/cm^2. The anode potential vs. MSE is plotted in figure 5.34. The anode potential was high and increased slightly during the first 10 hours of electrolysis. After electrolysis for 10 hours, the current was switched off while the anode remained in the electrolyte. Cyclic voltammetry was performed for 30 minutes, and then a new period of 10 hours electrolysis was started. The anode potential in the second electrolysis period was lower than in the first period. This decrease might have occurred because of dissolution of some of the deposited MnO_2, or change in the surface area during the cyclic voltammetry measurements.

Forsèn [7] studied lead anodes in sulphuric acid (100 g/l) containing Mn^{2+} ions at 35°C, and observed that MnO_2 adhered poorly to the lead anode and was

dispersed in the bulk electrolyte. In the present work, this was not observed because no forced convection was introduced. The electrolyte was red coloured, but no visible MnO_2 was suspended in the bulk electrolyte, as observed in Norzink's industrial cell. Only two electrolysis periods of 10 hours each were performed because the electrode surface area changed during the electrolysis, due to the formation of huge dendrites on the anode surface. It is suggested that the oxidation of Mn^{2+} occurred on the deposited MnO_2, otherwise the dendrites could not have grown that large.

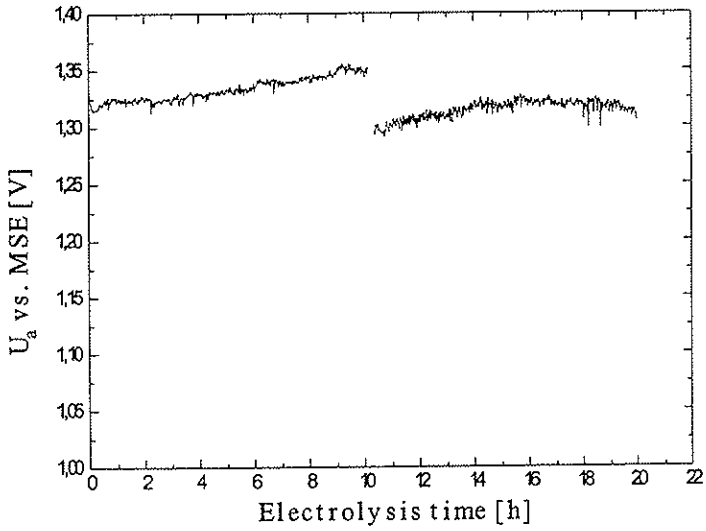

Figure 5.34: *The anode potential vs. MSE as a function of electrolysis time for Pb/Ag anode in 2M H_2SO_4 containing $c(Mn^{2+}) = 10$ g/l at $T = 35°C$ and $i = 0.05$ A/cm^2.*

Figure 5.35 shows an SEM image of the cross section of the Pb/Ag anode after electrolysis for 20 hours (2 electrolysis periods). The white area is the lead anode, while the dark grey phase is the deposited MnO_2. The bright areas in the MnO_2 deposit were found to be lead components. Small quantities of the lead anodes may have been smeared out on the deposit during the polishing before the SEM analysis, but it is also a possibility that Pb^{2+} ions from the corroded lead anode diffused through the porous MnO_2 deposit and into the bulk electrolyte. The occurrence of the lead components in the deposited MnO_2 may have increased its electronic properties.

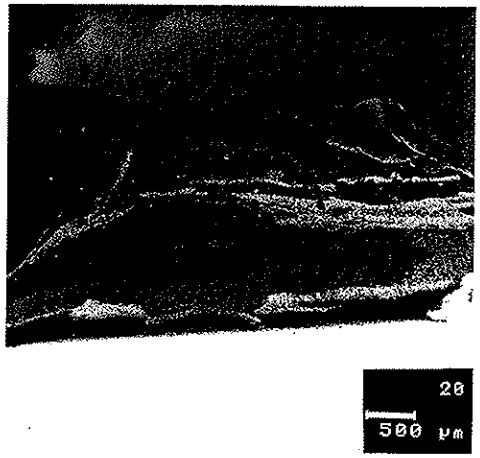

Figure 5.35: *SEM image of the cross section of a Pb/Ag anode after electrolysis for 20 hours in 2M H_2SO_4 containing $c(Mn^{2+}) = 10$ g/l at $T = 35°C$ and $i = 0.05$ A/cm^2. 20X.*

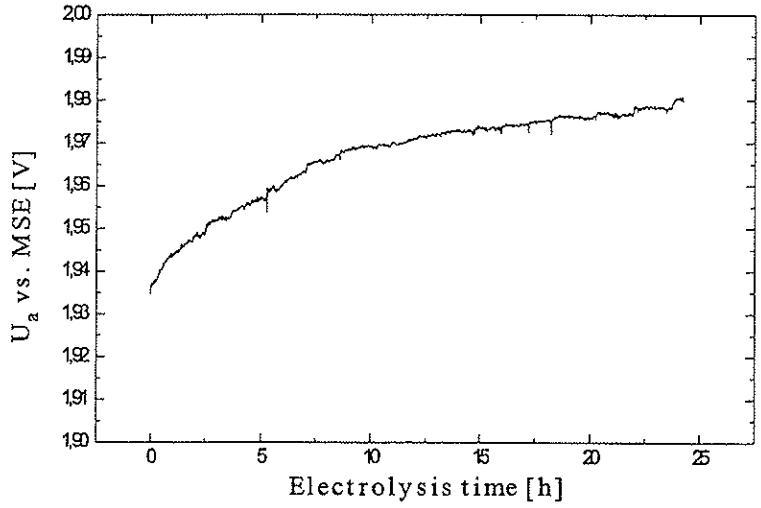

Figure 5.36: *Anode potential for Pt as a function of electrolysis time in 2M H_2SO_4 containing $c(Mn^{2+}) = 10$ g/l at $T = 35°C$ and $i = 0.05$ A/cm^2.*

When Pt was used as anode during electrolysis in 2M H_2SO_4 containing c(Mn^{2+}) = 10 g/l at T = 35°C and i = 0.05 A/cm^2, large quantities of suspended MnO_2 were observed in the bulk electrolyte. The anode potential as a function of electrolysis time is shown in figure 5.36. The increase in the anode potential was not as expected. The pure Pt electrode should obtain a higher anode potential than the Pt anode with deposited MnO_2, according to overpotential - log(i) curves reviewed by Trasatti [25]. The anode potential should decrease when MnO_2 deposited during electrolysis, but the opposite effect was observed. The suspended MnO_2 particles were also observed in the capillary tip after the electrolysis. Suspended MnO_2 particles may have increased the electrolyte resistance between the anode surface and the capillary tip, causing an increase in the measured anode potential.

When the Pt anode was taken out of the cell and washed in distilled water, most of the deposited MnO_2 fell off the electrode surface as small, fine crystals. The adherence of the MnO_2 deposit on the Pt surface was very poor compared to the Pb/Ag anode, and it led to huge quantities of dispersed MnO_2 in the electrolyte. The anode potential was observed to be higher for the Pt anode (1.94 V vs. MSE) than for the lead anode (1.30-1.35 V vs. MSE). Because of the high anode potential on the Pt, permanganate (MnO_4^-) may have been formed according to equation 3.30 in section 3.6.1. Parts of the dispersed MnO_2 may have been produced by the reaction between MnO_4^- and Mn^{2+} in the bulk as given by equation 3.31 in section 3.6.1.

5.4.3 Ti/IrO_2 - Ta_2O_5 as anode material in sulphuric acid containing Mn^{2+} ions

The periodic electrolysis was performed in the same way as for the Pb/Ag anode described in section 5.4.2. The electrolysis was run for 10 hours in 2M H_2SO_4 containing c(Mn^{2+}) = 10 g/l at T = 35°C and i = 0.05 A/cm^2. After the electrolysis period, the Ti/IrO_2 - Ta_2O_5 anode with MnO_2 deposit was used as working electrode in cyclic voltammetry, in the same electrolyte as the electrolysis was performed. Five electrolysis periods were conducted, separated by cyclic voltammetry on a Ti/IrO_2 - Ta_2O_5 anode as the working electrode. Figure 5.37 shows the anode potential as a function of the electrolysis time. It was assumed that changes in the Mn^{2+} concentration in the electrolyte could be neglected, since the current efficiency for MnO_2 is low in acid concentrations as high as 2M.

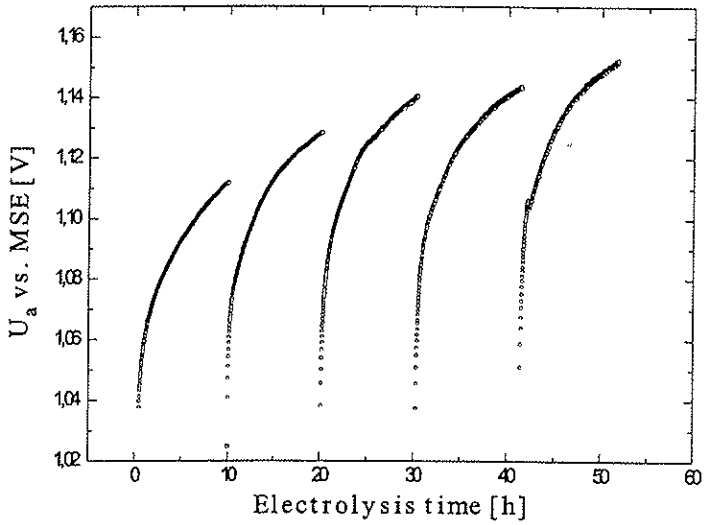

Figure 5.37: *The anode potential as a function of electrolysis time for periodic electrolysis with Ti/IrO_2 - Ta_2O_5 as the anode in 2M H_2SO_4 containing c(Mn^{2+}) = 10 g/l at T = 35° C and i = 0.05 A/cm^2. Each electrolysis period lasted for 10 hours.*

After each electrolysis period, the applied current was switched off and cyclic voltammetry was conducted in the same electrolyte at scan rate 10 mV/s. After the voltammetry measurement, the electrolysis was started for a new 10 hour period. When the current was applied and the oxygen evolution started, it was observed that the deposited MnO_2 fell off the anode as one flake. The initial anode potential after each cyclic voltammetry measurement was observed to be quite low, and then it increased rapidly to higher potentials. The anode potential at the end of each electrolysis period was higher than observed for the previous one, which may be caused by a thicker deposit layer. It is not known if all the deposited MnO_2 fell off when the oxygen evolution started after the break, or if a thin layer was left on the electrode surface.

The electrolyte was red coloured as observed in the electrolysis experiment with the lead anode, but no dispersed MnO_2 was observed in this experiment either. After electrolysis in 2M H_2SO_4 containing c(Mn^{2+}) = 10 g/l at T = 35°C for 10 hours with the Ti/IrO_2 - Ta_2O_5 as anode material, the electrolyte was studied by a spectrophotometer to see if the red colour was due to MnO_4^- or Mn^{3+} ions. Figure 5.38 shows that spent electrolyte after electrolysis contained Mn^{3+} ions and no MnO_4^-.

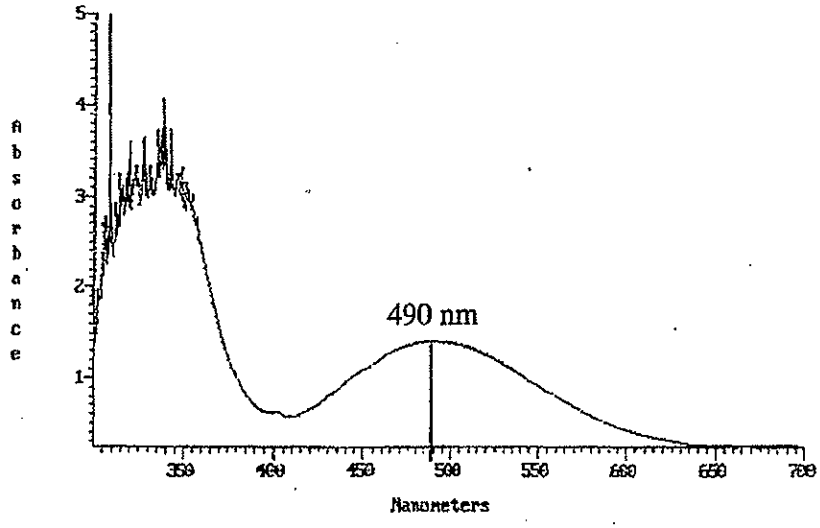

Figure 5.38: *The absorption spectrum of the Mn^{3+} in spent electrolyte after electrolysis in 2M H_2SO_4 containing $c(Mn^{2+}) = 10$ g/l at $T = 35°C$ and $i = 0.05$ A/cm^2 for 10 hours, with Ti/IrO_2 - Ta_2O_5 as anode material [72].*

5.4.4 Effect of Mn^{2+} ions on the anode potential

In section 5.4.1 we have seen that at 0.05 A/cm^2 current density in pure 2M H_2SO_4, there was no large changes in the anode potential. If Mn^{2+} ions are present in the electrolyte, deposition of manganese dioxide will occur as a parasitic reaction to the oxygen evolution, as described in section 1.1. We have also seen that deposition of manganese dioxide occurs at lower oxidation potentials than oxygen evolution on both Pt and Ti/IrO_2 - Ta_2O_5 electrodes (section 5.2). When MnO_2 is deposited on the anode surface, it covers the entire surface area and blocks the catalytic sites (IrO_2 crystals), reducing the active surface area. This will be shown later in SEM images. When MnO_2 is deposited on the anode surface, the anode potential increases because the deposited MnO_2 is less active (higher oxygen overvoltage) than the IrO_2 for oxygen evolution (see figure 3.8 in section 3.5). The ohmic resistance through the deposit layer may increase with the time of electrolysis due to thicker deposit.

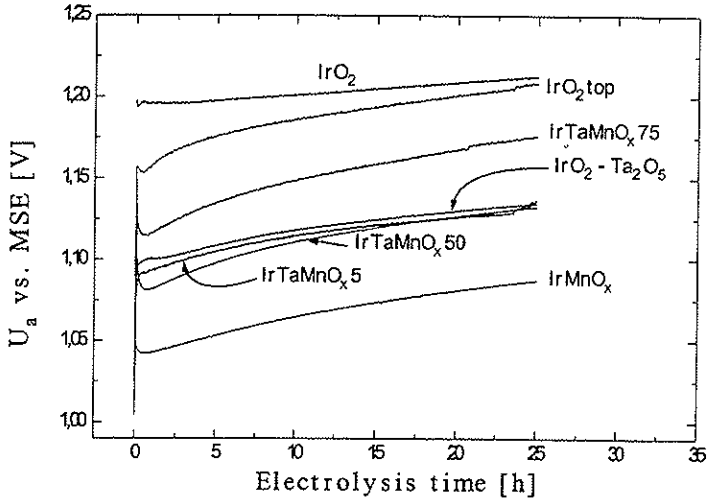

Figure 5.39: *Anode potential for various coatings, as a function of electrolysis time in 2M H_2SO_4, $c(Mn^{2+})$ = 10 g/l, T = 35° C and i = 0.05 A/cm^2.*

Figure 5.39 shows the anode potential vs. MSE for the various coatings as a function of the electrolysis time in 2M H_2SO_4 containing 10 g/l Mn^{2+} at standard electrolysis parameters. The anode potential increased very much during the first minutes, and then decreased initially for the coatings containing large amounts of manganese oxide (50-100 mol%). After 30 minutes of electrolysis, the anode potential started to increase again. The increase in anode potential was approximately the same for all coatings except for the pure IrO_2 coating. The low increase in electrode potential for the IrO_2 coating may be explained by some activation of the surface caused by deposition of manganese dioxide, because the IrO_2 coating did not cover the entire Ti base metal. For the other coatings, the effect of deposition of manganese dioxide is apparently independent of the composition of the coating.

After the electrolysis, the anodes were taken out of the electrolyte while they were polarized, and washed with distilled water, dried in air and weighed. The weight increase for the deposition and the current efficiency for MnO_2 on the various coatings are given in Table 5.4. These results show the same as observed in the cyclic voltammetry measurements on platinum and IrO_2/Ta_2O_5 coatings, i.e. that the oxidation of Mn^{2+} to MnO_2 is independent of the electrode material.

Table 5.4: *Amount of deposit and current efficiency for MnO_2 on the various coatings in 2M H_2SO_4 containing $c(Mn^{2+}) = 10$ g/l at $T = 35°C$ and $i = 0.05$ A/cm^2 after electrolysis for 25 hours.*

Coating	Δm [mg/cm^2]	S [%]
IrO_2	+3.83	0.19
IrO_2 - Ta_2O_5	+3.07	0.15
IrO_2top	+2.77	0.14
$IrTaMnO_x5$	+2.78	0.14
$IrTaMnO_x50$	+3.13	0.15
$IrTaMnO_x75$	+2.98	0.15
$IrMnO_x$	+3.08	0.15

The diffusion of Mn^{2+} ions to the electrode surface is controlling the rate of oxidation of Mn^{2+} to MnO_2, as suggested earlier in the literature [66], so the catalytic properties of the electrode materials are insignificant. When the first thin layer of manganese dioxide is formed/deposited on the electrode surface, the conditions for further deposition is similar for all electrode materials, since deposition of manganese dioxde occurs at the interface deposit/electrolyte as described by Jorgensen [43]. Very similar values for the current efficiency for the various coatings support this theory.

The surface of the deposited MnO_2 on the various coatings was investigated by SEM after electrolysis. The deposited MnO_2 looked similar for all the coatings, a dried-mud structure being observed as shown in figure 1.4 in section 1.1.1. From the SEM images taken of the electrode surface (Ti/IrO_2 - Ta_2O_5) during cyclic voltammetry of MnO_2 deposition (figures 5.23-5.26 in section 5.2.2) no cracks were observed on the deposit when it was very thin, while there were numerous cracks when the deposit thickness increased. The cracks may have been formed during electrolysis because of stresses as the deposit grew thicker.

5.4.5 Deposition of manganese dioxide on a Ti/IrO_2 - Ta_2O_5 anode as a function of the Mn^{2+} concentration

Electrolysis in 2M sulphuric acid containing various Mn^{2+} concentrations (0.01-10 g/l) was carried out to see if there existed a lower concentration limit for manganese dioxide deposition on the IrO_2 - Ta_2O_5 coating. Figure 5.40 shows the anode potential as a function of electrolysis time for various Mn^{2+} concentrations (0.01, 5 and 10 g/l). The anode potential was expected to increase with increasing Mn^{2+} concentration, because a thicker MnO_2 deposit would give higher ohmic resistance through the deposit. The lowest and highest anode potentials were observed for $c(Mn^{2+}) = 0.01$ g/l and $c(Mn^{2+}) = 10$ g/l respectively, as expected.

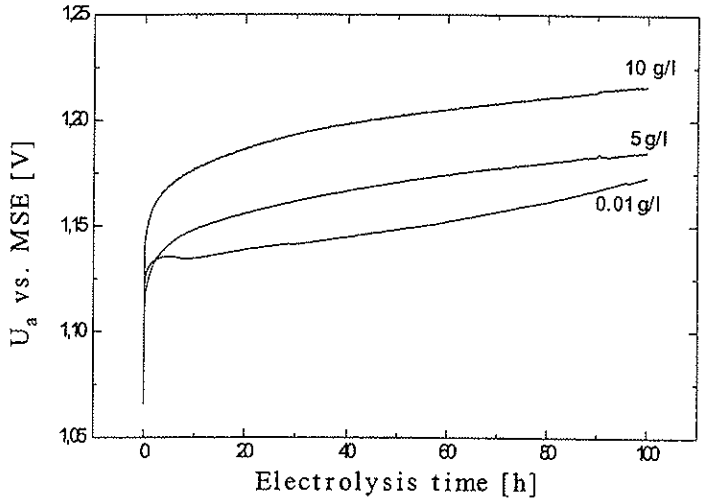

Figure 5.40: *Anode potential on Ti/IrO_2 - Ta_2O_5 as function electrolysis time and Mn^{2+} concentration in 2M H_2SO_4 containing $c(Mn^{2+}) = 0.01$, 5 and 10 g/l at $T = 35°C$ and $i = 0.05$ A/cm^2.*

Scanning Electron Microscope images of deposited manganese dioxide on a Ti/IrO_2 - Ta_2O_5 anode

Ti/IrO_2 - Ta_2O_5 anodes were used in electrolysis with various Mn^{2+} concentrations (0.01, 0.1, 1, 5 and 10 g/l), to study the MnO_2 deposit on the anode surface as a function of the Mn^{2+} concentration, and as a function of electrolysis time. The electrodes were taken out of the electrolyte at definite times (1, 10, 50 and 100 hours), washed with distilled water, dried in air, and examinated by SEM. Figures 5.41 - 5.60 show SEM images for the various Mn^{2+} concentrations and times of electrolysis. All the images were taken in secondary electron modus (SE) in the Scanning Electron Microscope instrument. The deposit layer was not investigated with element analysis, but the SEM images were compared with a new electrode, which had not been used in electrolysis.

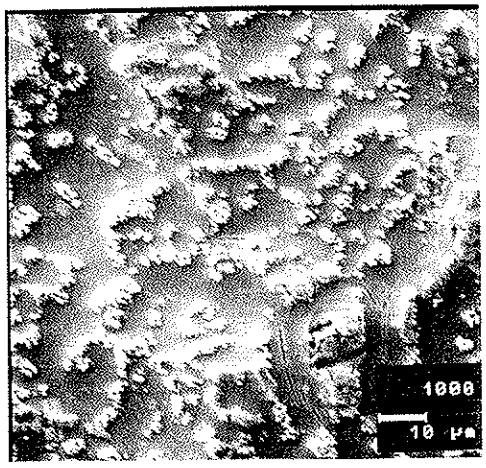

Figure 5.41: *Ti/IrO_2 - Ta_2O_5 used in electrolyte with $c(Mn^{2+}) = 0.01$ g/l for 1 hour. 1000X.*

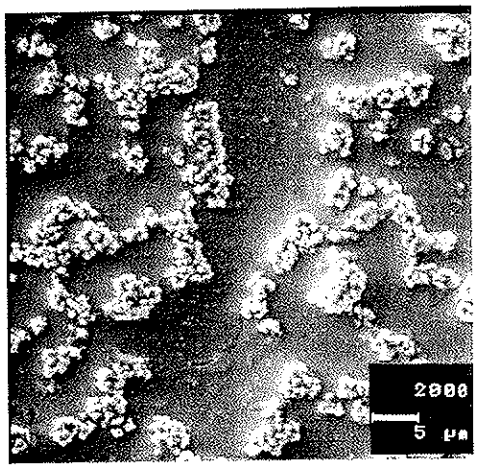

Figure 5.42: *Ti/IrO_2 - Ta_2O_5 used in electrolyte with $c(Mn^{2+}) = 0.01$ g/l for 10 hours. 2000X.*

After 1 hour of electrolysis with 0.01 g/l Mn^{2+}, no visible quantities of deposited MnO_2 were observed on the anode surface, as shown in figure 5.41. After ten hours of electrolysis (figure 5.42) it can be seen that the IrO_2 particles had grown bigger and were more diffuse because of nucleation of MnO_2. There were not observed any cracks in the deposit because it was very thin. Figure 5.43 presents the anode surface after electrolysis for 50 hours, and it can be observed that more MnO_2 had deposited, but still no cracks were observed. However, after electrolysis for 100 hours, small cracks were observed in the deposit on the Ta_2O_5-rich areas.

From these images it is clear that even as low concentration as 0.01 g/l of Mn^{2+}, leads to deposition of manganese dioxide during anodic polarization. Tanskanen et al. [69] studied the MnO_2 deposition on DSA® electrodes in sea water with 10 ppm Mn^{2+} and observed deposition of MnO_2.

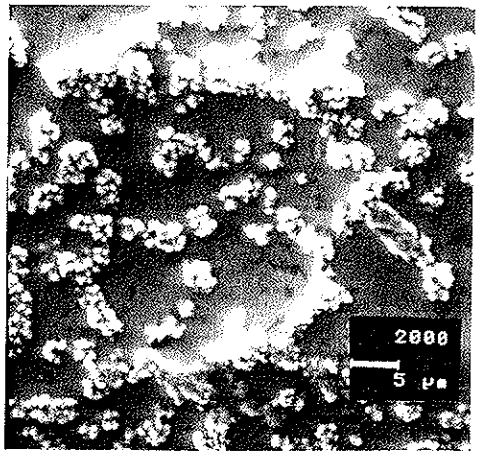

Figure 5.43: *Ti/IrO_2 - Ta_2O_5 used in electrolyte with c(Mn^{2+}) = 0.01 g/l for 50 hours. 2000X.*

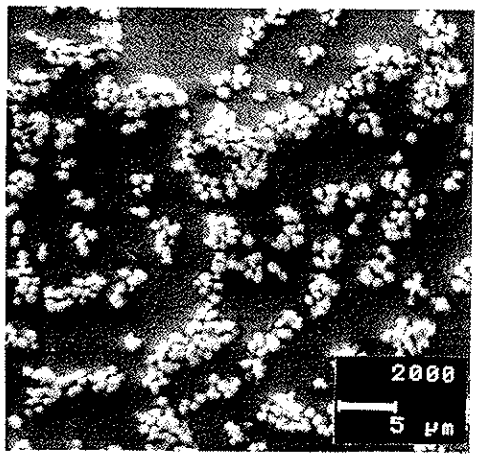

Figure 5.44: *Ti/IrO_2 - Ta_2O_5 used in electrolyte with c(Mn^{2+}) = 0.01 g/l for 100 hours. 2000X.*

When the Mn^{2+} concentration was increased ten times to 0.1 g/l, very small amounts of manganese dioxide were observed on the anode surface after electrolysis for 1 hour, as can be seen from figure 5.45, and no cracks were observed. After electrolysis for 10 hours most of the electrode surface was covered by MnO_2 (figure 5.46). Only a few cracks were observed in the deposit. Figure 5.47 shows that the entire anode surface was covered by MnO_2 with large cracks. The contours of IrO_2 particles were visible under the deposit. After electrolysis for 100 hours (figure 5.48) the deposit had grown thicker and the cracks were dividing the deposit in grains of about 10 μm size.

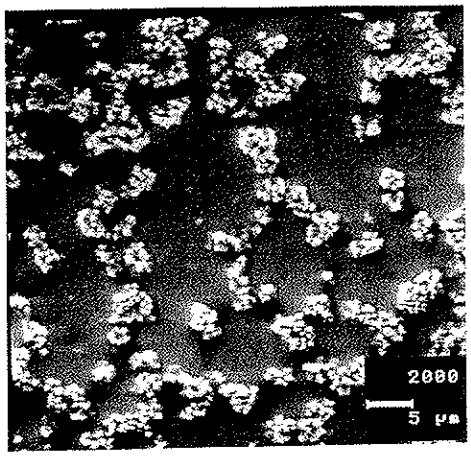

Figure 5.45: *Ti/IrO_2 - Ta_2O_5 used in electrolyte with $c(Mn^{2+}) = 0.1$ g/l for 1 hour. 2000X.*

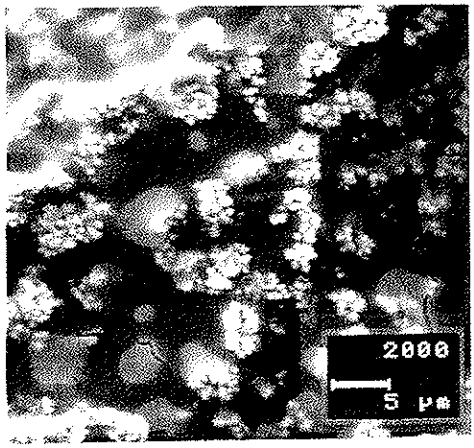

Figure 5.46: *Ti/IrO_2 - Ta_2O_5 used in electrolyte with $c(Mn^{2+}) = 0.1$ g/l for 10 hours. 2000X.*

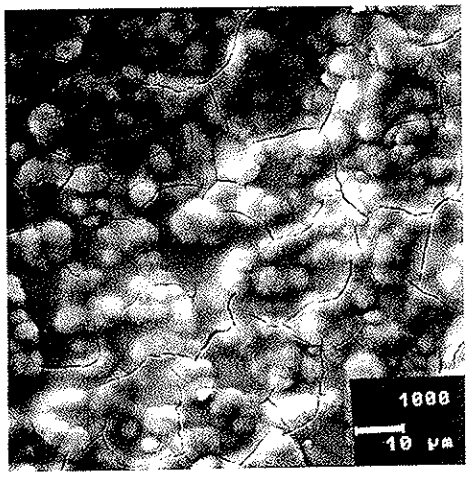

Figure 5.47: *Ti/IrO_2 - Ta_2O_5 used in electrolyte with $c(Mn^{2+}) = 0.1$ g/l for 50 hours. 1000X.*

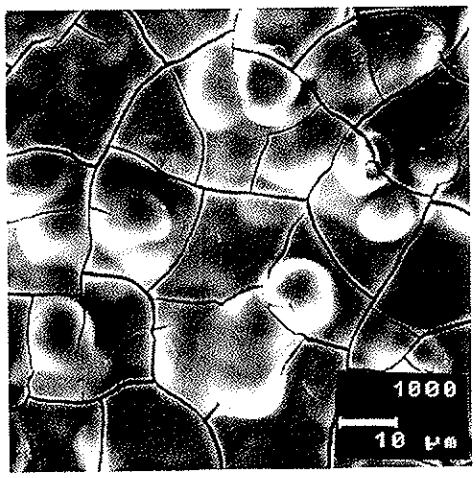

Figure 5.48: *Ti/IrO_2 - Ta_2O_5 used in electrolyte with $c(Mn^{2+}) = 0.1$ g/l for 100 hours. 1000X.*

When the Mn^{2+} concentration was increased to 1 g/l, the MnO_2 deposit had covered the entire anode surface after 1 hour of electrolysis, and the deposit contained some cracks (figure 5.49). After electrolysis for 10 hours the deposit was observed to break up on the Ta_2O_5-rich phase, as presented in figure 5.50. The entire anode area was covered by manganese dioxide after 50 hours (figure 5.51) and the deposit consisted of many small grains which had grown together.

After electrolysis for 100 hours the manganese dioxide deposit had grown thicker (figure 5.52). The bright areas observed on the surface of the deposit, were caused by the topography of the deposit.

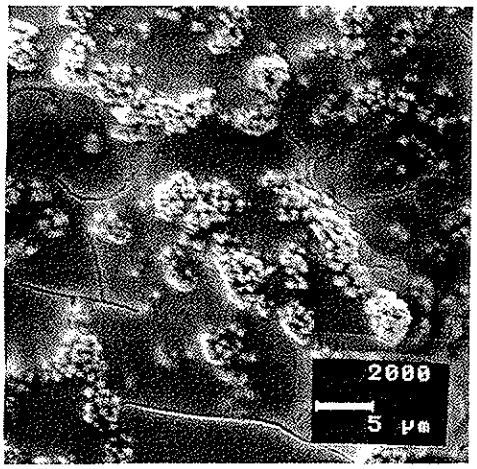

Figure 5.49: *Ti/IrO_2 - Ta_2O_5 used in electrolyte with $c(Mn^{2+}) = 1$ g/l for 1 hour. 2000X.*

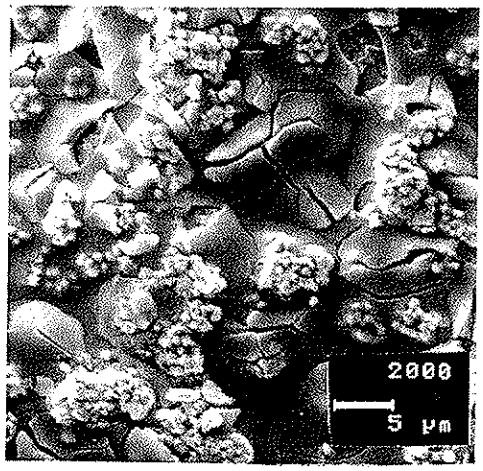

Figure 5.50: *Ti/IrO_2 - Ta_2O_5 used in electrolyte with $c(Mn^{2+}) = 1$ g/l for 10 hours. 2000X.*

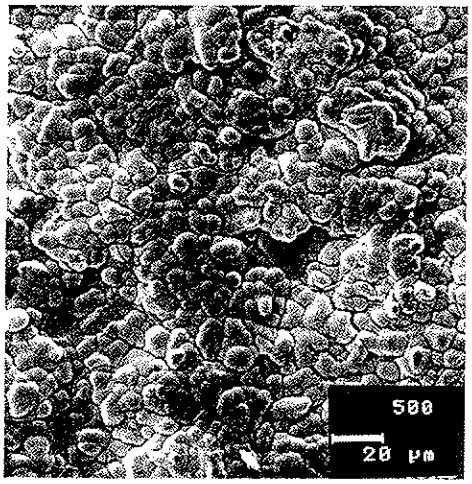

Figure 5.51: *Ti/IrO_2 - Ta_2O_5 used in electrolyte with $c(Mn^{2+}) = 1$ g/l for 50 hours. 500X.*

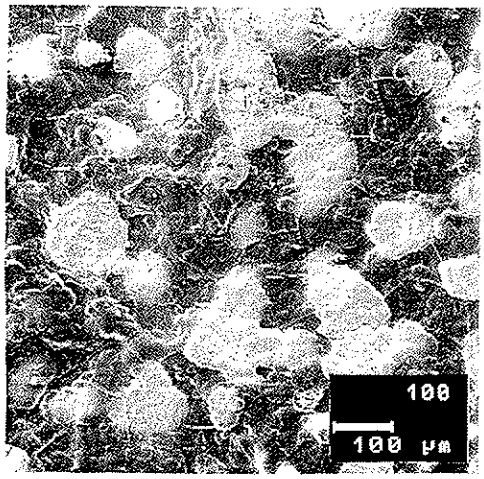

Figure 5.52: *Ti/IrO_2 - Ta_2O_5 used in electrolyte with $c(Mn^{2+}) = 1$ g/l for 100 hours. 100X.*

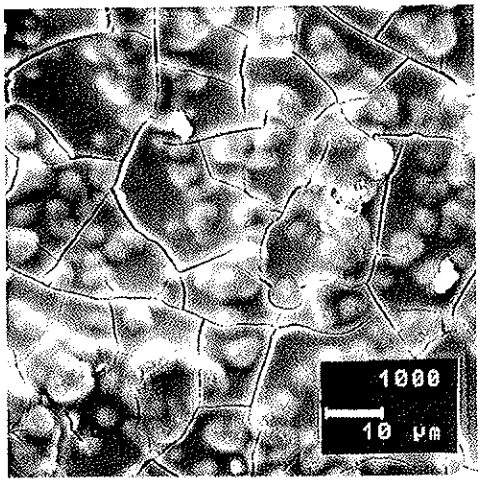

Figure 5.53: *Ti/IrO_2 - Ta_2O_5 used in electrolyte with $c(Mn^{2+}) = 5$ g/l for 1 hour. 1000X.*

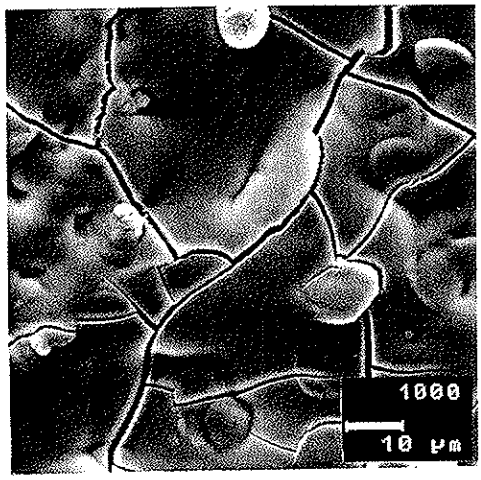

Figure 5.54: *Ti/IrO_2 - Ta_2O_5 used in electrolyte with $c(Mn^{2+}) = 5$ g/l for 10 hours. 1000X.*

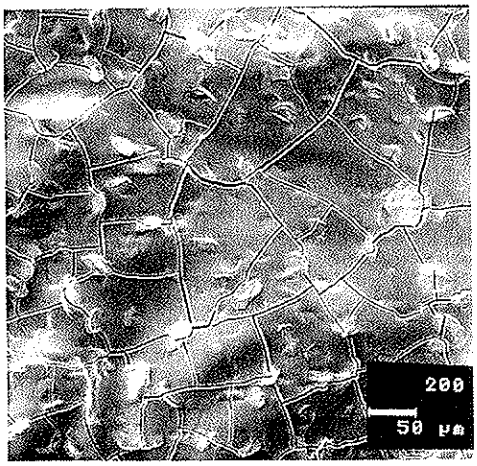

Figure 5.55: *Ti/IrO_2 - Ta_2O_5 used in electrolyte with $c(Mn^{2+}) = 5$ g/l for 50 hours. 200X.*

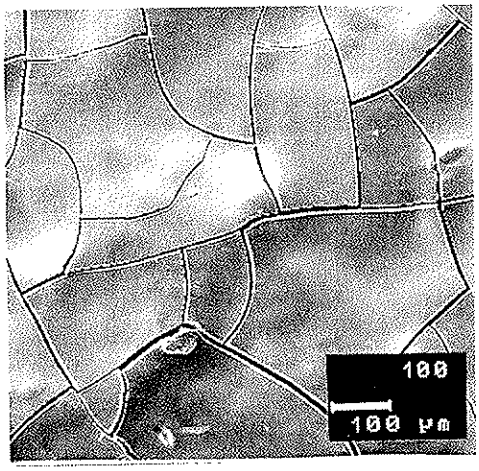

Figure 5.56: *Ti/IrO_2 - Ta_2O_5 used in electrolyte with $c(Mn^{2+}) = 5$ g/l for 100 hours. 100X.*

Increasing Mn^{2+} concentration raised the rate of deposition of MnO_2 on the anode surface, and the electrode surface was covered faster when the Mn^{2+} concentration in the electrolyte was increased. Figure 5.53 shows that the electrode surface was completely covered by MnO_2 deposit already after 1 hour of electrolysis. If the SEM image in figure 5.53 is compared to figure 5.47, the two images

are nearly identical. This comparison may indicate that if the Mn^{2+} concentration is 0.1 g/l, it will take about 50 hours to reach the same deposit thickness as the concentration 5 g/l uses 1 hour to reach. Figures 5.54 - 5.56 shows that the appearance of the deposit did not change much from 10 to 100 hours. The only difference was the size of the grains divided by the cracks. It can be observed that the grain size increased when the deposit layer grew thicker. The main reason for this observation may be that big grains are growing by "consuming" smaller grains.

For the Mn^{2+} concentration 10 g/l, the SEM images (figures 5.57 - 5.60) were very similar to those for 5 g/l. After 1 hour of electrolysis the entire surface was covered by MnO_2 deposit, but still the contours of IrO_2 particle groups were visible through the deposit. Also from these SEM images it can be observed that the grain size increased from about 20 μm after 10 hours to 200-400 μm after 100 hours of electrolysis. Some of the deposit fell off the anode while drying in air, as can be seen from the bright areas in figure 5.60. AUGER analysis of 1 μm (from the deposit surface) of the deposit after 100 hours of electrolysis, showed that no components of the coating were present in the deposit.

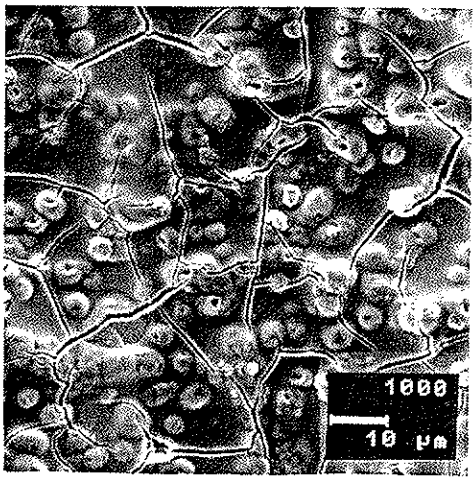

Figure 5.57: *Ti/IrO_2 - Ta_2O_5 used in electrolyte with $c(Mn^{2+}) = 10$ g/l for 1 hour. 1000X.*

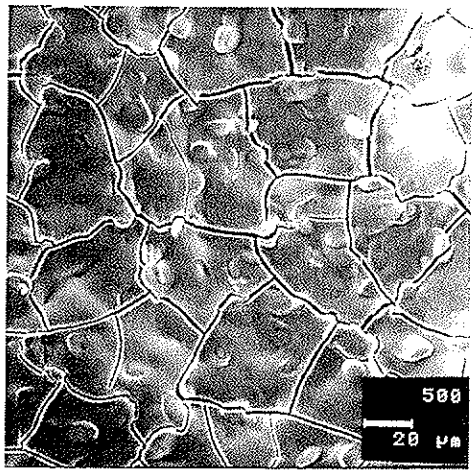

Figure 5.58: *Ti/IrO_2 - Ta_2O_5 used in electrolyte with $c(Mn^{2+}) = 10$ g/l for 10 hours. 500X.*

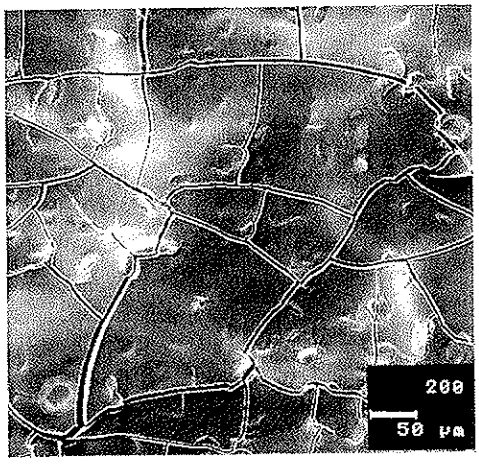

Figure 5.59: *Ti/IrO_2 - Ta_2O_5 used in electrolyte with $c(Mn^{2+}) = 10$ g/l for 50 hours. 200X.*

Figure 5.60: *Ti/IrO_2 - Ta_2O_5 used in electrolyte with $c(Mn^{2+}) = 10$ g/l for 100 hours. 50X.*

5.4.6 Deposition of MnO_2 on a rotating cylinder electrode as a function of the rotation velocity

Rodrigues and Dry [48] observed that deposition of MnO_2 on the anode could be avoided by agitating the electrolyte. In that way the Mn^{3+} ions were removed from the anode surface and into the bulk electrolyte, and the deposition of MnO_2 occurred in the electrolyte instead of on the anode surface. Electrolysis on rotating cylinder electrodes with IrO_2 - Ta_2O_5 coating (figure 4.2 in section 4.1) were conducted in 2M H_2SO_4 containing $c(Mn^{2+}) = 10$ g/l at T = 35°C and current density 0.05 A/cm^2, as described in section 4.3.4.

The scope of these experiments was to see if the rotation velocity had any effect on the deposition of MnO_2 on the anode surface. The peripheral rotation velocity was varied from 0 to 3.0 m/s. The anode potential could not be measured because of too much noise and disturbance. It was observed that no MnO_2 was deposited in the bulk electrolyte during electrolysis, and the electrolyte was red coloured due to Mn^{3+} ions.

When the applied current was switched off before the electrodes were taken out of the electrolyte, the deposited MnO_2 fell off the anode surface. The anodes were therefore taken out of the electrolyte while they were anodically polarized,

to avoid loss of the deposit. After electrolysis the electrodes were washed in distilled water, cast in epoxy and polished. Figures 5.61 - 5.64 show the SEM images of the cross section of the anodes after electrolysis for 10 hours with varying rates of rotation.

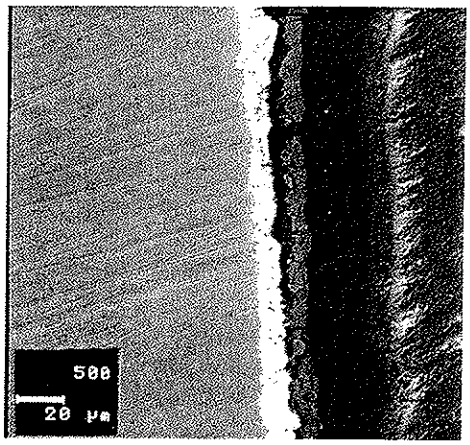

Figure 5.61: *Cross section of a cylinder electrode with IrO_2 - Ta_2O_5 coating after electrolysis in 2M H_2SO_4 containing $c(Mn^{2+}) = 10$ g/l at $T = 35°C$ and $i = 0.05$ A/cm^2, for 10 hours with no rotation. SE 500X.*

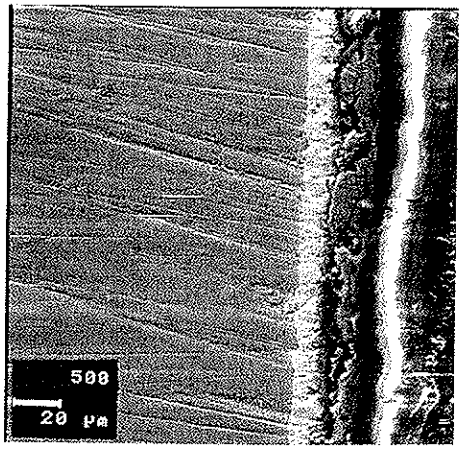

Figure 5.62: *Cross section of a cylinder electrode with IrO_2 - Ta_2O_5 coating after electrolysis in 2M H_2SO_4 containing $c(Mn^{2+}) = 10$ g/l at $T = 35°C$ and $i = 0.05$ A/cm^2, for 10 hours with rotation velocity 50 rpm = 0.052 m/s. SE 500X.*

The cross section of the cylinder electrode after galvanostatic electrolysis for 10 hours in 2M H_2SO_4 containing $c(Mn^{2+}) = 10$ g/l with no rotation of the anode, is presented in figure 5.61. The bright grey phase (to the left) was the Ti substrate, the white phase was the IrO_2 - Ta_2O_5 coating, while the dark grey phase to the right of the IrO_2 - Ta_2O_5 coating, was MnO_2 deposit. The thickness of the coating was about 10-20 μm and it contained a few cracks, but none of them penetrated into the base metal. The deposited MnO_2 (10 μm) was full of cracks, and it was released from parts of the electrode surface. The detachment of the MnO_2 may have happened during the polishing procedure. No particles of the IrO_2 - Ta_2O_5 coating were observed in the MnO_2 deposit.

The SEM image of the cross section of the rotating electrode used in electrolysis with rotation velocity 50 rpm (0.052 m/s), is shown in figure 5.62. This SEM image was very similar to the cross section of the electrode with no rotation, and

the thickness of the deposited MnO_2 was about 10-20 μm thick.

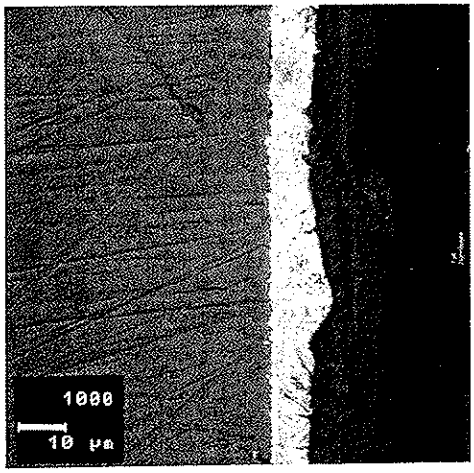

Figure 5.63: *Cross section of a cylinder electrode with IrO_2 - Ta_2O_5 coating after electrolysis in 2M H_2SO_4 containing $c(Mn^{2+}) = 10$ g/l at $T = 35°C$ and $i = 0.05$ A/cm^2, for 10 hours with rotation velocity 300 rpm = 0.3 m/s. SE 1000X.*

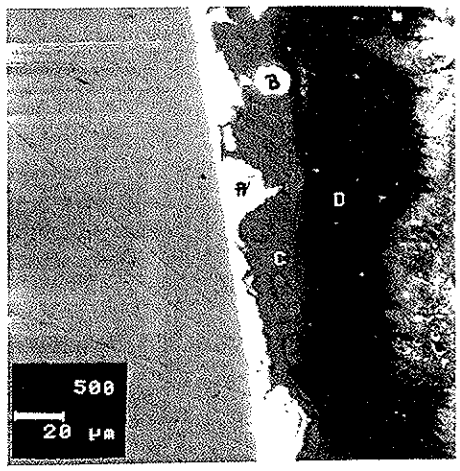

Figure 5.64: *Cross section of a cylinder electrode with IrO_2 - Ta_2O_5 coating after electrolysis in 2M H_2SO_4 containing $c(Mn^{2+}) = 10$ g/l at $T = 35°C$ and $i = 0.05$ A/cm^2, for 10 hours with rotation velocity 3000 rpm = 3.1 m/s. SE 500X.*

When the rotation rate was increased to 300 rpm (0.3 m/s), the deposited MnO_2 was observed to be very compact and it adhered very well to the electrode surface (figure 5.63). The thickness of the MnO_2 deposit did not differ very much from those with lower rotation velocity, and it was observed to be 10-20 μm.

Cross section of the electrode used in the experiment with rotation velocity 3000 rpm (3 m/s) is presented in figures 5.64 and 5.65. The deposited MnO_2 was observed to be up to 20 μm thick, and small particles of the catalytic coating (IrO_2-Ta_2O_5) were observed as inclusions in the MnO_2 deposit. These particles may have been detached because of the high rotation speed or during polishing. Figure 5.65 shows another part of the cylinder electrode where the electrocatalytic coating was thicker than 20 μm and contained pores and cracks. The thickness of the deposited MnO_2 was found to be less than 10 μm, and MnO_2 deposit was observed inside the cracks and pores.

Figures 5.66 - 5.68 show element analyses of the various phases in the cross section of the electrode in figure 5.64.

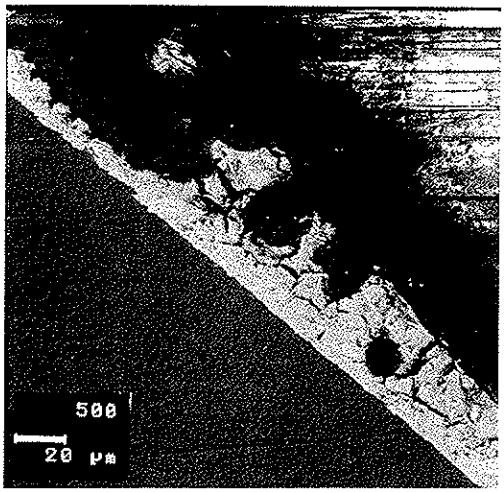

Figure 5.65: *Cross section of a cylinder electrode with IrO_2 - Ta_2O_5 coating after electrolysis in 2M H_2SO_4 containing $c(Mn^{2+}) = 10$ g/l at $T = 35°C$ and $i = 0.05$ A/cm^2, for 10 hours with rotation velocity 3000 rpm = 3.1 m/s. SE 500X.*

Figure 5.66: *Element analysis of the area A in figure 5.64.*

Figure 5.67: *Element analysis of the area B in figure 5.64.*

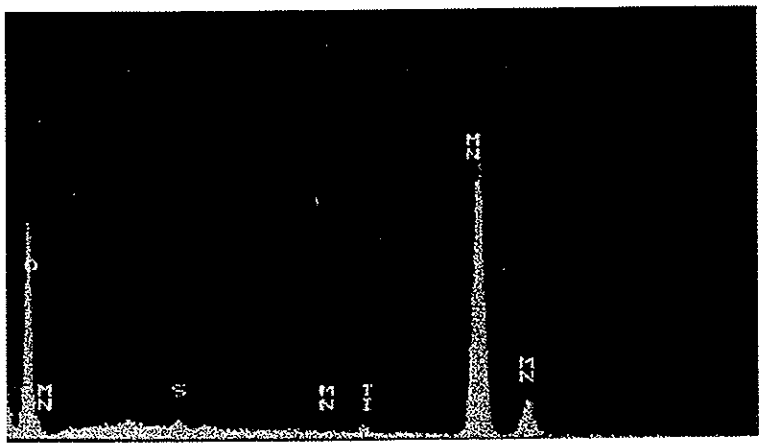

Figure 5.68: *Element analysis of the area C in figure 5.64.*

From the results presented above it can be concluded that deposition of MnO_2 cannot be avoided on the IrO_2 - Ta_2O_5 coating, even at very high rotation velocities (3 m/s), and the thickness of the MnO_2 deposit seemed to be independent of the rotation velocity of the electrode. The MnO_2 deposit was observed to fall off the electrode surface when the current was switched off, and remained attracted

to the coating when the anode was polarized. The attraction between the MnO_2 deposit and the anodically polarized coating may have been coulombic.

5.5 Current efficiency for manganese dioxide deposition

As mentioned earlier in section 1.1, deposition of manganese dioxde occurs as a parasitic reaction to the oxygen evolution on the anode. In the following experiments, the current efficiency as a function of electrolysis time will be discussed. The electrolysis was run in 2M H_2SO_4 with c(Mn^{2+}) = 10 g/l at T = 35°C and i = 0.05 A/cm^2. The anode material used was Ti/IrO_2 - Ta_2O_5, and the electrolysis time was varied from 2 to 96 hours.

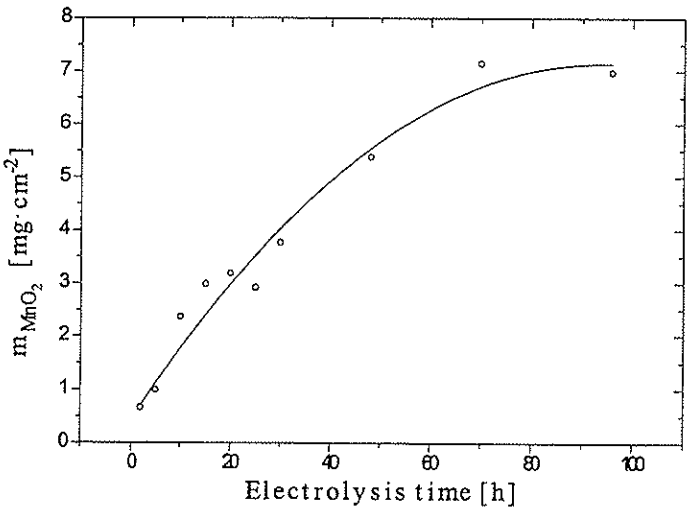

Figure 5.69: *Deposition of manganese dioxide on a Ti/IrO_2 - Ta_2O_5 electrode, as a function of electrolysis time in 2M H_2SO_4, c(Mn^{2+}) = 10 g/l at T = 35 °C and i = 0.05 A/cm^2. The anode area was 6 cm^2.*

Figure 5.69 presents the quantity of deposit as a function of electrolysis time. As can be seen from the figure, deposition of manganese dioxide increased approximately linearly with electrolysis time for the first 20-30 hours, and thereafter the

rate of deposition varied non-linearly with electrolysis time. After 80 hours of electrolysis, an apparent limiting value was reached.

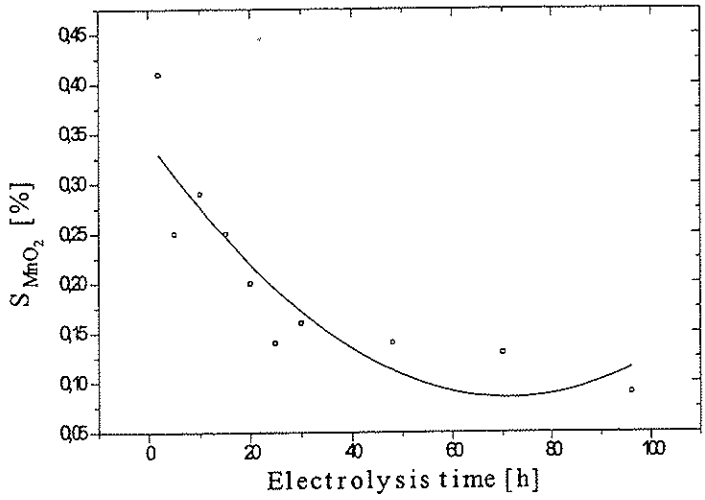

Figure 5.70: *Current efficiency for deposition of MnO_2 on a i/IrO_2 - Ta_2O_5 electrode, as a function of electrolysis time in 2M H_2SO_4, $c(Mn^{2+}) = 10$ g/l at $T = 35°C$ and $i = 0.05$ A/cm^2.*

It was observed that the current efficiency of MnO_2 deposition decreased with increasing electrolysis time (figure 5.70). This decrease supports the observation that deposition of manganese dioxide was not proportional to the electrolysis time.

Forsèn [7] also observed that the current efficiency for the deposition of MnO_2 was highest for new lead anodes in the beginning of the electrolysis. The deposition of MnO_2 may have slowed down further oxidation of Mn^{2+}, which led to decrease in the current efficiency.

5.6 Dissolution of deposited manganese dioxide

As observed earlier in this chapter (section 5.4), it is impossible to prevent deposition of MnO_2 on the anode during anodic polarization, if Mn^{2+} ions are present in the electrolyte. The amount of deposit was reduced when the Mn^{2+} concentration was reduced, but after some time the entire electrode surface was covered by MnO_2 deposit, which blocked the electroactive sites for oxygen evolution. We have also seen from cyclic voltammetry in section 5.2, that MnO_2 deposited on the anode, may be completely reduced during the cathodic scan (800-0 mV). In addition to electrochemical reduction, deposited MnO_2 may be reduced by H_2O_2, as described in section 3.6.2.

5.6.1 Electrochemical dissolution by pulse

From the cyclic voltammograms in section 5.2 it was observed that at potential 0.4 V vs. MSE, deposited MnO_2 was completely reduced. The "cathodic" potentials used in these experiments, were cathodic relative to the oxidation potential for Mn^{2+} (850 mV vs. MSE). The electrochemical reduction was achieved by cathodic pulses at various frequencies and reduction potentials. The current at the working electrode was difficult to measure during the pulse experiments. The experiments were performed as described in section 4.3.5, and the results for changes in weight after pulsing for 100 hours are given in table 5.5, where E_a was the anodic potential applied, E_c was the cathodic potential, t_a was the time interval for the anodic pulse, and t_c was the time interval for the cathodic pulse.

Table 5.5: *Experiments with potential pulse to reduce deposited MnO_2 on a Ti/IrO_2 - Ta_2O_5 anode. E_a was the anodic potential applied, E_c was the cathodic potential, t_a was the time interval for the anodic pulse, and t_c was the time interval for the cathodic pulse.*

Pulse experiment	E_a [V]	E_c [V]	t_a [s]	t_c [s]	Δm [mg/cm^2]
Pulse1	1.1	0.2	1	0.1	+ 0.0071
Pulse2	1.2	0.2	0.1	0.01	-34
Pulse3	1.2	0.3	0.1	0.01	0

It was expected that cathodic pulses should reduce the deposited MnO_2 on the anode surface. From the Pulse1 experiment a slight weight increase was observed. The amount of deposit was observed to be 35 % less than MnO_2 deposited during

galvanostatic electrolysis at the same conditions. The electrode surface was grey, which indicated that there was MnO_2 deposit present. From the SEM image of the electrode surface after 100 hours of pulsing shown in figure 5.71, a thick smooth layer of MnO_2 was observed.

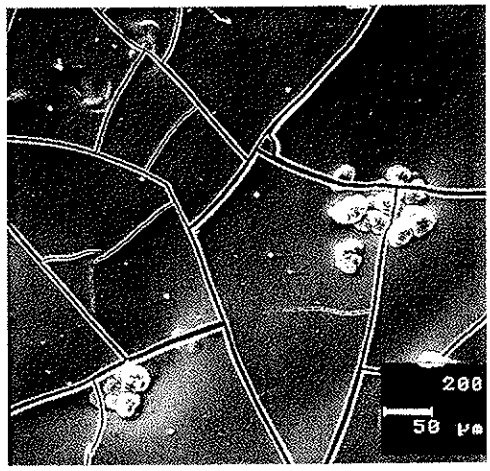

Figure 5.71: *SEM image of the surface of the MnO_2 deposited on a Ti/IrO_2 - Ta_2O_5 anode after pulsing (Pulse1) in 2M H_2SO_4, $c(Mn^{2+}) = 10$ g/l, $T = 35°C$ for 100 hours. The pulse experiment was performed as described in table 5.5.*

Since MnO_2 deposit was observed in the Pulse1 experiment, it was decided to decrease the anodic and cathodic intervals in the Pulse2 experiment. During Pulse2 a reduction in weight of 34 mg/cm^2 was observed. The electrode surface was similar as the one in Pulse1 after pulsing for 100 hours. The same was observed for Pulse3 where no mass difference was measured. These observations may indicate that the coating, or the Ti substrate might not be stable during cathodic pulsing for long times. Some MnO_2 deposit might have been reduced during the cathodic pulses, but it was not completely reduced. The conclusion of these experiments is that pulsing the Ti/IrO_2 - Ta_2O_5 electrode with cathodic potential pulses, does not prevent deposition of MnO_2 on the electrode surface, however it may dissolve the catalytic coating or the base metal.

5.6.2 Chemical dissolution

In section 3.6.2 it was described that deposited MnO_2 may be reduced by H_2O_2. It was believed that if H_2O_2 was added to the electrolyte during electrolysis, deposited MnO_2 on the anode surface might dissolve according to equation 3.43 in section 3.6.2. It was tried to dissolve electrolytically deposited MnO_2 in boiling 2M H_2SO_4 at 100°C, but the black deposit was not reduced. When 10 ml of 30 wt% H_2 O_2 was added to the electrolyte at 75°C, the black deposit dissolved immediately and gas evolution was observed on the electrode surface.

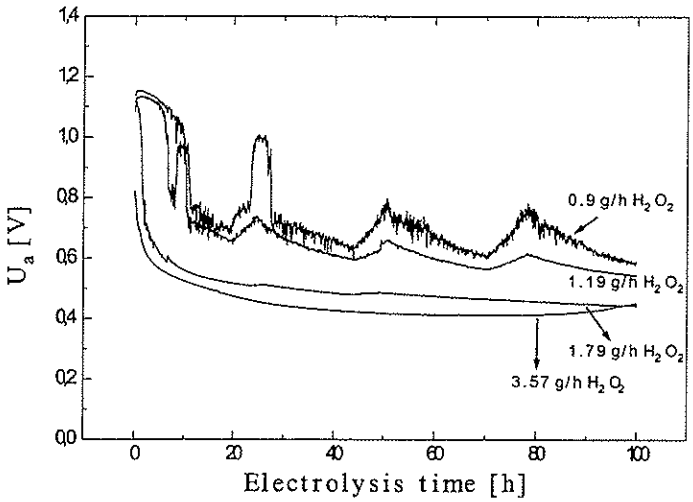

Figure 5.72: *Anode potential for a Ti/IrO_2 - Ta_2O_5 electrode during electrolysis in 2M H_2SO_4, $c(Mn^{2+}) = 10$ g/l at $T = 35$ °C and $i = 0.05$ A/cm^2, when various quantities of H_2O_2 (0.9, 1.19, 1.79 and 3.57 g/h) was added continuously to the electrolyte. The addition of H_2O_2 were about 8-9 ml/hour and convection was induced by bubbling air through the electrolyte.*

Figure 5.72 presents the anode potential on a Ti/IrO_2 - Ta_2O_5 electrode anode during electrolysis in 2M H_2SO_4 containing $c(Mn^{2+})$ = 10 g/l at T = 35°C and i = 0.05 A/cm^2, when various quantities of H_2O_2 (0.9-3.57 g/h) were added continuously to the electrolyte with an injection pump. In the experiment with addition of ~3.57 g/h H_2O_2 to the electrolyte, there was 4.2 g of H_2O_2 in the electrolyte before the electrolysis started. For the other experiments, no H_2O_2 was added to the electrolyte prior to electrolysis, and the addition of H_2O_2 was stopped for

3-4 hours once a day to reduce the H_2O_2 concentration in the electrolyte.

During addition of ~1.79 g/h H_2O_2, the anode potential became constant when the H_2O_2 feed was stopped. For both ~0.9 and 1.19 g/h H_2O_2, the anode potential increased when the feed of H_2O_2 was stopped. This observation indicates that addition of ~0.9-1.19 g/h H_2O_2 may be the lowest amount of H_2O_2 which should be added to avoid deposition of MnO_2 on the anode surface.

The colour of the electrode surface did not change after electrolysis for 100 hours, and no MnO_2 deposit was visible on the anodes when ~0.9-1.19 g/h H_2O_2 was added to the electrolyte. The electrolyte was not red coloured (because of Mn^{3+} ions) as observed earlier, but was faintly pink ($MnSO_4$ in H_2SO_4). This observation indicates that the Mn^{3+} ions formed at the anode, may have been reduced by the hydrogen peroxide to Mn^{2+} in the electrolyte, according to equation 3.44.

When ~3.57 g/h H_2O_2 was added, the electrolyte turned yellow after 75 hours, which might be explained by dissolution of the substrate forming titanium peroxide complexes in the electrolyte. Mraz and Krysa [30] also observed a weak yellow colour in the electrolyte in the end of the accelerated life-tests of the Ti/IrO_2 - Ta_2O_5 anode in sulphuric acid, and explained it by formation of peroxotitanic acid. Large sections of coating had also fallen off the electrode during electrolysis.

The low anode potentials may be due to the decomposition of H_2O_2 (equation 5.1) at the anode, in addition to deposition of MnO_2 and O_2 evolution. The H_2O_2 worked as a depolarizer on the anode potential, and the anode potential was reduced by 500 to 700 mV compared to the standard electrolysis in 2M H_2SO_4 containing $c(Mn^{2+})$ = 10 g/l. The curves for 1.79 and 3.57 g/h H_2O_2 were very smooth, while those for 0.9 and 1.19 were irregular. At high additions of H_2O_2 (1.79 g/h $\leq$) no MnO_2 may have deposited on the anode. It is suggested that the intermediate, Mn^{3+}, may have been reduced before it was hydrolyzed. At low additions of H_2O_2 ($\leq$ 1.19 g/h), MnO_2 might have been deposited and reduced simultaneously as oxygen evolution and decomposition of H_2O_2 occurred on the anode surface, giving an irregular anode potential.

$$O_2 + 2H^+ + e^- \rightleftharpoons H_2O_2 \qquad E^\circ_{NHE} = 0.68V \tag{5.1}$$

The electrodes were weighed before and after electrolysis. The differences in weight are given in table 5.6. As can be seen from the table, addition of ~3.57 g/h H_2O_2 to the electrolyte was obviously too much, and it destroyed/reduced the catalytic coating. It might also happen that H_2O_2 in some way affected

Table 5.6: *Change in weight of anode (Ti/IrO_2 - Ta_2O_5) before and after electrolysis in 2M H_2SO_4, $c(Mn^{2+}) = 10$ g/l at $T = 35°C$ and $i = 0.05$ A/cm^2 with different additives of H_2O_2 (0.9-3.57 g/h) for 100 hours.*

H_2O_2 [g/h]	Δm [mg/cm^2]
0.95	-0.05
1.19	-0.05
1.79	-0.07
3.57	-34.0

the adherence between the substrate and the catalytic coating. H_2O_2 additions between ~0.9-1.19 g/h were found to be enough to reduce the deposited MnO_2 on the anode surface, and to avoid coverage of the catalytic sites by MnO_2. The small negative change in weight may be due to dissolution of the coating, but the weight reduction lies within the uncertainty of the scales used.

These experiments were carried out to study the reducing effect of H_2O_2 on the deposited MnO_2 in sulphuric acid. Further experiments might be conducted to study the concentration of H_2O_2 in the electrolyte as a function of time, and to establish the accurate quantities of H_2O_2 needed to avoid deposition of MnO_2 for various Mn^{2+} concentrations in the electrolyte.

Chapter 6

Conclusions

The deposition of manganese dioxide from sulphuric acid electrolyte containing Mn^{2+} ions, has been studied on various electrode materials (Pt, Pb/Ag, Ti/IrO_2 - $Ta_2O_5/(MnO_x)$), by cyclic voltammetry, linear voltammetry and galvanostatic electrolysis.

Cyclic voltammetry was conducted on platinum and Ti/IrO_2 - Ta_2O_5 as working electrodes in 2M H_2SO_4 containing Mn^{2+} ions at T = 35°C. The oxidation of Mn^{2+} to MnO_2 was found to be mass transfer controlled, and followed an ECE mechanism (electrochemical-chemical-electrochemical) as given by equations 6.1 - 6.3, because two oxidation peaks were observed.

$$Mn^{2+} \rightarrow Mn^{3+} + e^- \tag{6.1}$$

$$Mn^{3+} + 2H_2O \rightarrow MnOOH + 3H^+ \tag{6.2}$$

$$MnOOH \rightarrow MnO_2 + H^+ + e^- \tag{6.3}$$

The presence of the Mn^{3+} ions in the electrolyte during the anodic scan, was detected by a spectrophotometer. The intermediate product MnOOH was found to be insulating, giving very sharp oxidation peaks at low scan rates (≤ 10 mV/s).

Low sulphuric acid concentrations ($\leq$ 2M) were observed to favour deposition of MnO_2, while high acid concentrations (4 $\leq$) inhibited the deposition.

Introduction of stirring in the electrolyte enhanced the oxidation of Mn^{2+}, and inhibited the deposition of MnO_2 on the platinum electrode surface. For the Ti/IrO_2 - Ta_2O_5 electrode, only small amounts of MnO_2 were deposited compared to experiments with no stirring.

The MnO_2 deposited during the anodic scan, was found to be reduced completely in the cathodic scan. The reduction mechanism is suggested to be a combination of electrochemical and chemical dissolution steps, as described in equations 6.4 - 6.7. The Mn^{2+} concentration (10 g/l $\leq$) had a large effect on the production of Mn^{3+} ions during the cathodic scan. The Mn^{3+} ions were reduced in the end of the cathodic scan according to equation 6.7. The first reduction step is suggested to take place in the interior of the MnO_2 deposit where the electrons from the electrode and protons from the electrolyte meet. The diffusion of protons to the interior of the deposit is suggested to be the rate determining step in the reduction of MnO_2.

$$MnO_2 + H^+ + e^- \rightarrow MnOOH \tag{6.4}$$

$$MnOOH + 3\ H^+ \rightarrow Mn^{3+} + 2\ H_2O \tag{6.5}$$

$$1/2\ MnO_2 + 1/2\ Mn^{2+} + 2\ H^+ \rightarrow Mn^{3+} + H_2O \tag{6.6}$$

$$Mn^{3+} + e^- \rightarrow Mn^{2+} \tag{6.7}$$

The IrO_2 - Ta_2O_5 coating was modified by replacing parts of the Ta_2O_5 content with various quantities of MnO_x (5, 50, 75 and 100 mol%), while the quantity of IrO_2 was the same for all coatings. The morphology of the coating changed from consisting of a smooth phase of Ta_2O_5 with crystalline agglomerates of IrO_2 for the IrO_2 - Ta_2O_5 coating, to an apparent one phase coating with no agglomerates of IrO_2 for high concentrations of MnO_x (50-100 mol%). The coating with 5 mol% MnO_x was observed to have the lowest anode potential for oxygen evolution, while the coating with pure IrO_2 was observed to be less active for oxygen evolution because of partial passivation of the Ti substrate.

The deposition of MnO_2 on the various electrode coatings was nearly independent of the coating composition in galvanostatic electrolysis, and it is suggested that oxidation of Mn^{2+} occurred at the interface deposited MnO_2/electrolyte. The current efficiency with respect to MnO_2, was observed to decrease as a function of electrolysis time.

Manganese dioxide was observed deposited on rotating cylinder electrodes during galvanostatic electrolysis, and the deposit thickness (20μm) was observed to be nearly independent of the rotation velocity (0 to 3 m/s).

Increasing concentration of Mn^{2+} ions in the electrolyte led to faster blocking of the catalytic sites of the IrO_2 - Ta_2O_5 coating leading to higher anode potential. The spent electrolyte was studied by a spectrophotometer and the absorption spectrum of Mn^{3+} was obtained. No permanganate was detected in the red coloured electrolyte.

When Pt was used as an anode in electrolysis in 2M H_2SO_4 containing Mn^{2+} ions, huge quantities of dispersed MnO_2 were observed in the bulk electrolyte. The MnO_2 adhered poorly to the Pt surface, while it adhered very well to the IrO_2 - Ta_2O_5 coating and polished lead (Pb/Ag) anode (no dispersed MnO_2 was observed). It is suggested that differences in surface tensions may affect the adherence of the deposited MnO_2 to the anode surface.

Cathodic pulses were applied to the Ti/IrO_2 - Ta_2O_5 electrode during electrolysis (for 100 hours), to reduce the deposited MnO_2. The deposition of MnO_2 was not avoided, but the coating or the Ti substrate was dissolved, and a decrease in weight was observed. However, when H_2O_2 ($\sim$0.9-1.19 g/h) was added to the electrolyte during electrolysis, the deposited MnO_2 and the Mn^{3+} ions were reduced by the H_2O_2. I addition a depolarizing effect was observed due to the decomposition of H_2O_2 on the anode, and the anode potential was reduced by 500 to 700 mV compared to the standard electrolysis in 2M H_2SO_4 containing $c(Mn^{2+}) = 10$ g/l.

Bibliography

[1] X. G. Zhang. *Corrosion and Electrochemistry of Zinc.* Plenum Press, New York, (1996).

[2] J. Thonstad. *Elektrolyseprosesser.* NTH, Trondheim, (1994).

[3] F. Porter. *Zinc Handbook (Properties, Processing and Use in Design).* Marcel Dekker, Inc., New York, (1991).

[4] D.H. Magoon, K.A. Metcalfe, A.R. Babcock, and W.A. Van Beek. Equipment and processes for roasting zinc concentrates. In T. S. Mackey and R. D. Prengaman, editors, *Lead~ Zinc '90*, pages 389–412, (1990).

[5] D. R. Spink, K. D. Nguyen, and E. Marrella. New process to upgrade zinc concentrate to using partial desulphurization technique. In T. S. Mackey and R. D. Prengaman, editors, *Lead~ Zinc '90*, pages 717–731, (1990).

[6] K. Bouzek, K. Børve, O. A. Lorentsen, K. Osmundsen, I. Rousar, and J. Thonstad. Current distribution at the electrodes in zinc electrowinning cells. *J. Electrochem. Soc.*, 142(1):64–69, (1995).

[7] O. Forsèn. *Manganjonens inverknad på blyanoden under elektrolys i sulfatbad.* PhD thesis, Tekniska Högskolan i Helsingfors, 1979.

[8] J. J. Lander. Further studies on the anodic corrosion of lead in H_2SO_4 solutions. *J. Electrochem. Soc.*, 103(1):1–8, (1956).

[9] C. Rerolle and R. Wiart. Kinetics of Pb-Ag anodes for zinc electrowinning, formation of $PbSO_4$ layers at low polarization. *Electrochim. Acta*, 40(8):939–948, (1995).

[10] Jr. E. R. Cole and T. J. O'Keefe. Insoluble anodes for electrowinning zinc and other metals. Technical report, U. S. Bureau of Mines, (1981). Report number. BuMines RI 8531.

[11] S. Trasatti. Electrocatalysis in the anodic evolution of oxygen and chlorine. *Electrochim. Acta*, 29(11):1503–1512, (1984).

[12] L. N. Kulikova, V. N. Fateev, A. De Battisti, and V. D. Rusanov. The electrochemical behaviour of iridium dioxide modified by ion implantation. *Russian Journal of Electrochem.*, 32(6):691–695, (1996).

[13] T. A. F. Lassali, S. C. De Castro, and J. F. C. Boodts. Structural, morphological and surface properties as a function of composition of Ru + Ti + Pt mixed-oxide electrodes. *Electrochim. Acta*, 43(16-17):2515–2525, (1998).

[14] Ch. Comninellis and G. P. Vercesi. Characaterization of DSA-type oxygen evolving electrodes: choise of a coating. *J. Appl. Electrochem.*, 21:335–345, (1991).

[15] J. Krysa, J. Maixner, R. Mraz, and I. Rousar. Effect of coating thickness on the properties of IrO_2 - Ta_2O_5 anodes. *J. Appl. Electrochem.*, 28:369–372, (1998).

[16] M. Vukovic. Oxygen evolution reaction on thermally treated iridium oxide films. *J. Appl. Electrochem.*, 17:737–745, (1987).

[17] L. A. da Silva, V. A. Alves, M. A. P. da Silva, S. Trasatti, and J. F. C. Boodts. Oxygen evolution in acid solution on IrO_2 + TiO_2 ceramic films. a study by impedance, voltammetry and SEM. *Electrochim. Acta*, 42(2):271–281, (1997).

[18] F. Cardarelli, P. Taxil, A. Savall, Ch. Comninellis, G. Manoli, and O. Leclerc. Preparation of oxygen evolving electrodes with long service life under extreme conditions. *J. Appl. Electrochem.*, 28:245–250, (1998).

[19] V. A. Alves, L. A. Da Silva, J. F. C. Boodts, and S. Trasatti. Kinetics and mechanism of oxygen evolution on IrO_2-based electrodes containing Ti and Ce in acid solutions. *Electrochim. Acta*, 39(11/12):1585–1589, (1994).

[20] S. Kulandaisamy, J. P. Rethinaraj, S. C. Chockalingam, S. Visvanathan, K. V. Venkateswaran, P. Ramachandran, and V. Nadakumar. Performance of catalytically activated anodes in the electrowinning of metals. *J. Appl. Electrochem.*, 27:579–583, (1997).

[21] A. Nidola, F. Zioni, R. J. Ornelas, and U. Nevosi. Anodes for oxygen evolution in electrolytes containing manganese and fluorides. Australian Patent Office AU-A-83179/98, (1998).

[22] G. N. Martellia, R. Ornelas, and G. Faita. Deacivation mechanism of oxygen evolving anodes at high current densities. *Electrochim. Acta*, 39(11/12):1551–1558, (1994).

[23] G. P. Vercesi, J. Y. Salamin, and Ch. Comninellis. Morphological and microstructural study of the Ti/IrO_2 - Ta_2O_5 electrode: Effect of the preparation temperature. *Electrochim. Acta*, 36(5/6):991–998, (1991).

[24] J. Krysa and R. Mraz. Experimental investigation of the double layer capacity, X-ray diffraction and the relative surface content of TiH_2 during the pretreatment of titanium used for the preparation of dimensionally stable anodes with RuO_2 and/or IrO_2 coating. *Electrochim. Acta*, 40(12):1997–2003, (1995).

[25] S. Trasatti, editor. *Electrodes of conductive metallic oxides.* Part B. Elsevier, Amsterdam, (1980).

[26] R. Otogawa, K. Soda, S. Yamauchi, Y. Nagatoishi, M. Morimitsu, and M. Matsunaga. Morphological deterioration of iridium oxide - tanalum oxide anode by oxygen evolution. *Denki Kagaku*, 65(12):987–991, (1997).

[27] G. P. Vercesi, J. Rolewich, and Ch. Comninellis. Characterization of DSA-type oxygen evolving electrodes. choise of base metal. *Thermochim. Acta*, 176:31–47, (1991).

[28] R. F. Savinell, R. L. Zeller III, and J. A. Adams. Electrochemically active surface area. voltammetric charge correlation for ruthenium and iridium dioixde electrodes. *J. Electrochem. Soc.*, 137(2), (1990).

[29] J. Krysa, L. Kule, R. Mraz, and I. Rousar. Effect of coating thickness and surface treatment of titanium on the properties of IrO_2-Ta_2O_5 anodes. *J. Appl. Electrochem.*, 26:999–1005, (1996).

[30] K. Mraz and J. Krysa. Long service life of IrO_2/Ta_2O_5 electrodes for electroflotation. *J. Appl. Electrochem.*, 24:1262–1266, (1994).

[31] R. Kötz, H. J. Lewerenz, and S. Stucki. Xps studies of oxygen evolution on Ru and RuO_2 anodes. *J. Electrochem. Soc*, 130(4):825–829, (1983).

[32] Yu. E. Roginskaya, O. V. Morozova, E. N. Loubnin, a. V. Popov, Yu. I. Ulitina, V. V. Zhurov, S. A. Ivanov, and S. Trasatti. X-ray diffraction, transmission electron microscopy and X-ray photoelectron spectroscopic characterization of $IrO_2 + Ta_2O_5$ films. *J. Chem. Soc. Farady Trans.*, 89(11):1707–1715, (1993).

[33] G. Lodi, A. De Battisti, G. Bordin, C. De Asmundis, and A. Benedetti. Microstructure and electrocal properties of IrO_2 prepared by thermal decomposition of $IrCl_3 \cdot xH_2O$. role played by the conditions of thermal treatment. *J. Electroanal. Chem.*, 277:139–150, (1990).

[34] G. Foti, C. Mousty, V. Reid, and Ch. Comninellis. Characterization of DSA type electrodes prepared by rapid thermal decomposition of the metal precursor. *Electrochim. Acta*, 44:813–818, (1998).

[35] S. Gottesfeld and S. Srinivasan. Electrochemical and optical studies of thick oxide layers on iridium and their electrocatalytic activities for the oxygen evolution reaction. *J. Electroanal. Chem.*, 86:89–104, (1978).

[36] H. Remy. *Treatese on inorganic chemistry*, volume 2. Elsevier, Amsterdam, (1956).

[37] K. V. Kordesch, editor. *Batteries (Manganese dioxide)*, volume 1. Marcel Dekker, INC, New York, (1974).

[38] S. Trasatti, editor. *Electrodes of conductive metallic oxides.* Part A. Elsevier, Amsterdam, (1980).

[39] P. Ruetschi. Cation-Vacancy Model for MnO_2. *J. Electrochem. Soc.*, 131(12):2737–2744, (1984).

[40] W-H Kao. Effect of particle size on transformation of EMD during digestion in sulphuric acid continaing Mn(II). *J. Electrochem. Soc.*, 135(6):1317–1320, (1988).

[41] A. M. Pande, K. N. Gupta, and V. A Altekar. Single cell extraction of zinc and manganese dioxide from zinc sulpide concentration and manganese ores. *Hydrometallurgy*, 9:57–68, (1982).

[42] W. H. Kao and V. J. Weibel. Electrochemical oxidation of manganese(II) at a platinum electrode. *J. Appl. Electrochem.*, 22(1):21–27, (1992).

[43] F. R. A. Jorgensen. Cell voltage during the electrolytic production of manganese dioxide. *Electrochemical Technology*, 117(2):275–278, (1970).

[44] W. C. Vosburgh. The manganese dioxide electrode. *J. Electrochem. Soc.*, 106(9):839–845, (1959).

[45] M. Fleischmann, H. R. Thirsk, and I. M Tordesillas. Kinetics of electrodeposition of γ-manganese dioxide. *Trans. Faraday Soc.*, (58):1865–1877, (1962).

[46] J. Y. Welsh. The role of manganic ion in the prodution of electrolytic manganese dioxide. *Electrochemical Technology*, 5(11-12):504–507, (1967).

[47] J. Ph. Petitpierre, Ch. Comninellis, and E. Plattner. Oxydation du $MnSO_4$ en dioxyde de manganese dans H_2SO_4 30%. *Electrochim. Acta*, 35(1):281–287, (1990).

[48] J. M. S. Rodrigues and M. J. Dry. The production of particulate manganese dioxide during zinc electrowinning. In *Electrometallurgical plant practice*, pages 199–220.

[49] S. Bodoardo, J. Brenet, M. Maja, and P. Spinelli. Electrochemical behaviour of manganese dioxide electrodes in sulphuric acid solutions. *Electrochim. Acta*, 39(13):1999–2004, (1994).

[50] R. L. Paul and A. Cartwright. The mechanism of the deposition of manganese dioxide, Part II. electrode impedance studies. *J. Electroanal. Chem.*, (201):113–122, (1986).

[51] G. Davies. *Coordination Chemistry Reviews*. Elsevier Publishing Company, Amsterdam, (1969).

[52] R. L. Paul and A. Cartwright. The electrodeposition of manganese dioxide: Theory and practice. pages 453–461, (1985).

[53] S. Rodrigues, N. Munichandraiah, and A. K. Shukla. A cyclic voltammetry study of the kinetics and mechanism of electrodeposition of manganese dioxide. *J. Appl. Electrochem.*, (28):1235–1241, (1998).

[54] D. Velayutham, M. Noel, and S. Chidambaram. Influence of acid strength and other addition agents on the electrochemical production of manganic sulphate from manganous suplhate. *Bulletin of Electrochemistry*, 2 and 3(9):99–102, (1993).

[55] J. A. Lee W. C. Maskell and F. L. Tye. The electrochemical reduction of managanese dioxde in acidic solutions, Part I. *J. Electroanal. Chem.*, 79:79–104, (1977).

[56] J. A. Lee, W. C. Maskell, and F. L. Tye. The electrochemical reduscction of managanese dioxde in acidic solutions, Part III. *J. Electroanal. Chem.*, 110:145–158, (1980).

[57] W. C. Maskell. The electrochemical reduscction of managanese dioxde in acidic solutions, Part II. *J. Electroanal. Chem.*, 199(1):127–137, (1986).

[58] N. C. Cahoon and M. P. Korver. The influence of the active surface on the cathodic reduction of MnO_2. *J. Electrochemical Soc.*, 109(1):1–6, (1962).

[59] Southampton Electrochemstry Group. *Instrumental Methods in Electrochemistry*. Ellis Horwood Limited, England, (1990).

[60] K. S. Jeon, D. Y. Shin, and T. Kang. The application of coated titanium electrodes for zinc electrowinning processes. In C. Shi, H. Li, and A. Scott,

editors, *The first pacific Rim International Conference on Advanced Materials and Processing (PRICM-1)*, The Minerals, Metals and Materials Society, pages 565–568, (1992).

[61] A. Michas, F. Andolfatto, M. E. G. Lyons, and R. Durand. Gas evolution reactions at conductive metallic oxide electrodes for solid polymer electrolyte water electrolysis. *Key Engineering Materials*, 72-74:535–550, (1992).

[62] O. De Nora, G. Bianchi, A. Nidola, and G. Trisogli. Method of electrowinning metals. United States Patent 3,926,751, (1975).

[63] Ch. Comninellis and G. P. Vercesi. Problem in DSA coating deposition by thermal decomposition. *J. Appl. Electrochem.*, 21:136–142, (1991).

[64] W. P. Griffith, C. J. Raub, and E. Raub. *Gmelin Handbuch der Anorganischen Chemie.* Springer Verlag, Berlin, 8 edition, (1978). Ir.

[65] K. Swars, editor. *Gmelin Handbuch der Anorganischen Chemie.* Verlag Chemie, GMBH, Weinheim/Bergstr., 8 edition, (1970). Ta.

[66] C. C. Liang. *Encyclopedia of Electrochemistry of the Elements.* Marcel Dekker, Inc., New York, (1973).

[67] P. S. Tutundzic and S. Mladenovic. Quantitative elektrolytische erzeugung von permanganationen. *Anal. Chim. Acta*, 12:382–389, (1955).

[68] R. G. Selim and J. J. Lingane. Coulometric titration with higher oxidation states of manganese. electrolytic generation and stability of +3 manganese in sulfuric acid media. *Anal. Chim. Acta*, 21:536–544, (1959).

[69] P. Tanskanen, J. Aromaa, and O. Forsen. Manganese deposition on inert anodes during cathodic protection. Technical report, Helsinki University of Technology, Laboratory of Corrosion and Material Chemistry, (1996).

[70] G. Dominguez and D. D. Makwana. Redox control in the electrodeposition of metals. United States Patent 5,833,830, (1998).

[71] J. L. Fussi, O. Quintero, A. Cornaglia, and C. Morosini. Electrowinning of high purity zinc metal from a Mn-containing leach solution preceded by cold electrolytic demanganization. European Patent, EP 0 885 976 A1.

[72] T. Bjørnarå. Dimensjonsstabile elektroder i sink elektrolysen. Technical report, Department of Materials Science and Electrochemistry, NTNU, (1999).

APPENDIX

Appendix A

Cyclic voltammetry on Pt

Peak current density and peak potential as a function of scan rate

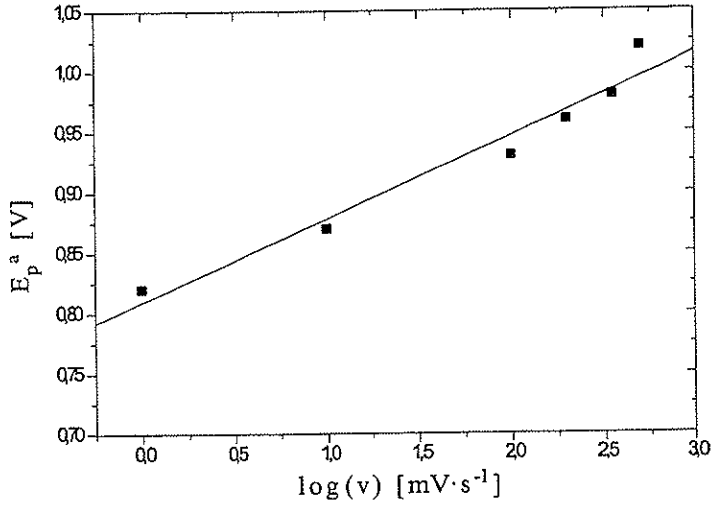

Figure A.1: *The anodic peak potential as a function of log(v).*

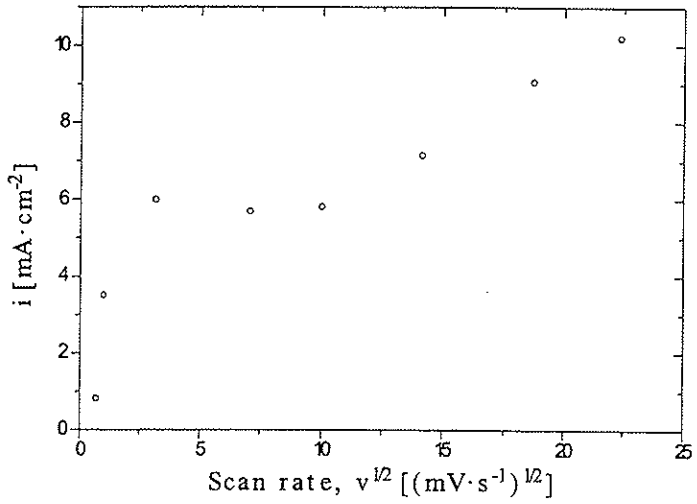

Figure A.2: *The anodic peak current density as a function of the square root of the scan rate.*

Appendix B

AC Impedance

AC impedance measurements on Ti/IrO_2 - Ta_2O_5 in 2M H_2SO_4

The figures B.1-B.4 present Nyquist diagrams for a Ti/IrO_2 - Ta_2O_5 electrode in 2M H_2SO_4 at T = 35°C and various applied potentials.

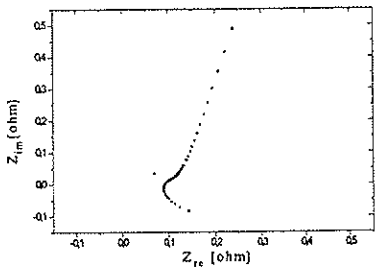

Figure B.1: *Impedance plot (10-100kHz) on a Ti/IrO_2 - Ta_2O_5 electrode at open circuit potential.*

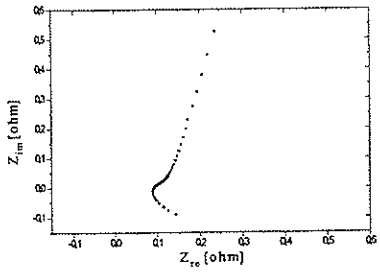

Figure B.2: *Impedance plot (10-100kHz) on a Ti/IrO_2 - Ta_2O_5 electrode at applied potential 0.5 V vs. MSE.*

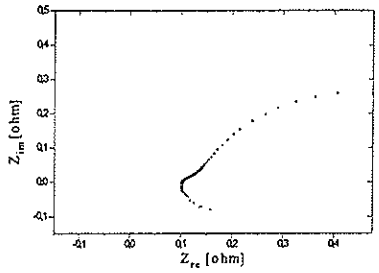

Figure B.3: *Impedance plot (10-100kHz) on a Ti/IrO_2 - Ta_2O_5 electrode at applied potential 1.0 V vs. MSE.*

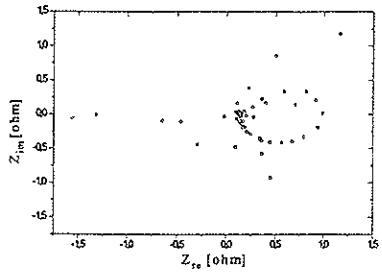

Figure B.4: *Impedance plot (10-100kHz) on a Ti/IrO_2 - Ta_2O_5 electrode at applied potential 2.0 V vs. MSE.*

The noise in the measurements when 2.0 V was applied to the electrode, was due to the oxygen evolution on the Ti/IrO_2 - Ta_2O_5 electrode.

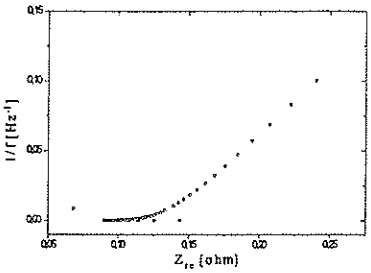

Figure B.5: *Plot of inverse frequence (10-100kHz) as a function of Z_{Re} at open circuit potential on a Ti/IrO_2 - Ta_2O_5 electrode.*

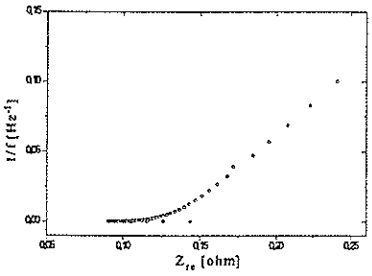

Figure B.6: *Plot of inverse frequence (10-100kHz) as a function of Z_{Re} at applied potential 0.5 V vs. MSE on a Ti/IrO_2 - Ta_2O_5 electrode.*

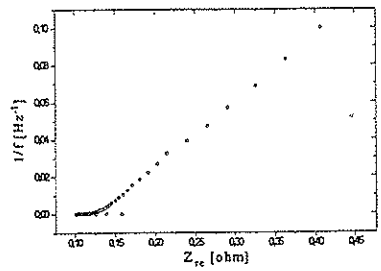

Figure B.7: *Plot of inverse frequence (10-100kHz) as a function of Z_{Re} at applied potential 1.0 V vs. MSE on a Ti/IrO_2 - Ta_2O_5 electrode.*

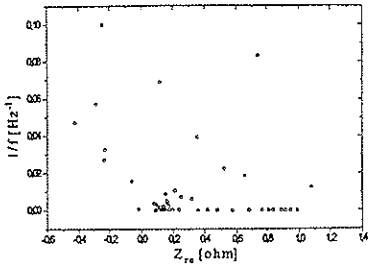

Figure B.8: *Plot of inverse frequence (10-100kHz) as a function of Z_{Re} at applied potential 2.0 V vs. MSE on a Ti/IrO_2 - Ta_2O_5 electrode.*

The electroyte resistance between the electrode surface and the luggin capillary tip, was performed by extrapolate the curve to 1/f = 0 and read the resistance from the Z_{Re}.

Table B.1: *The electrolyte resistance between the electrode surface and the luggin capillary tip, when various potentials were applied to the working electrode.*

Applied Potential [V]	Electrolyte resistance [Ω]
OCP=0.3	0.09
0.5	0.09
1.0	0.1
2.0	0.1

Appendix C

Polarization curves in sulphuric acid

Polarization curves in 2M H_2SO_4

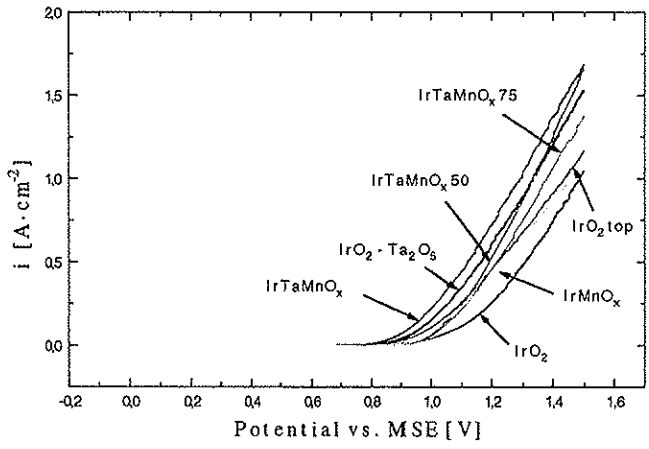

Figure C.1: *Polarization curve on IrO_2 - Ta_2O_5, IrO_2top, IrO_2, $IrTaMnO_x5$, $IrTaMnO_x50$, $IrTaMnO_x75$ and $IrMnO_x$ coating in 2M H_2SO_4 at $T = 35°C$ and scan rate 1 mV/s. Interval 0-1.5 V vs. MSE. Second experiment.*

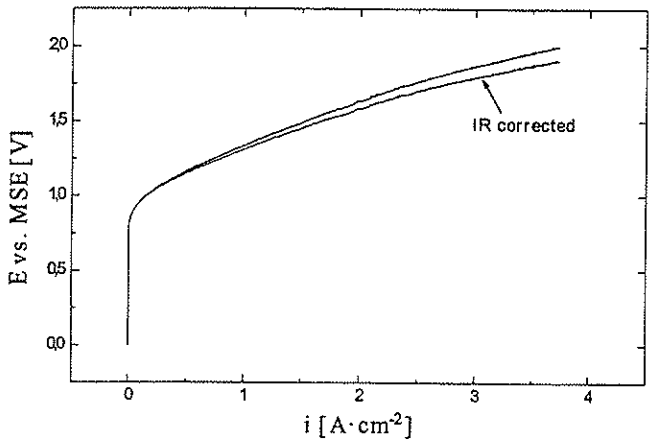

Figure C.2: *Polarization curves on a Ti/IrO_2 - Ta_2O_5 electrode in 2M H_2SO_4 at $T = 35°C$ and scan rate 1 mV/s. Interval 0-2 V vs. MSE. The effect of IR correction when the electrolyte resistance is 0.1 Ω.*